Microstructure and Mechanical Performance of SiC/BMAS Glass-Ceramic Matrix Composite

Grant West

Thesis submitted for the award of

Doctor of Philosophy

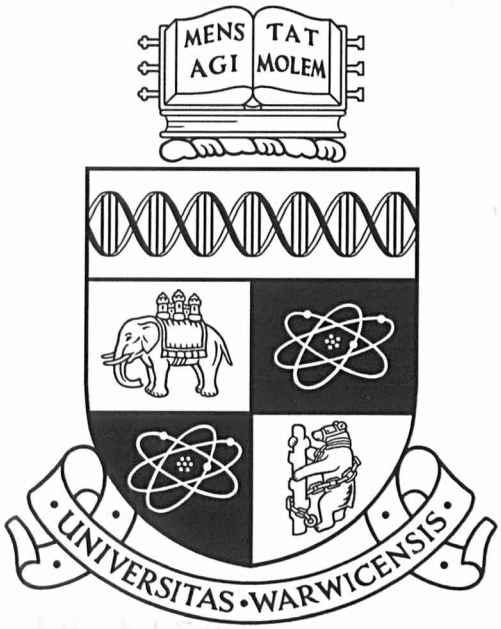

Centre for Advanced Materials

University of Warwick

July 1997

To Sally, Hayley and Sophie

Acknowledgements

During this PhD I have received help from a great many sources. In particular I would like to thank Professor Mike Lewis for providing the opportunity to work at the University of Warwick and his help and guidance as my supervisor. Thanks also to my former supervisor Professor David Taplin.

It has been my pleasure and privilege to work alongside colleagues in this field who have inspired me and been great friends. In particular, gratitude is due to Drs Markys Cain and Aldo Boccaccini for numerous informative discussions. I must also thank past and present friends from the Department of Physics such as Drs Kevin Plucknett, Tony Chamberlain, Astrid Nordmann, John Lumby as well as Rebecca Cain.

Technical assistance has been gratefully received from many sources within the department such as Gerry and Steve on the electron microscopes, Adrian Lovejoy for his electronics guidance and noise detection on the Instron and Dave Hammond for his aid with the Instron and dilatometer.

Having worked on this project at two different Universities I must also thank the staff of the University of Plymouth, David Short and Dr David Plane particularly, for their help.

Most of all wholehearted thanks to Hayley who is understanding and loving and has been a pillar of support throughout.

Declaration

This thesis is entirely my own work unless otherwise referenced and has not been submitted for award of a degree at any other University. The thesis is set out as as per the guidelines issued by the Warwick Graduate School (September 1996). Parts of this work have appeared in numerous publications as listed below:

Cyclic creep response and creep recovery of continuous fibre reinforced glass and glass-ceramic matrix composites,
G West, A R Boccaccini, J Janczak, D M R Taplin and M H Lewis, *Submitted to ICSMA-11, Prague, 25-29 August 1997*

Mechanical behaviour and environmental stability of continuous fibre-reinforced glass-ceramic matrix composites,
G West, D M R Taplin, A R Boccaccini, K Plucknett and M H Lewis, *Glass Science and Technology, Glastech Berichte, Feb 1996, Vol 69, No 2, pp34-43*

Cyclic creep response of continuous fibre reinforced glass-ceramic matrix composites,
G West, A R Boccaccini, D M R Taplin and M H Lewis, *ECCM-7, The Institute of Materials, Woodhead Publishing Ltd, London, 1996 Vol 1, 455-60*

Creep and creep fatigue behaviour of continuous fibre reinforced glass ceramic matrix composites,
G West, A R Boccaccini and D M R Taplin, *Materielwissenschaft und Werksofftechnik 26, 368-73, (1995)*

Ceramic matrix composites; microstructure and thermostructural performance limits,
M H Lewis, A Tye, G West and M G Cain, *Presented at NATO Advanced Research Workshop, Kiev, Ukraine, June 2-6 1997*

Mechanical properties of silicate matrix SiC yarn reinforced composites,
D M R Taplin, G West, A R Boccaccini and M H Lewis, *ICF-9 in Advances in Fracture Research, Vol 2, Eds Karihaloo B L, Mai Y-W, Ripley M I and Rotchie R O, Pergamon (1997), pp1127-34*

Tensile behaviour and cyclic creep of of continuous fiber-reinforced glass matrix compoistes at room and elevated temperatures,
A R Boccaccini, G West, J Janczak, M H Lewis and H Kern, *Journal of Materials Engineering and Performance, Vol. 6, No 3, 1997, pp344-348*

KriechermYdungserscheinungen von faserverstSrkten Glaskeramikmatrix-Verbundwerkstoffen,
A R Boccaccini, G West, D M R Taplin and M H Lewis, *Werkstoffwoche '96, Stuttgart, 28-31 May 1996. (Poster presentation).*

Fracture behaviour and creep fatigue response of fibre reinforced glass-ceramic matrix composites,
A R Boccaccini, G West and D M R Taplin, *Physicochemical Mechanics of Materials, Vol. 32, 1, (1996), 81-90*

Environmental ageing effects in a silicon carbide fibre-reinforced glass ceramic matrix composite,
K P Plucknett, S Sutherland, A M Daniel, R L Cain, G West, D M R Taplin & M H Lewis, *J. of Microscopy, Vol. 177, Pt 3, March 1995, 251-263*

Continuous fibre reinforced glass ceramic matrix composites: microstructure, mechanical behaviour and environmental stability,
K P Plucknett, G West, D M R Taplin, A M Daniel, S Sutherland, R L Cain and M H Lewis, *In Proceedings of the Eighth Int. Conf. on Fracture (Advances in Fracture and Structural Integrity 1994), Kiev, Ukraine, June 1993. pp597*

Summary

A diverse range of microscopy techniques and mechanical testing methods have been used to characterize glass and glass-ceramic composites. The focus of the work has been a commercially available Barium Magnesium Aluminosilicate matrix reinforced by Tyranno SiC based yarn type fibres. The mechanical behaviour has been related to the microstructure through use of models from the literature. The temperature range of study has been from room temperature to 1300°C in air.

The microstructure of the BMAS/Tyranno was a diphasic mixture of celsian and indialite/cordierite although the manufacturers intention was a monophasic bariumosumilite. The carbon rich interface was found to be thin (10-15nm) but the composite displayed impressive strength when compared to similar glass-ceramic composites reported in the literature. The matrix could be converted to the equilibrium bariumosumilite phase by heating in an inert atmosphere at 1370°C (or possibly lower) but matrix elemental diffusion into the fibres is likely to impair fibre strength.

Tensile failure was by conventional matrix microcracking with load transfer to the in line fibres. However the composite strength was found to be dependent upon the strain rate as was the microcracking threshold associated with cracking of the 0° plies. Failure of the UD BMAS/Tyranno was by longitudinal splitting before the expected ultimate strength (from the 0,90° results) was reached. This was due to an apparent notch sensitivity in this fibre architecture, a trait not observed in the 2-D composite.

Direct measurement methods were used to establish the interfacial shear strength and these were compared to various models. These were based on matrix cracking thresholds, matrix crack spacing and a relatively new method where an 'inelastic strain index' was found from loading and unloading curves or hysteresis loop widths. Greatest fidelity with the direct methods was found with the last of these models.

As with all composites with carbon enriched interfaces oxidation of the interface and fibres was found to impair strength when tested in air at temperatures as low as 600°C and possibly below this when testing at lower strain rates. At high strain rates, near room-temperature-strengths were achieved, even at 1100°C, as the degrading effects of the oxidizing environment had less time to act. Long term exposure at high temperatures (1200°C) was responsible for formation of an embrittled surface layer up to 70μm thick. Within this layer the fibres were severely degraded and strong bonding prevailed at the interface.

At temperatures in excess of the expected fibre pyrolysis temperature, (1100°C), the composite was seen to shrink along the length of the fibre axis and dilate normal to it which was attributed to fibre instability. Stabilising the fibres by heat treatments at 1200°C for 24 hours was seen to improve the creep performance in terms of the total strain accumulated within the 100 hours of the creep tests. The creep was comparable to other commercial glass ceramics (CAS/Nicalon and BMAS/BN/SiC/Nicalon) indicating the dominance of fibre creep properties on those of the composite.

Cycling of the creep load seemed to result in a greater embrittled depth from the surface but failure at 100MPa and 1200°C was not observed within 240 hours of testing.

Other systems were investigated such as the CAS/Nicalon, MAS/Nicalon and AS/Nicalon. Of these the AS/Nicalon was used for modelling the creep behaviour since it represented a simple system where matrix creep was accompanied by elastic deformation of the fibres. A model from the literature was used to explain an apparent increase in the elastic modulus during load cycling at high temperature and also the lower strain accumulation seen during load cycling compared to conventional creep tests.

Contents

Abbreviations

τ	Interfacial Shear Stress
Γ	Debond Energy
ACK	Publication by Aveston Cooper and Kelly (see references)
ADR	Actuator Displacement Rate
AS	Aluminosilicate
BAS	Barium Aluminosilicate
BMAS	Barium Magnesium Aluminosilicate
BMC	Brittle Matrix Composite
CAS	Calcium Aluminosilicate
CMAS	Calcium Magnesium Aluminosilicate
CP	Cross Ply
CTE	Coefficient of Thermal Expansion
EDS	Electron Dispersive Spectroscopy
GMC	Glass Matrix Composite
GCMC	Glass-Ceramic Matrix Composite
ITM	Inverse Tangent Modulus
LAS	Lithium Aluminosilicate
LDE	Large Debond Energy
LFRC	Long Fibre Reinforced Composite
MAS	Magnesium Aluminosilicate
RT	Room Temperature
SDE	Small Debond Energy
SEM	Scanning Electron Microscope
TEM	Transmission Electron Microscope
UD	Unidirectional
XRD	X-Ray Diffraction

Chapter 1 Introduction

1.1 High Temperature Engineering Materials

It is the highest temperature applications that drive most of the current research into advanced structural ceramic materials as this is the area where the highest financial rewards would accrue. In this high temperature arena ceramics must compete directly with nickel based superalloys.

Particular applications have been identified which would maximise the potential of ceramic composites such as chemical processing equipment, where high temperature aggressive environments limit component longevity, or reciprocating parts for the mass produced car market where raising the engine's maximum temperature capability and reducing the reciprocating weight would respectively improve efficiency and maximum engine speeds. However one of the most difficult applications for these highly complex metal alloys is in the gas turbine engine where, as turbine blades, they perform at up to 80% of their melting temperature (for nickel based superalloys T_m~1250°C (Raj1993)).

The ideal efficiency of the gas turbine engine (η) is governed by the turbine entry temperature (TET, T_2):

$$\eta = 1 - \frac{T_1}{T_2} \tag{1.1}$$

where T_1 is the heat sink temperature. If the maximum turbine temperature can be increased by using materials with higher temperature capability, the overall efficiency improves. However the main advantage of incrementing T_2 comes from the power improvement which is a linear function of temperature. Clearly improvement in the power to weight ratio means either physically smaller engines can be employed or the possibility of greater payloads. In order to reach such temperatures, superalloy turbine blades rely on a constant supply of cooling air forced centrifugally through small holes on the surface of the blade. This air cushions the blade from the extreme temperatures of the combustion process but can form up to 12% of the total turbine airflow (Stohr 1993). This cooling impairs the overall efficiency but does not negate the benefits of increasing the overall temperature capability.

Operating at high temperatures means turbine blades must be resistant to creep,

oxidation, thermal fatigue and thermal shock. The implications of blade failure in jet engines imposes the further criterion of fracture toughness for dealing with broken compressor blades and bird strike debris. A possible specification could put a maximum stress of ~250MPa at take off and a limit of 0.1% creep over 30 hours at 850°C. Under such conditions grain boundary sliding and cavitation can be the limiting creep strength mechanisms. Two major developments have seen these mechanisms lessen in importance in turbine blades. In the 1950s the oxygen content was reduced by vacuum melting. The second development introduced in the 1970s reduced the amount of grain boundary perpendicular to the loading direction by the process of directional solidification. Columnar grains can be grown parallel to the applied stress. This reduces the driving force for grain boundary sliding to zero and lowers grain boundary cavitation. The logical conclusion to this method is blades consisting of only one grain. Thus the diffusional creep distances too are maximized.

Such developments have seen thrust to weight ratios more than treble from 3:1 to 10:1 and TETs increase from 800 to 1400°C from 1940 to the present day. Development of nickel based superalloys has reached a point where there is limited scope for further enhancement of maximum use temperature. It is hoped that ceramics will be able to replace superalloy blades directly and, in doing so, dispense with the extra cooling with an immediate impact on power and efficiency.

Use of more refractory metals with suitably low coefficients of thermal expansion (CTE) has been considered as an alternative to nickel based alloys but invariably candidates such as tantalum, molybdenum and tungsten suffer from poor oxidation resistance.

1.2 Ceramics

Ceramics have the highest temperature capability of the three material groups. Generically ceramics display good specific strength and stiffness to high temperatures, exhibit high tolerance to oxidative and corrosive environments, have low thermal expansion, are both thermal and electrical insulators and have wear and erosion resistance due to their high hardness. This favourable blend of properties has resulted in applications such as high temperature kiln equipment, furnace insulation and space shuttle thermal protection, (where refractoriness is the main property required), cutting tools and bearings, (high hardness), chemical plant, (resistance to aggressive

environments) and radomes, (low coefficient of thermal expansion). A material displaying all of these characteristics would seem ideal for most structural engineering applications. Ceramics, however, have a major failing: inherent brittleness which leads to a lack of reliability. This unreliability stems from the small size at which defects become critical. The ceramic under load may fail unpredictably. Other considerations lie in the processing of high temperature ceramics: their refractory nature necessitates high processing temperatures. Their hardness also makes it difficult and expensive to machine to the desired net shape as diamond grinding could be necessary. It is for these reasons of unreliability, lack of ductility, forming problems and the necessity for near net shape forming which has limited the development of industrial structural ceramics to date.

Strength predictions for glass based on σ_u=E/10 arguments suggest strengths of up to 10GPa. However such theoretical strengths are not approached in reality. It is the presence of flaws that limits the fracture strength. These flaws may be present as pores, surface scratches, isolated inclusions or other stress concentrating defects. The flaws may be pre-existing within the bulk of the material from manufacture or result from machining damage or even environmental attack. The small size at which these defects affect the ceramic's fracture strength means they are difficult to detect. Study of the effects of stress raisers such as defects and flaws has produced the discipline of fracture mechanics.

1.3 Fracture Mechanics

Under an applied load a material will deform elastically. Stress will concentrate at flaws. If the load is continuously increased a critical stress may be reached sufficient to propagate a crack from the critical flaw. If the energy used to create the new fracture surfaces is equivalent to or exceeds the elastic energy lost from the system the crack remains stable at its new length. If not, the elastically stored energy will provide the driving force for catastrophic failure. In metals the stress at a crack tip creates a plastic process zone, a consequence of which is a reduced elastic energy and a lower driving force for crack propagation, i.e. crack shielding occurs through plastic processes at the crack tip. A typical ceramic has no method of reducing the stress intensity at a crack tip so crack propagation can continue unabated under such conditions.

It was Inglis, (1913), who documented the stress concentrating effects around flaws

which were considered as elliptical holes:

$$\sigma_m = 2\sigma(a/r)^{1/2} \tag{1.2}$$

Where a and r are the crack length and crack tip radius respectively and σ_m the maximum stress at the crack tip. The smaller the value for r the greater the maximum stress at the crack tip. It was Griffith (1920) who related the fracture strength of the material (σ_f) to the flaw size (a), modulus of elasticity (E) and the surface fracture energy (γ). By energy balance arguments he found what has become the cornerstone of fracture mechanics:

$$\sigma_f = (2E\gamma/\pi a)^{1/2} \tag{1.3}$$

Irwin (1958), through work on the stress field at a crack front, defined a material property called the critical stress intensity factor (K_C), or K_{IC} for plane strain conditions, more usually called the fracture toughness. This is a measure of a materials resistance to fracture and is given in:

$$\sigma_f = K_{IC}/Ya^{1/2} \tag{1.4}$$

Where Y is a dimensionless constant dependent on loading and specimen geometry. For monolithic ceramics the fracture toughness can vary from 0.2MPa.m$^{1/2}$ for concrete up to 5MPa.m$^{1/2}$ for alumina and silicon nitride to 8MPa.m$^{1/2}$ for diphasic 'Syalon' (Lewis, 1989). Equations 1.2 to 1.4 show the importance of the length and acuity of a crack or flaw on the fracture strength. The size and distribution of flaws therefore has a statistical effect on the fracture stress and therefore dictates the maximum strength. This means large factors of safety (FOS) must be used whenever ceramics are used structurally. The magnitude of the FOS necessary can be assessed by statistical methods.

1.4 Weibull Statistics

Due to the inability of ceramics to relieve stress concentrations at flaws the strength of individual ceramic components can be highly variable depending on the size of the critical flaw. The size of a critical flaw in a low toughness ceramic (K_{IC} ~ 5MPa.m$^{1/2}$) can be difficult to detect as the threshold may be much lower than 100μm (Lewis 1989a). In order to quantify the reliability of ceramics, statistical methods can be employed. The most widely used method is Weibull statistics (Weibull, 1951). In this

approach it is assumed failure occurs at a critical flaw by weakest link theory. For ceramics the Weibull function can be expressed as:

$$f(\sigma)=\left(\frac{\sigma-\sigma_{\mu}}{\sigma_0}\right)^m \tag{1.5}$$

where σ_{μ} is the threshold stress below which no failure is expected, σ_0 is a parameter taken as the stress which represents a probability of failure of 63.2% and m is the Weibull modulus. Large m values represent narrow flaw distributions and small flaw sizes and hence low strength data scatter. The volume of a component stressed has a large effect on data scatter since a larger sampling volume is likely to experience a larger flaw population. When a volume dV is considered, the probability of failure (F) is found to be:

$$F = 1 - \exp\left[-\int_v \left(\frac{\sigma-\sigma_{\mu}}{\sigma_0}\right)\right]^m dV \tag{1.6}$$

The m value is a measure of reliability or predicted reliability. For different loading regimes the volume under consideration varies considerably. In uniaxial tensile loading the whole gauge section volume is considered, for other modes the effective volume is less.

Methods of improving the reliability of ceramics can therefore concentrate on two different approaches (Evans, 1990): reduce the quantity and size of flaws or somehow improve the ceramics fracture toughness. The former method relies on identifying the stages during processing at which flaws are introduced and eliminating them. Toughening methods will now be discussed as the material systems used within this work are based on this approach.

1.5 Toughening Methods

Toughening of ceramics is an approach which recognizes flaws are inherent and cannot be completely removed. A major failing of the flaw reduction approach to improving the fracture strength of ceramics comes from the possibility of post processing damage which can be introduced in final machining or in service. Toughening accepts such imperfections and permits a degree of damage tolerance.

To increase the fracture resistance of a brittle ceramic its flaw sensitivity must be reduced. This can be achieved by microstructural modifications, prestressing,

martensitic phase transformations and reinforcement with a second phase. These methods rely on preventing crack initiation or once developed, impeding crack propagation.

1.5.1 Transformation toughening

This method of toughening relies on the metastable phase transformation of tetragonal zirconia to the monoclinic equilibrium structure in the presence of a large elastic strain. The monoclinic phase has a less efficient atomic packing and so tries to assume a larger volume (~3% volume increase). The martensitic reaction therefore applies a closing force on the advancing crack. Toughening is therefore improved as the crack grows, this is referred to as rising resistance or R-curve behaviour (Evans, 1990). The tetragonal phase is retained within the structure by cooling from above the phase transformation temperature of 1150°C. The fracture toughness can be increased to ~10MPa.$m^{1/2}$. Toughening can be compromised with rising temperature as the driving force for the tetragonal phase conversion to monoclinic is reduced.

1.5.2 Pre-stressing

This method of improving the strength depends on reducing the tensile stress at likely crack initiation sites in a brittle solid thereby reducing the crack opening force when a load is applied. In this way a crack can only propagate from a flaw when a force large enough to overcome the compressive stress and reach the critical stress at the critical flaw is applied. The pre-stress can be achieved in several ways. For glass, surface prestressing by rapid quenching can be used where the surface cools more rapidly than the interior. Ion exchange can also be used to induce surface compression by substitution of larger ions at the glass surface.

Long fibres can also be used to compress ceramics as with concrete where steel rods are elastically stretched. The concrete is then poured around them and allowed to set. Releasing the fibre stress pulls the concrete matrix into compression.

1.5.3 Microstructural Modifications

In materials of the lowest fracture toughness (e.g. glass) the resistance to a propagating crack is minimal and fracture surfaces are planar. Impediment to an advancing crack can be provided by polycrystallinity which can force a crack to deflect and deviate by

the random grain orientation thus crack propagation requires greater energy. Further toughness enhancement can be provided by elongation of the grain structure.

1.5.4 Second Phase Reinforcement

Toughness increments can be achieved by inclusion of a second phase such as particles to form a composite. The shape and volume fraction of the particles greatly affects the degree of toughening. The degree of toughening generally follows the aspect ratio of the second phase with the maximum toughness supplied by long fibre reinforcement. The aspect ratio and reinforcement alignment determine how successfully a crack can be bridged and therefore the amount of force acting to close the crack. Crack bridging is not the only mechansim active when a second phase is incorporated. Microcrack toughening and crack deflection are also active but make small contributions compared to that of crack bridging. Spherical, platelet, rod, whisker and fibre reinforcement are all examples of this toughening method.

1.5.5 Long Fibre Reinforcement

Toughening by long fibres involves several different mechanisms. A propagating crack's progress can be impeded, or arrested, at the reinforcement or deflected at the interface. Bridging by the fibres in the crack wake may resist further extension. All of these mechanisms absorb energy so greater energy is necessary to cause failure. Further cracks will form leading to a microcracked matrix which in itself provides a degree of toughening. Intuitively the energy necessary to drive a number of cracks through a material is more than that needed to drive a single crack as more new surfaces are created. Ultimately, with increasing load, the bridging fibres fail and pull-out of the matrix and in doing so dissipate energy by frictional sliding.

Brittle matrices such as glass, glass-ceramic and ceramic matrices can be reinforced in this way to improve fracture toughness and strength. The important feature which governs the properties of such composites systems is the region between the fibre and the matrix. The interfacial bonding between the fibre and the matrix must be strong enough to transfer load yet weak enough to prevent crack propagation of the first crack through matrix and fibre.

The objective of this research is to understand the basic mechanics and fracture of long fibre reinforced glass and glass-ceramic composites (GMCs and GCMCs respectively)

over a wide range of loading conditions and temperatures. The applicability of the composite systems for critical engineering purposes is evaluated through the experimental work presented in chapters 3 to 6. A review of the pertinent literature is presented in Chapter 2. The mechanical testing methods and equipment are detailed in Chapter 3 the latter half of which is concerned with microstructural characterization of the composites investigated in the subsequent chapters. The microstructural characterization within Chapter 3 is utilised in chapter 4 to explain the results from room temperature (RT) property investigations in both flexural and tensile testing modes at varying testing speeds and loading configurations. These RT properties are then compared in Chapter 5 with the mechanical performance at temperatures from RT to 1200°C, which approximates to the melting point of nickel based superalloys. The effects of loading rate are also considered across the temperature range in air. The time dependent properties at high temperatures are studied in Chapter 6 by single and multiple loading (cyclic) creep tests for periods up to 240 hours. Attempts have been made to model some of these effects. The major findings of the current study are reviewed and conclusions drawn in Chapter 7 with possible avenues of future research identified.

Chapter 2 Review of Long Fibre-Reinforced Brittle Matrix Composites (BMCs)

Research into 'modern' glass and glass-ceramic composites is not a recently developed field, rather an extension of work into brittle matrix composites (BMCs) that can be traced back to work on fibre reinforced cements. One of the goals of current research into BMCs across the globe is the development of tough, environmentally inert, high temperature structural composites for use in advanced applications such as the aerospace market. Strength and stiffness increments, although welcome, are secondary desiderata to toughness.

Within this chapter the current work is placed within an historical perspective by review of pertinent areas of research which attempt to achieve this goal with glass and glass-ceramic matrix composites (GMC and GCMCs).

2.1 Glass and Glass-Ceramic Matrix Composites

Marked increases in the work of fracture (WoF) of several reinforced brittle matrices were achieved by Sampbell and Bowen (1972a,b). This was attributed to the effects of fibre pull-out. This early work on glass and glass-ceramic composite systems which incorporated carbon fibres in several matrices including glass, glass ceramic and ceramic matrices. Continuous reinforcement improved the flexural strength from less than 100MPa for the monolithic to 680MPa for the long-fibre reinforced Lithium Aluminosilicate (LAS) and borosilicate. However the oxidation of the carbon fibres above 400°C overshadowed the low temperature property improvements and precipitated a decline in research activity.

The renaissance of the early eighties was due to the development of a new silicon carbide yarn manufactured from a polycarbosilane precursor route by Yajima et al (1978). The yarn's greater oxidation resistance imparted a higher temperature potential.

The commercial availability of the Nippon Carbon Company produced Nicalon fibre was first capitilized on by Prewo and Brennan in a series of papers on GMCs (Prewo and Brennan, 1980 and 1982) and GCMCs (Brennan and Prewo, 1982).

The manufacture of composite tiles with the Nicalon fibres was first undertaken by

Prewo and Brennan (1980) who successfully managed to produce a unidirectional glass matrix composite which displayed impressive flexural strength and toughness at temperatures up to 700°C. The strength was limited by softening of the borosilicate matrix. This was sufficient to prove the potential of SiC yarn reinforced composites.

The manufacturing technique utilized a slurry infiltration processing route pioneered at UKAEA Harwell for production of carbon fibre composites (Sampbell and Bowen, 1972b). Manufacture began with desizing of the fibres by passing through a Bunsen flame. The yarn was then passed through a glass slurry (fig 2.1) which infiltrated the fibre tows. The slurry consisted of the matrix material finely powdered, a resin binder and solvent. The tows were dried on a drum. Plies were then cut from the dried tapes. The plies were stacked in a die for hot pressing. Densification was achieved by melting the glass and hot pressing. The processing of GCMCs was ostensibly the same but with a devitrification step, sometimes called 'ceraming', at an elevated temperature giving a highly crystalline matrix with as little as 4% residual glass phase.

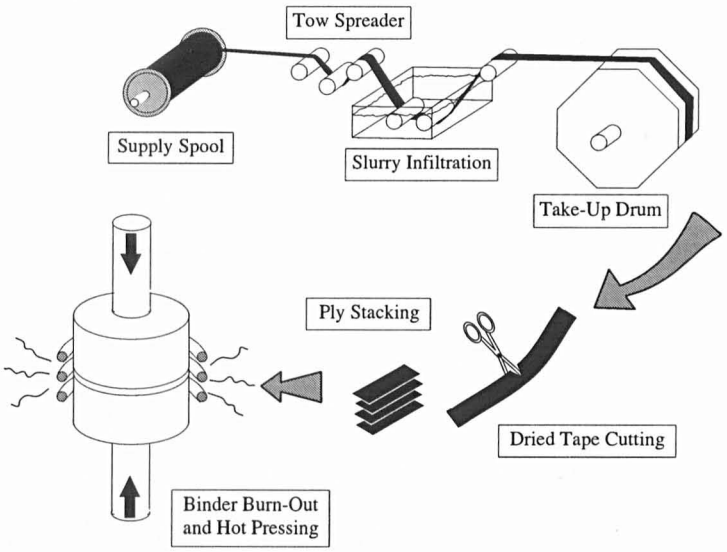

Figure 2.1 Schematic representation of hot pressing of slurry infiltrated fibre pre-forms

During fabrication a delicate balancing procedure is required to maximize the toughness potential through weak interface development, minimise the level of porosity and fibre degradation and control of matrix crystallization.

Different processing parameters can lead to great variations in the depth of the interface: Pippel (1993) observed a Tyranno/SiC composite with a ~10nm C-rich layer while Lewis and Murthy (1991) produced Nicalon/BAS with a 250nm Carbon interface. Lowden (1991) has shown the interface thickness is inversely proportional to τ in a Nicalon/SiC composite thereby demonstrating a potent method for controlling

composite mechanical behaviour through control of interfacial thickness.

The hot pressing pressure, temperature and time are critical to the composite properties. Temperatures above the glass liquidus enhance infiltration but may cause chemical damage and fibre grain growth. Conversely, selection of a low hot pressing temperature may lead to poor densification and mechanical damage of the fibre by hard glass particles. Crystallization of the matrix must then be controlled as unwanted phases may induce excessive residual stresses at the interface and matrix such as cristobalite in borosilicate glass (Murthy and Lewis, 1989). Stresses at the interface can lead to high values of debond and sliding resistance from high fibre clamping forces whilst within the matrix, microcracking and premature matrix failure can result.

Inevitably fibre damage cannot be avoided but processing can be optimized to minimize it. Prewo (1986) tested fibres before and after incorporation into a LAS matrix and found both the Weibull modulus and average strength (down from 2300 to 1500MPa) were compromised. Beyerle et al (1992a) measured fracture mirror radii of in-situ tested fibres and calculated the fibre bundle strength to be 0.42GPa against 1.8GPa for pristine fibres.

The Prewo and Brennan papers showed a borosilicate glass could be reinforced with Nicalon fibres giving a toughness approaching 20MPam^{½} (fibre strength ~ 2GPa). The flexural strength with temperature was only limited by the glass softening point. The delamination failure mode was indicative of a weak interface which they suggested was probably carbon on the fibres' surface. Oxidative stability of the composite was found to be excellent when exposed to air at 540°C (Prewo and Brennan, 1982). The temperature range was extended by use of a high silica matrix (Prewo and Brennan 1982) which displayed impressive flexural properties to 1200°C in air.

The availability of Lithium Aluminosilicate (LAS) GCMC developed jointly by United Technologies Research Center (UTRC) and Corning resulted in the SiC/LAS system becoming the focus of early mechanical (Brennan and Prewo, 1982; Mah et al 1985a,b; Stewart et al, 1987) and microstructural (e.g. Brennan, 1986; Chaim and Heuer, 1987) characterization studies. Patent applications at the time for LAS (Brennan et al, 1980) and BMAS (Brennan et al, 1984) suggested the possible application of GCMCs in gas turbines. More recently the Corning Calcium Aluminosilicate (CAS) system has received the greatest attention (e.g. Beyerle et al, 1992a,b; Walter and Ravichandran,

1995; Wang, 1992). Other glass ceramics based on the aluminosilicate system have been investigated but few have been available commercially. Such matrices include MAS, AS, CMAS, YMAS. A system made by AEA Harwell comprising the smaller diameter Tyranno SiC fibres and a Barium Magnesium Aluminosilicate matrix has been sold to several of the British Universities (Plymouth, Warwick, Queen Mary and Westfield College) and has been selected as the basis of the current work.

2.2 Fibres

Two fibres based on silicon carbide dominate the market for fibre reinforcement of GMC and GCMCs. These fibres are Nicalon (Si-C-O) and Tyranno (Si-Ti-C-O). Both of these fibres are produced by pyrolysis of polycarbosilane precursors to form very fine grained off-stoichiometric yarns with diameters of ~14μm and ~8.5μm respectively. Nicalon, produced by Yajima et al (1978) was the first to gain market penetration after becoming commercially available from 1979-80 under Nippon Carbon Company (Japan) production. UBE Industries (Japan) have subsequently introduced a rival fibre under the name Tyranno, first tested by Yamamura et al (1987 & 1988) and Fischbach et al (1988).

The two fibres are not drastically different: both have nominally SiC compositions. In fact the majority is SiC (49mol% for Nicalon) present as a nanometer scale dispersion of β-SiC crystals (~3nm for Nicalon but less for Tyranno in the as received state). Free carbon is present within the structure as ~1nm aggregates in Nicalon and surrounds the β-SiC crystals in several turbostratic layers in Tyranno (Bunsell et al, 1995). The remainder of the fibres is an amorphous phase consisting of mixed coordination tetrahedra (SiO_xC_{4-x}), (Lewis et al, 1993). Typical compositions of the fibres are presented in Table 2.1.

Table 2.1 Mechanical properties and chemical compositions of Nicalon and Tyranno fibres. Nicalon data from Ichikawa et al, 1995; Tyranno from Berger et al, 1996.

Properties	Nicalon NL-200	Hi-Nicalon	Hi-Nicalon 'S'	Tyranno Lox-M	Tyranno Lox-E
Diameter (μm)	14	14	12	8.5	11
Tensile Strength (GPa)	3	2.8	2.6	2.5	2.9
Elastic Modulus (GPa)	220	270	420	180	199
Failure Strain (%)	1.4	1.0	0.6	1.4	1.46
Density (g/cm)	2.55	2.74	3.1	2.4	n/a
Approx. Grain Size (nm)	2.2	5.4	10.9	<2	2
Chemical Composition					
Si wt%	56.6	62.4	68.9	57	55
C	31.7	37.1	30.9	28	38
O	11.7	0.5	0.2	13	5
Ti				2	2

The mechanical performance of Nicalon and Tyranno when tested as isolated fibres is presented in Table 2.1. These strengths and elastic moduli appear high but must be compared to stoichiometric SiC which has an elastic modulus in excess of 410GPa. The properties of both Nicalon and Tyranno are known to suffer in aerobic environments. Pysher et al, (1989), tested Nicalon and Tyranno in air and found the strength for both degraded above 800°C. Above this temperature the strength stabilized at approximately 1.5GPa for Nicalon and Tyranno up to 1200°C. Strength and stiffness rapidly decreased above this temperature. Ishikawa et al, (1987), studied the effects of thermal exposure in air at 800, 100, 1200 and 1400°C, the strengths when tested under room temperature conditions were not affected at 800°C for exposure durations of 10 hours or less. Exposure to 1000°C seemed to show a similar result with a minor drop of less than 200MPa over the same period. The thermal exposure results of Kim and Moorhead (1991) on Nicalon have shown degradation occurs at lower temperatures. Heat treatments at 800°C in air with room temperature tensile testing has shown a rapid strength degradation for the first 1 to 5 hours from ~2.8GPa to ~1.9GPa (average values). Mah et al, (1984), explained the fibre weakening due to the reaction of the free carbon within the fibre with oxygen. The escaping oxidation product (CO) was believed to leave a hole behind which, with ongoing oxidation, could form a deep notch and consequently lower fibre strength. The evolution of CO has been seen in inert atmospheres (e.g. Jia et al, 1993) where it was attributed to the decomposition of the amorphous silicon oxycarbide phase. Low oxygen partial pressures can also result in SiO formation. Grain growth at elevated temperatures has also been observed for both fibre types but is generally limited to 8nm or less in Tyranno (Berger et al, 1996), at the

temperatures investigated, by the Ti additions (Table 2.1). This phenomenon has been used to explain fibre shrinkage at high temperatures (1200°C and over) for Nicalon (Simon and Bunsell, 1984) and Tyranno (Bunsell et al, 1995) and also extended primary creep regimes during creep testing of individual fibres (Jia et al, 1993) and composites (Wu and Holmes, 1993). The grain growth is normally associated with temperatures in excess of 1000°C but Kim et al (1991) claim grain growth at temperatures as low as 700°C for long periods at temperature in Nicalon (164 hours) although similar findings are not available in the literature. The fibres also undergo a passive oxidation of the fibre surface which produces a silica layer the depth of which increases with time and temperatures as low as 700°C (Huger et al, 1993). The SiO_2 layer can protect the fibre from oxidation (Mah et al, 1984) but as the depth increases fibre embrittling may take place (Kim and Moorhead, 1991).

From the above it can be inferred the non-crystalline portion of these fibres controls the ultimate high temperature stability. The degree of non-crystallinity can be related to the oxygen content of the fibre implying greater stability can be imparted for compositions nearer to stoichiometric SiC. Recent developments of the Nicalon fibre have seen oxygen levels as low as 0.2 wt% for the new Hi-Nicalon 'S' due to a new electron beam irradiation method in an oxygen free atmosphere which prevents oxygen entering the fibre during the curing process (Okamura, 1987). The elastic modulus has been shown to increase dramatically with lower O content (Ichikawa et al 1995), see table 2.1. The fibre is not freely available yet but provides an exciting prospect for CMC and MMC development at high temperatures in the immediate future with its oxidation resistance to 1400°C and creep resistance to 1200°C (Ichikawa et al, 1995). Tyranno have also produced a fibre by a similar route but the introduction of titanium to the fibre in the polymer precursor state as titanium alkoxide accounts for most of the final oxygen content of ~5% (Berger et al, 1996). The lower oxygen fibres also have proven superior creep resistances over their original counterparts (Bunsell et al, 1995).

Several authors (Stewart et al, 1987; Murthy et al, 1989; Cooper and Chyung, 1987) have found oxidation to be more rapid for fibres in composite form. Processing into composite matrices also reduces fibre ultimate strength and Weibull modulus (Prewo, 1986). However the ultimate high temperature potential of the fibre seems to be increased by as much as 150°C in composites with uncracked matrices (Prewo et al, 1989; Fillipuzzi et al, 1994) due to low SiO and O partial pressures in the matrix

(Fillipuzzi et al, 1994).

The newest low oxygen fibres with their apparently superior properties, were not available at the initiation of this research. At the outset of this research programme composite manufacturers had selected the Nicalon 200 series or, to a lesser extent, the Tyranno LoxM fibres for composite reinforcement over the other fibres of Table 2.2 (Lewis, 1996). With greater availability of the recently developed low oxygen fibres, at reasonable cost, a new generation of GMCs, GCMCs and CMCs may become available.

Table 2.2 Fibre types suitable for GMC, GCMC and CMC applications

Type	Manufacturer	Constitution	Diameter (μm)	Modulus E (GPa)	Strength (GPa)
Nicalon SiC	Nippon Carbon Co. (Japan)	Si-O-C	10-20	180	2
Tyranno SiC	Ube Industries (Japan)	Si-O-C-Ti	10-20	175	2
HPZ	Dow Corning	Si-N-C-O	10-12	180-230	1.9-2.58
SiN Tonen	Tonen	Si-N	10	250	2.5
SiC (CVD) -SCS6	Textron	SiC	140	406	3.5
Saphikon Al O c-axis filament	Sapikon Inc.	Al_2O_3	70-250	380	3.1
Nextel 610	3M	αAl_2O_3 (99%) + Fe_2O_3, SiO_2	10-12	370	1.9

2.3 Monotonic Stress-Strain Behaviour

Brittle materials suffer catastrophic failure when an applied load is sufficient for crack initiation from a critical stress concentrating defect. In such materials propagation is largely unimpeded.

In 'tough' fibre reinforced brittle matrix composites (BMCs) an applied load extends the composite elastically. At some critical strain a matrix crack will form. In the presence of a 'weak' interface the crack can circumvent the fibres, deflect at the fibre/matrix interface, (Cook and Gordon, 1964) and leave fibres bridging the crack in its wake (Fig. 2.2).

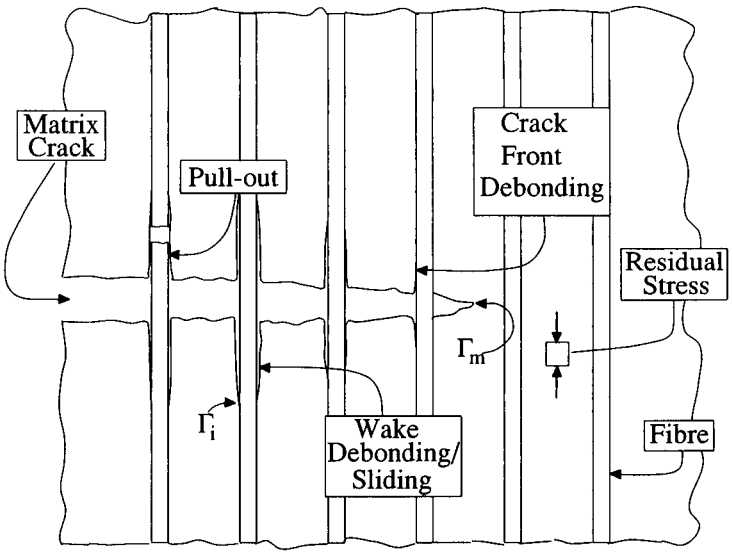

Figure 2.2 Toughening mechanisms in a tough BMC (After Evans and Zok, 1994)

The fibres provide bridging tractions which reduce the stress intensity at the crack tip. At the crack the fibres assume all of the load. The matrix stress recovers with distance from the crack faces within a characteristic slip length at a rate which is governed by the fibre/matrix interfacial shear stress (τ). In this manner further cracks may develop throughout the matrix. The cracks, which form perpendicular to the applied load when the fibres are aligned in the loading direction, reach a saturation spacing when the slip lengths overlap (Aveston et al, 1971). This microcracking introduces inelastic strains.

Once crack saturation has been achieved linear stress-strain behaviour may be reinstated but with a lower elastic modulus as the fibres assume the additional stress. Ultimately the fibres fail and, due to statistical flaw distributions, may fracture away from the final failure plane. Further toughening is provided as these broken fibres 'pull-out' of the blocks of matrix.

Thus various damage stages occur (fig 2.3):

I No damage, II Matrix cracking, III Fibre crack bridging and IV Fibre failure culminating in composite failure.

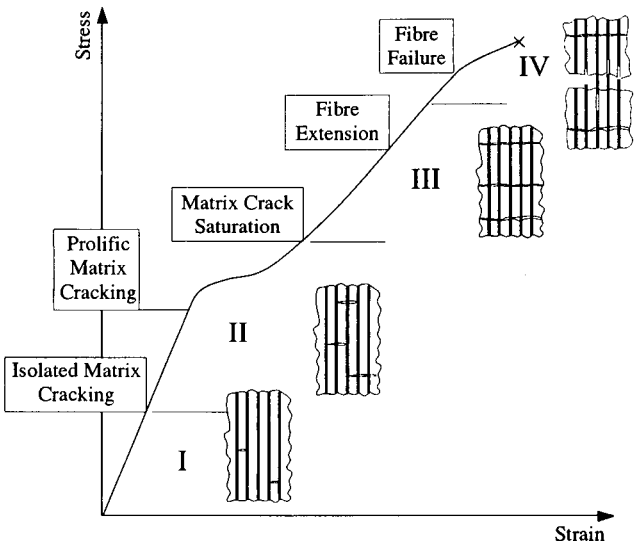

Figure 2.3 Schematic representation of composite damage evolution during tensile loading. Based on Holmes, 1995

2.3.1 UD BMCs

Stage I: Within stage I no significant damage is manifest on a stress strain plot but various authors have shown isolated cracking events occur in matrix rich regions which have little effect on the elastic modulus as the cracks do not span the specimen (Kim and Pagano, 1991; Zawada and Butkus, 1991). The elastic modulus at this stage is given by the Voigt model or rule of mixtures (ROM):

$$E_c = E_f V_f + E_m V_m \tag{2.1}$$

where the matrix volume fraction is: $V_m = (1-V_f)$, where (V_f) is the fibre volume fraction,

Stage II: The matrix microcracking initiation condition for BMCs (stage II :σ_{mc}) where the fibre failure strain is greater than the matrix is given by Aveston et al (1971) with an allowance for the matrix residual stress by Budiansky et al, (1986):

$$\frac{\sigma_{mc}}{E_c} = \left(\frac{6\tau\Gamma_m E_f V_f^2}{E_c E_m^2 R V_m}\right)^{1/3} - \frac{q}{E_m} \tag{2.2}$$

where τ is a unique value for the fibre/matrix interfacial shear stress, Γ_m the matrix fracture energy, R the fibre radius and q the residual axial matrix stress which may develop due to the high fabrication temperatures and thermal expansion mismatch between fibre and matrix which affects the cracking level. The matrix cracking level can be increased by increasing τ or decreasing R and q. An important implication is the prediction of enhanced failure stress and strain for the matrix.

The above equation has been verified by numerous studies but arbitrary selection of Γ_m and q can lead to disparities between different investigations (Beyerle et al, 1992a). The model provides a lower limit for multiple matrix microcracking which occurs over a range of stresses due to the distribution in the inherent matrix flaw sizes (Marshall et al, 1985, McCartney, 1987). Matrix cracking forms an important design parameter as it signifies the onset of irreversible damage (Zawada and Butkus, 1991).

Toughening of BMCs is highly dependent on the fracture toughness of the fibre/matrix interface (Γ_i). This places a limitation on the ACK model (2.2) which suggests τ can be increased indefinitely. However in the presence of a 'strong' interfacial bond, fibres are prone to rupture in the crack path. With a 'weak' interface fibre/matrix debonding occurs in the crack path. He and Hutchinson (1989) place the following limitation for debonding in the presence of a zero elastic mismatch:

$$\Gamma_i / \Gamma_f \lesssim 0.25 \qquad (2.3)$$

Where Γ_f represents the fibre fracture toughness, (fig 2.4).

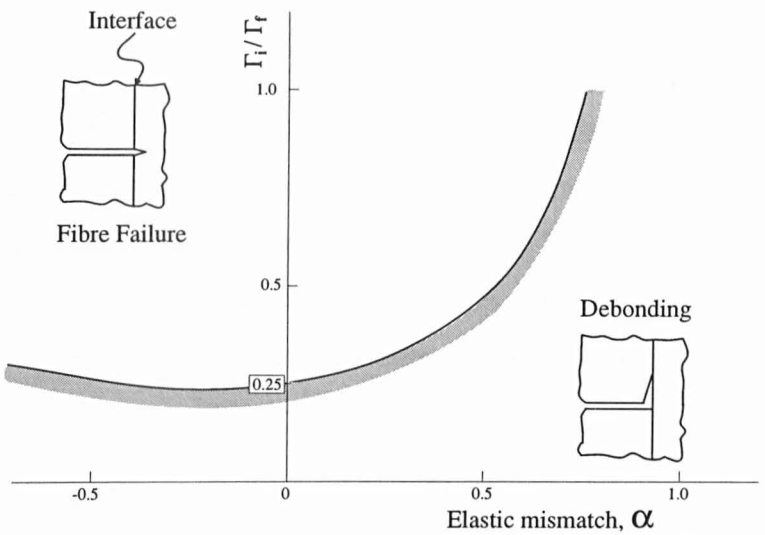

Figure 2.4 Interfacial fracture toughness requirements for debonding to occur. After He and Hutchinson, (1989)

Further debonding may also occur in the crack wake (Charalambides and Evans, 1989). The stability of the debonding stress is governed by the residual stress state at the interface. Unstable, extensive debonding can prevail when the interface is in tension, lower levels of debonding are indicative of residual compression (Evans and Marshall, 1989). The effects of interfacial sliding stress and matrix residual stress state are illustrated in figure 2.5.

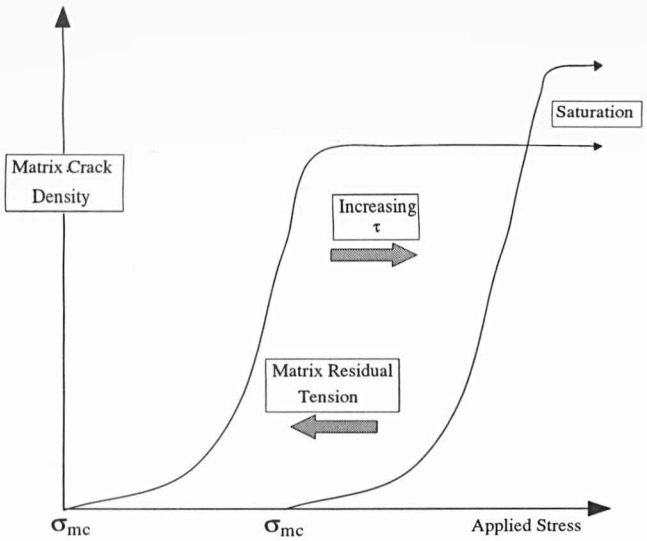

Figure 2.5 Effects of interfacial shear stress and matrix residual stress state on matrix cracking density and initiation stress after Beyerle et al (1992a)

Once the interface has debonded, the sliding resistance (τ) controls the load transfer from fibre back to the matrix (Aveston et al, 1971). To a first approximation τ is the product of the compressive stress at the interface and the coefficient of friction (μ), i.e. $F=\mu N$. With a sufficiently low value of τ, fibre failure is more likely to occur remote from the matrix crack plane. The fibre 'pull-out' of the matrix at failure was resisted by τ which adds a toughening contribution. Extensive 'pull-out' has been seen for several GMC (Prewo and Brennan, 1980) and GCMCs (Brennan and Prewo, 1982).

Matrix cracking continues until a saturation crack spacing develops when the slip lengths of neighbouring cracks overlap. The mean final crack spacing lies between one and two times the fibre to matrix load transfer length, x. This spacing therefore contains information on τ for small debond energy composites. Kimber and Keer (1982) give the mean final crack spacing as $1.3376 \times x$. Aveston et al (1971) calculated

$$x = \left(\frac{V_m}{V_f}\right)\frac{\sigma_{mu} r}{2\tau} \tag{2.4}$$

where σ_{mu} represents the unreinforced matrix failure stress.

Stage III: With saturation cracking of the matrix, load is accommodated by elastic extension of the fibres. Thus it may be predicted that for fibres slipping within the matrix 'blocks' the elastic modulus is simply the product of the fibre stiffness and fibre volume fraction ($E_c=V_fE_f$).

Various studies have shown the final tangent modulus is actually lower than this prediction (e.g. Spearing and Zok, 1993). Evans and Zok (1994) identify changes in τ

due to Poisson contraction of the fibres and fibre failures for the discrepancy.

Stage IV: Ultimately the fibres fail according to a statistical strength distribution. Global load sharing ensures the composite does not fail with the first fibre fracture as the matrix blocks distribute the load to intact fibres across the plane in which the fibre failed (Curtin, 1991, Davis et al, 1993). By this method the composite failure strain can actually exceed dry fibre bundle failure strains. Within a stress-strain plot the process of fibre failure can sometimes be seen as a reduction in the elastic modulus.

2.3.2 Cross Ply BMCs

For cross-ply laminates the stress-strain behaviour is similar but other damage stages are necessary to describe the complete failure behaviour.

Stage I described previously is terminated by transverse microcracking in the 90° plies by a tunnelling mechanism (Hutchinson and Suo, 1991). The applied stress at which cracking initiates depends on the residual stresses within the ply, the flaw sizes and distribution, matrix fracture toughness, fibre volume fraction and the ply thickness. The cracks form perpendicular to the applied load and reach a saturation crack spacing which is proportional to the ply thickness (Garrett and Bailey, 1977). These transverse cracks generally terminate at the 0° ply boundaries but may penetrate to several fibre depths (Wang, 1992).

At a second microcracking level, cracking in the 90° plies may extend into and across the 0° plies coincident with crack initiation within the aligned ply. After this threshold stress a comparison can be made between different fibre architectures by considering the fibre volume fraction in the loading orientation. For UD and 0,90° specimens which share the same volume fraction the 0,90° stress-strain behaviour (post 0° microcracking) can be approximated by multiplying the UD stress by one half (Evans and Zok, 1994).

2.4 Interfaces

Low debond and sliding stresses have been identified as prerequisites for 'graceful' failure behaviour. Such an interface can be provided in GMC and GCMCs reinforced with non-stoichiometric nanocrystalline Nicalon (Si-C-O) or Tyranno (Si-Ti-C-O) fibres by a fortuitous reaction between fibres and matrix (Brennan, 1986). Fibres can

also be coated prior to composite fabrication with C or BN with the same effect (e.g. Cain et al, 1993).

Prewo and Brennan (1980) suggested the delamination failure mode of a Nicalon reinforced borosilicate glass was due to a weak interface, probably carbon present on the surface of the nicalon fibres. Brennan (1986) identified an essentially amorphous, carbon rich interface and felt it was formed from the particular chemistry or microstructure of the fibres used. Brittle and tough composites were investigated: the carbon layer was absent in the weak, brittle composite. However, Cooper and Chyung (1987) claimed the cryptocrystalline interface formed depended on the reaction of oxygen with silicon carbide in addition to the excess carbon present in Nicalon fibre by the reaction:

$$SiC + O_2 \rightarrow SiO_2 + C \qquad (2.5)$$

or by Benson et al (1988):

$$SiC + 2CO \rightarrow SiO_2 + 3C \qquad (2.6)$$

Cooper and Chyung (1987) gave the silica concentration gradient as the driving force for the interface formation. The oxidation reaction of silicon carbide has also been shown to occur with pure silicon carbide whiskers in an alumina matrix (Lin et al, 1988) but not when a silica layer exists on the as received whisker surface (Schoenlein et al, 1988). Chaim and Heuer (1991) found an in-situ reacted carbon interface could also be formed in α-SiC and cordierite reaction couples. Thus reactions 2.1 and 2.2 could occur in stoichiometric SiC and non-stoichiometric silicon oxycarbides. However the kinetics of the two reactions were found to be enhanced for the off-stoichiometric fibres.

The carbon rich layer has also been identified as amorphous (eg Chaim and Heuer, 1987; Bischoff et al, 1989). Chaim and Heuer (1991) attributed the finding to different thermal histories as the variation could occur in ostensibly identical compositions by different manufacturers (Bonney and Cooper, 1990). Lewis et al, (1992), suggested low temperature fabrication (<1200°C) resulted in amorphous carbon interfaces and higher temperature hot pressing in graphitic interfaces. The depth of the in-situ reacted interface has been found to depend on fining agent additions (Brennan, 1986), the hot pressing temperature and the duration of hot pressing and the basicity of the matrix

(Cooper and Chyung, 1987): The matrix SiO_2 activity is determined by the basicity thereby dictating the SiO_2 concentration gradient and the interface reaction kinetics. Cooper and Chyung (1987) suggested the reaction rate of the interface formation was more rapid due to the excess carbon in Nicalon and Tyranno fibres.

During interface formation matrix elements may diffuse into the fibre catalysing the nucleation and growth of β-SiC. The diffusion band can be seen in TEM investigations (Murthy et al, 1989). Tyranno has been shown to develop a thinner carbon rich interface than Nicalon under identical processing conditions in a borosilicate matrix due to a lower level of free carbon and formation of TiC precipitates. In contrast the fibre diffusion band was much larger at 450nm v 250nm for the Nicalon fibre (Murthy et al, 1990) caused by Tyranno's greater disorder and higher oxygen content.

2.4.1 Interfacial Shear Stress Evaluation

Many ways have developed to either measure the interfacial shear stress directly or find it by inference from the mechanical behaviour of the composite.

Of the direct methods a fibre can be either pulled out of the matrix of a specially manufactured test-piece, pushed-in by an indentor or pushed-through with similar equipment. A recent method which may also be utilised in the near future involves measurement of fibre strain in the presence of a matrix crack and applied stress by Laser Raman Spectroscopy (Bollet et al, 1996).

The most widely used methods for direct measurement are the indentation techniques. Specimen preparation for push-in testing is the least laborious and does not require special fabrication, unlike fibre pull-out testing. For composites with weak interfaces the preparation of thin specimens for fibre push-though can also prove difficult. Fibre indentation was first employed by Marshall and Evans, (1985). Individual fibres are indented until fibre debonding and sliding are observed. The analysis for τ evaluation in the current study is taken from Marshall and Oliver, (1987), in which the slope of indent load (F) squared versus fibre displacement (u) provides a means for calculating the interfacial shear stress (τ) and the intercept provides the interface debond energy ($2\Gamma_i$) since:

$$u = \frac{F^2}{4\pi^2 R^3 E_f \tau} - \frac{2\Gamma_i}{\tau} \qquad (2.7)$$

Problems exist with this analysis since Poisson expansion of the fibre under load is likely to increase the apparent sliding and debond resistances. Also the analysis assumes shear cracking (mode II) at the interface whereas mixed mode (I and II) may prevail at the debond crack tip. The former problem is only evident for large debond energy composites and is not generally of concern for GMCs and GCMCs. The latter point will tend to underestimate Γ_i ,(Lewis, 1996).

Indirect methods where τ can be inferred from macroscopic mechanical behaviour include crack spacing measurements, matrix cracking stress, hysteresis loop widths, crack opening and pull-out lengths. Of the indirect methods calculation from matrix crack spacing (l) has proved the most popular using (Marshall and Evans, 1985):

$$l = \frac{\lambda R \sigma_{mc} V_m E_m}{2\tau V_f E_c} \tag{2.8}$$

Where σ_{mc} represents the nominal matrix crack initiation stress, λ is a universal numerical factor given by Kimber and Keer, (1982), as 1.3337 and the other symbols have their usual meanings.

Compared to the matrix crack spacing method measuring pull-out lengths can be laborious. As an alternative hysteresis loop widths have been the subject of a recent trilogy of papers from Santa Barbara and remain to be independently validated (see Chapter 4). However the accuracy of the indirect methods is dependent on the model initially but also unknowns such as values for the matrix fracture energy and the matrix residual stress as well as the individual moduli for the composite constituents.

2.4.2 Interface Stability

Flexural testing of GMC and GCMCs in vacuum or inert atmospheres showed composite strengths could be retained to temperatures as high as 1200°C (Brennan and Prewo, 1982). However an Achilles heel was discovered in the mid 80's by several research groups (Stewart et al, 1986; Prewo, 1983; Mah et al, 1985b). At temperatures in excess of 600°C in air a severe strength degradation was observed. Mah et al (1985) identified oxygen as the embrittling specie in Nicalon/LASII by varying the O content in an Ar-O mix. The minimum strength, which occurred at 900°C in air, was found to coincide with the matrix cracking stress at room temperature. It was postulated diffusion of oxygen was very fast and probably gained access to the fibre/matrix interface via the first matrix crack. This explained why the embrittlement only occurred

under load. Only one crack was observed in each specimen tested at high temperature in air. This contrasted with the parallel microcracks they had previously observed at room temperature (Mah et al 1985a).

Stewart et al (1986) reported similar findings for Nicalon/LASIII and also in Nicalon/ BMASIII. The rate of oxidation was probed by testing at two strain rates. No oxidation effects were apparent for Nicalon/LASIII at the faster rate. While the degradation was also less severe at the higher rate for the BMAS composite it did appear more susceptible to oxidation at the testing rates selected. The strength degradation was attributed to fibre oxidation rather than clamping between matrix and fibre.

Cooper and Chyung (1987) oxidized foils and found the carbon rich interface removed and replaced with a silica layer by the reaction:

$$SiC + O_2 \longrightarrow SiO_2 + C \qquad (2.9)$$

subsequent to the carbon removal (Pharaoh et al, 1993):

$$C + O_2 \rightarrow CO_2 \qquad (2.10)$$

The silica formed by this reaction strongly bonded the matrix to the fibre. At 900°C the reaction was noted within one minute. The ramifications are evident if equation 2.3 is considered: as Γ_i increases and Γ_f decreases it becomes increasingly unlikely the interface/fibre fracture toughness ratio can be sustained below 0.25. With the τ increments associated with SiO_2 formation the failure mode undergoes a transition from tough to brittle behaviour portrayed schematically in fig 2.6 where S_f is the fibre bundle failure stress. Heat treatments by Bischoff et al (1989) and Thouless et al, (1989) on LAS/Nicalon at 800°C showed silica formation at the interface was parabolic and filled the gap left by carbon removal within 16hours due to the 80% net volume increase associated with SiC oxidation. Huger et al, (1993), provide a means for estimating the time of closure of the annular ring left by carbon removal by evaluating the silica growth rate on as received Nicalon fibres from mass changes during oxidising heat treatments in air for temperatures from 700 to 1200°C. However Stewart et al (1986) and Cooper and Chyung (1987) noted the composite's fibre oxidation rate was far greater than that of as received Nicalon possibly due to the cross-diffusion of matrix elements during composite fabrication. Nicalon in turn suffers higher oxidation rates than pure SiC (Fillipuzzi et al, 1992).

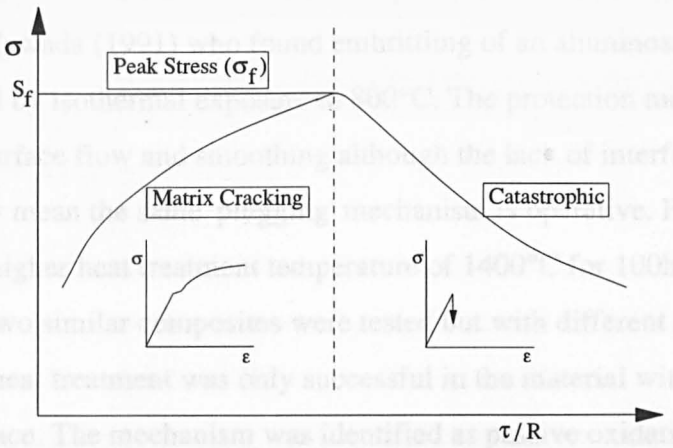

Figure 2.6 Schematic representation of composite property trends after Evans and Marshall, 1989

Pharaoh et al (1992) examined the effects of oxidation on τ by using Marshall's indentation technique for heat treated CAS/Nicalon. Three temperature regimes were identified. Below 500°C no effect was evident but at 500-800°C τ was found to be highly variable. Low τ values were related to carbon removal by 'piped' diffusion and high to silica bridging. At high temperatures a passivating plug was formed at exposed fibre surfaces thus preventing further oxygen ingress to the interface. Indentation showed that interfaces within the interior were similar to as received material. Interfaces within 30μm of the composite surface were found to suffer from oxygen diffusion through the matrix at very high temperatures (from 1200°C), (Fig.2.7; Lewis et al, 1993b). This slower rate of oxidation was expected to be more rapid for matrices with higher glassy content.

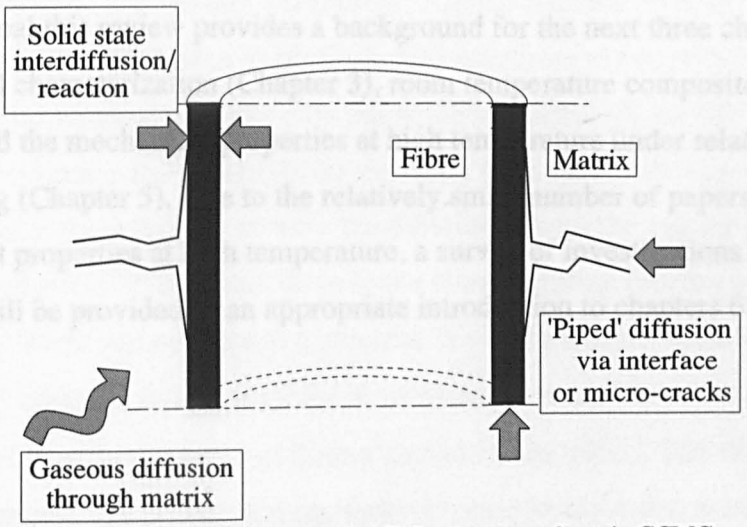

Figure 2.7 Oxidation pathways for Carbon rich interfaces in GCMCs (after Murthy et al, 1989)

Passivation 'plugging' of exposed fibre ends has been used as a heat treatment to prevent piped diffusion of the interface in BMAS/Tyranno at 1100°C (Plucknett et al,

1994 and 1995). Heat treatments have also been performed at lower temperatures, e.g. Wetherhold and Zawada (1991) who found embrittling of an aluminosilicate/Nicalon system was halted by isothermal exposure to 800°C. The protection mechanism was presumed to be surface flow and smoothing although the lack of interface microscopy could conceivably mean the same 'plugging' mechanism is operative. Frety et al (1992) have also used a higher heat treatment temperature of 1400°C for 100hours for a SiC/ SiC composite. Two similar composites were tested but with different interface thicknesses. The heat treatment was only successful in the material with the thinner carbon rich interface. The mechanism was identified as passive oxidation at the composite surface however the thicker interface could not be 'plugged' before gross interface degradation had occurred. Fillipuzzi et al (1994a,b) proposed a model for interface protection which calculated the rate at which the interfacial gap was closed by passive oxidation of the fibre and matrix (SiC) once carbon had been oxidized. The time necessary to close the pore entrance was found to be proportional to the pore size squared.

Surface sealing heat treatments enable high temperature investigations in aerobic environments but offer no protection once the matrix cracking threshold is exceeded. In such instances the mechanical behaviour becomes highly notch sensitive, i.e. matrix cracking and composite failure are concurrent (fig. 2.6).

The emphasis of the current work is to link the microstructure of GCMCs to the room temperature properties with special attention to high temperature mechanical behaviour. To fulfil this goal this review provides a background for the next three chapters on microstructural characterization (Chapter 3), room temperature composite properties (Chapter 4) and the mechanical properties at high temperature under relatively short duration testing (Chapter 5). Due to the relatively small number of papers published on time dependent properties at high temperature, a survey of investigations into creep and cyclic-creep will be provided as an appropriate introduction to chapters 6.

Chapter 3 Experimental Techniques and Materials Characterization

3.1 Composite Systems

Within the period of this work various material systems have been available. The original material supply was a unidirectionally Nicalon reinforced Magnesium Aluminosilicate (MAS) supplied by Pilkington. Unfortunately the "ceraming" stage of the processing was under pressureless conditions outside the die. During the heat treatment bloating of the plies occurred resulting in poor quality composite. Very little data will therefore be presented here due to the low reproducibility of its mechanical properties.

A Corning Calcium Aluminosilicate/Nicalon system was also available in limited supply. This has proved sufficient for flexure testing at various temperatures and indentation and push-through studies.

Towards the end of this study an aluminosilicate glass matrix/Nicalon composite supplied by Schott of Germany via Dr. Boccaccini has been tested in the tensile mode. The lower temperature capability of the matrix has proved useful for testing under temperature conditions where the fibres are elastic but the matrix creeps extensively.

The bulk of the results presented concentrate on the material supplied by AEA Technology, Harwell. The Barium Magnesium Aluminosilicate (BMAS) has Tyranno fibre reinforcement and has been available in UD and Cross ply (0,90°) lay-ups. Harwell have also supplied a matrix only tile of BMAS although, as will be shown later, the microstructure and phases differ markedly from that of the composite. Early supply problems were overcome as were the difficulties with the quality of the product. Reinstatement of a binder 'burn-out' stage to the manufacturing process has reduced matrix porosity levels and resulted in composite Weibull modulus values as high as 19.8. Table 3.1 contains details of all the most recent tiles used in this work (Information from AEA Harwell and Sutherland and Cain, 1995). The Weibull moduli, flexural strength and standard deviations were obtained from 4 point bend testing of at least 20 specimens. The fibre volume fractions (V_f) were supplied by the manufacturers. These values were calculated from the weight of the matrix powder and fibres used to manufacture each tile and have been independently verified by the

Leuven partner of BRITE programme BE-4610. The original BMAS/Tyranno (designated 'OBM' from now on) was of a broadly acceptable standard, quality then deteriorated for the processing reasons described above. The tiles from 'NPP5' and onwards have been the most consistent and have shown the best mechanical properties. Therefore three BMAS/Tyranno designations exist: Original (OBM), very poor quality (BNB1) and the most recent high quality tiles (NPP5 to 20). The composite was made via the slurry infiltration route and is purported to be hot pressed at 950°C and crystallized to bariumosumilite ($BaMg_2Al_6Si_9O_{30}$) at 1350°C for three hours, (Churchman-Davies, 1996).

Table 3.1 Quality assessment of AEA Harwell supplied BMAS/Tyranno

Tile	Fibre Architecture	Flexural Strength (MPa)	Std. Dev. (MPa)	Weibull Modulus	V_f (%)
NPP5	CP	649	64	10.7	~41.0
NPP7	CP	711	103	7.5	38.8
NPP10	CP	731	54	15.4	35.7
NPP11	CP	704	60	13.4	39.1
NPP12	UD	1231	118	11.5	38.9
NPP14	UD	991	103	8.0	34.0
NPP17	UD	1180	82	16.2	33.0
NPP18	UD	1284	63	19.8	35.0

3.2 Mechanical Testing Techniques

The preferred manufacturing route for the composites tested here is by the hot pressing of pre-impregnated plies. This manufacturing technique does not lend itself to the production of intricate shapes. For this reason the product was supplied in plate form generally less than 3.5mm thick. Two sizes of plate were supplied, nominally 100x100x3.5mm and 220x220x2.5mm.

3.2.1 Mechanical Test Specimen Preparation

Samples for testing in flexure and tension testing were cut from the plates by different methods. The simple shape of flexural test bars (nominally 3x3x50mm) could be cut by several passes of a grinding wheel on a surface grinder (Jones & Shipman, 1400 model). Each pass of the table past the wheel removed 0.0007" (~18μm) to avoid damage to the specimens. Once cut the mounting wax was removed by ultrasonic

cleaning in a heated methanol bath. The specimens were tested in the 'as cut' state.

The selected shape (fig 3.1) of the tensile specimens required CNC machining. The cutting was by a single pass of a diamond tipped tool bit mounted in a pneumatic high speed spindle head on the Beaver NC5 145 CNC machine.

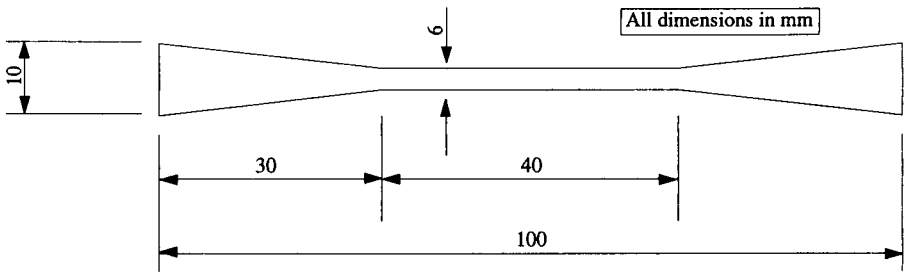

Figure 3.1 Schematic diagram of the tensile test geometry used within this programme

3.2.2 Flexural Testing

The testing of composites in flexure is subject to many inherent errors. Lewis et al (1985) point out the failure mode (compression, tensile or shear) of a flexure specimen is highly dependent upon the loading configuration and specimen dimensions. A minimum specimen span to depth ratio has been stipulated by many authors in order to accentuate tensile failure (Lewis et al, 1985; Davidge and Davies, 1988; Larsen et al, 1985) ranging from 20 to 32 for four bend loading. Even if this caveat is addressed the final failure stress is not representative of an ultimate strength, as measured through a tensile test. Calculations for composite stress are taken from linear elastic equations and provide a value for the maximum tensile and compressive stresses on the outer faces of the test piece. With a damage mechanism such as matrix cracking the beam's neutral axis is able to shift towards the compressive side of the beam invalidating the stress calculations. This is exemplified by Evans and Marshall, (1985), who show matrix crack arrest at approximately the mid plane of a LAS/Nicalon specimen. Despite these shortcomings, the ease of testing and the economical use of material have ensured the bend test is widely used as a research tool. The values presented here for the flexural strength are up to twice as high as the tensile properties on the same material, see for example Sutherland et al, (1995). However the results have followed the same trends such as oxidation embrittlement at elevated temperatures and greater degree of strength retention at the highest test temperatures as well as elastic moduli variations. Therefore flexural strength tests do not be provide absolute values but the method has merit as a research tool for demonstrating property trends.

The flexural facility was supplied by Instron (High Wycombe) as a 'High Temperature Ceramics Testing System'. The long split furnace was manufactured by Severn Furnaces Ltd (Bristol) and heated by six molybdenum disilicide elements. The flexure testing jig (Fig 3.2) had four pins, three of which rested on articulated rollers and the fourth rested on a rectangular section block and provided the alignment datum for the other articulated pins. The upper and lower jigs which held the pins and rollers had fixed spans of 20 and 40mm (upper and lower respectively). All of the components of the flexure jig were made from silicon carbide. Long alumina rods supported the fixture. The upper rod was solid and contacted the jig by a roller so as not to induce unwanted bend or torsion in the specimen. The lower rod was hollow. Deflection at the centre of the specimen was measured by an LVDT with ±1mm of travel which contacted the specimen through a hole in the bend jig and the hollow lower support rod. The location and remoteness of the LVDT ensured it was not affected by the test temperature. At the base of the rod a thumbwheel permitted precise adjustment of the transducer zero point.

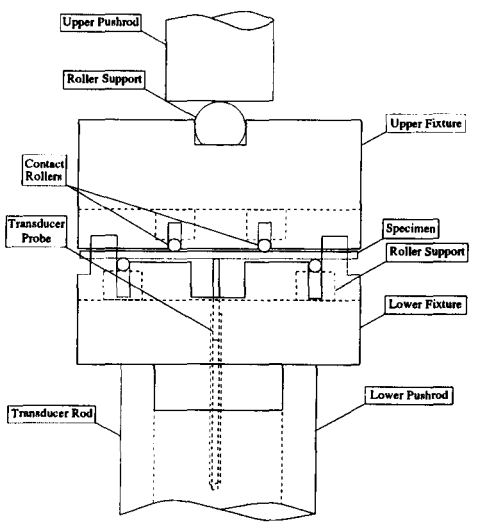

Figure 3.2 Schematic diagram of high temperature flexural testing facility

The rods were mounted on water cooled alignment rings and extra cooling for the 10kN load cell was provided by a heat shield above the furnace. The flexure testing equipment was mounted inside the load frame of a servohydraulic Instron 8501. This provided the ability to control in either position or load modes from the Instron console. For high temperature work the temperature was ramped at a maximum rate of 15°C/ min. The temperature was allowed to equilibrate for 15 minutes before testing commenced.

Logging of the outputs from the Instron was by an Archimedes A5000 computer with

an ADC/DAC podule capable of logging ±10V at up to 10kHz supplied by SiPlan Electronics Research (Stratford-upon-Avon). "Basic" programs supplied by SiPlan were modified and tailored for the logging task with various sampling rates used from several hundred data points per second when strain rate testing at the highest rates to one point every two second for long term testing. The data from such tests were analysed for discrepancies and 'pruned' down for reasonable file sizes for graphical presentation.

Monotonic loading in bend was at an actuator displacement rate of 0.5mm/min. For strain rate testing this rate was changed to a maximum of 100mm/min and a minimum of 0.001mm/min. For creep and cyclic creep testing load control was used for ramping to the selected load.

3.2.3 Tensile Testing

Testing in the tensile mode at Warwick on the Instron 1185 ball-screw driven universal testing machine has proved problematic. Electrical noise and temperature fluctuations within the room and water cooling and temperature instability of the extensometer due to proximity of the furnace have all had to be overcome or minimised before meaningful results could be attained. The laboratory heating switched off at 2000hrs and on again at 0730hrs, these times were previously obvious in the long duration creep curves. This time scale does not affect short term testing but can lead to erroneous data during a typical creep test. To overcome such temperature differentials over the course of a test a lower capacity load cell was purchased (10kN as opposed to 100kN) as the drift specified by the manufacturers was quoted as a maximum temperature sensitivity of ±0.001%/°C of the load cell capacity. The extensometer was enclosed in a temperature controlled box and the aluminium vertical bar on which the extensometer is mounted was drilled centrally to allow water cooling to maintain it at a constant temperature. Water was supplied at a constant pressure to the pull-rod cooling collets, the alignment rings, extensometer and extensometer heat shield and mounting bar in series. The water was heated from the mains to the chosen temperature. The load cell was therefore maintained at a constant temperature as it was directly connected to the alignment rings.

The extensometer proved susceptible to electrical noise and it was necessary to supply a highly stabilised excitation voltage and ensure isolation from the Instron load frame.

The electrical ground was therefore supplied by the computer via the logging podule. The specially built strain gauge amplifier (RS 435-692) was chosen for its temperature stability and low noise. The extensometer (model no. 632.59C-01) was supplied by MTS (Minneapolis, USA). The gauge length was set at 25mm and the gain on the strain gauge amplifier was set to give a ±10V output for ±0.5mm extension giving a maximum measurable strain approaching 4%. The rods contacted the specimen as chisel edges. Positioning on the specimen was maintained by a contact load of 100g per rod. This force induced a bending moment in the specimen. The side the rods contact experienced a compressive stress and similarly a tensile stress in the oppposite side.

The specimen geometry was based on a design by Holmes (1992). The specimens' widths have been varied during the test: to reduce the bending stress imposed by the contact extensometer thicker gauge widths were used generally for high temperature testing. This was a particular problem for the aluminosilicate/Nicalon composite which could viscously deform under such transverse loads at the upper testing temperatures. For room temperature testing of UD materials it was necessary to use a thinner section to prevent shear failure of the gripped ends. The pull rods were CNC machined from a mechanically alloyed steel designated MA956. The pull-rods were located outside the furnace hot zone but the 'warm gripping' precluded the use of normal steel alloy. The gripping arrangement and tensile test apparatus can be viewed in figure 3.3.

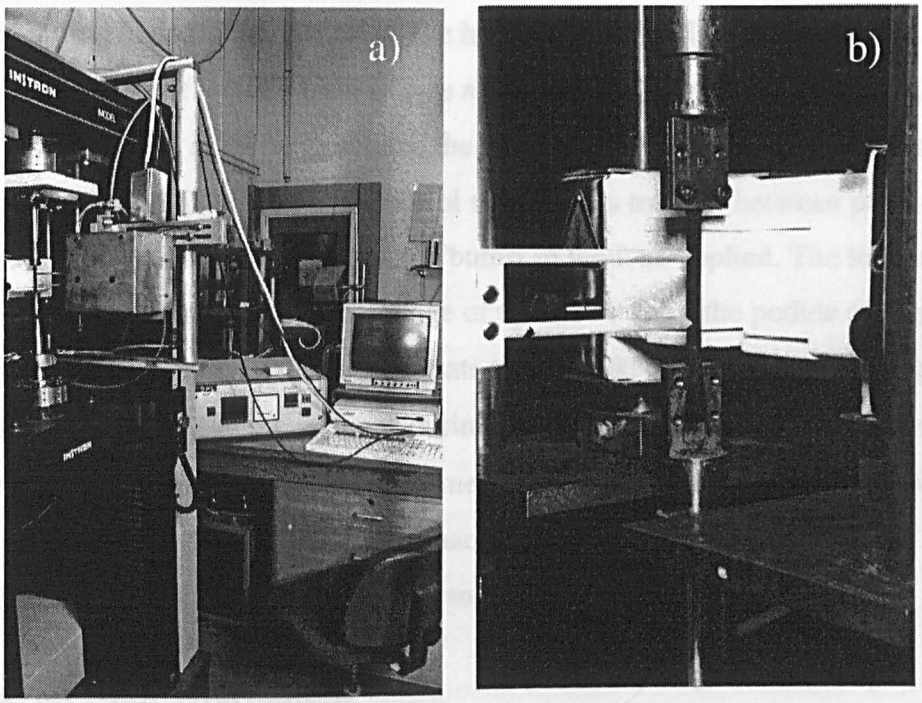

Figure 3.3 Photographs of tensile testing facility. a) logging equipment, furnace controller extensometer within heat shield and Instron universal testing machine
b) close up of sample and gripping method

The alignment of the pull-rods was crucial for eliminating bending strains from the gripping and thus ensuring failure within the gauge length. Once the angle of the rods was set, they were locked into place in the alignment rings. The rings then permitted adjustment of up to 2mm for a 1m length in any direction. A dial gauge was used to position the rods accurately. Once a specimen had been loaded the wedge shape of the sample lodged in the grips. To remove the broken specimen a lateral force was applied by a grub screw. In this way alignment of the rods was maintained and the specimen gauge length was not damaged. The rods were oriented so the extensometer contacted the side face of a specimen thereby minimising the stress on the composite outer faces since the stress was inversely proportional to the square of the depth. To exploit this further, specimens were machined with wider gauge sections (5mm as opposed to ~3mm).

Testing at high temperatures in air was possible using the Severn Furnaces Ltd. (Bristol) 1500°C single zone short furnace (MDS 1060). The hot zone was limited to 40mm. It was necessary to design and manufacture a sliding assembly to enable the furnace to be located after the tensile specimen was mounted. With the furnace positioned additional insulation was placed to close the gaps between the pull-rods and the furnace insulation. The extensometer then slid into position and the gauge length was set by positioning the rods individually until they were perpendicular to the specimen. Due to expansion during heating a minimal load (20N) was applied and maintained during temperature ramping. The heating rate for all tests in the tensile mode was 20°C/min. At least 30minutes was allowed for the temperature to equilibrate. For basic tensile testing at all temperatures the cross head speed was controlled at a rate of 0.2mm/min. For cyclic testing load control was used as transfer between position and load control involved a significant transient 'bump' in the load applied. The loading ramp was supplied to the Instron as a voltage of up to 10V from the podule card in the A310 Archimedes computer. This could equate to 1 or 10kN depending on settings chosen on the Instron. If failure occurred during a long term test the cross head would continue trying to apply the load. The outcome of this was that the specimen in the lower pull rod would descend out of the furnace until the lower travel limit was reached. During all tests the extension, load and time data were gathered.

3.3 Material Characterization

Various techniques have been used to characterize the as received composites. The

remainder of this chapter details the techniques used, reports the findings and concludes with a discussion of the results.

3.3.1 Electron Microscopy (SEM & TEM)

Microstructures have been investigated by scanning electron microscopy (SEM) using a JEOL 6100 with Link Oxford ISIS analytical equipment. Three window configurations were possible: Be, thin and windowless. The backscattered electron detector was manufactured by KE. The SEM was used due to the limitations of resolution and depth of field of reflected light microscopy.

Initial observations of the composites were made by Scanning Electron Microscopy (SEM). Sample preparation was critical to ensure the microscopy observations were real and not artefacts of the grinding and polishing operations. The specimens were mounted in bakelite in an automatic mounting press (Beuhler, Metaserv). Grinding to ensure a planar surface could remove the weakly bonded fibres at the surface especially in longitudinal sections. Due to this damage it was necessary to use the less harsh grinding wheels (maximum of 25μm). Silicon Carbide paper (1200 grit) was also used when preparing samples manually and for single specimen preparation. Two polishing stages of 6 and 1μm diamond on napped cloth were used prior to the final stage with colloidal silica on softer napped cloth. These stages could be manual or automatic on the Motopol 12 (Beuhler Metaserv) automatic polisher. Fracture faces of tensile and flexural tests could also be observed by mounting them on stubs or in a sample holder specially made to house several broken samples at once. To prevent charging by the build up of electrons on the non-conductive specimen surface all specimens had to be coated with a thin conducting layer of carbon or gold before examination.

The transmission electron microscope (TEM) used was a JEOL 2000FX. The preparation of thin foils for TEM was a more laborious process than sample preparation for SEM. Thin slices of composite 3mm in diameter and 250μm thick were cut using an annular saw 0.25mm thick (Capco). This slicing introduced very little damage when observed under an optical microscope. Several slices were mounted on a single brass stub with melted modelling wax. These slices were then thinned on 1200 grit paper by hand and polished as above to a 1μm finish on the exposed side. A scalpel was then used to cut the wax away. Copper apertures were then glued to the polished surface with a two part thermosetting glue. Further thinning of the central section was produced

using a 'dimpling' machine (South Bay Technology model 515). Diamond paste (6 and 1μm) was applied to the dimpling wheel to thin the central region to less than 60μm. The final stage thinned the central region until a small perforation was formed in the centre of the foil. The process was by ion beam thinning in an Ion Tech Ltd. 700 series thinner. The perforation ensured an electron transparent area was created around the hole, suitable for microscopy.

BMAS/Tyranno

Low magnification images of cross ply and UD BMAS/Tyranno specimens (tiles NPP5 & 18) (Fig 3.4) revealed several points of note: small levels of porosity were evident, the fibres were concentrated in bundles and, correspondingly, matrix rich regions existed generally between the fibre bundles.

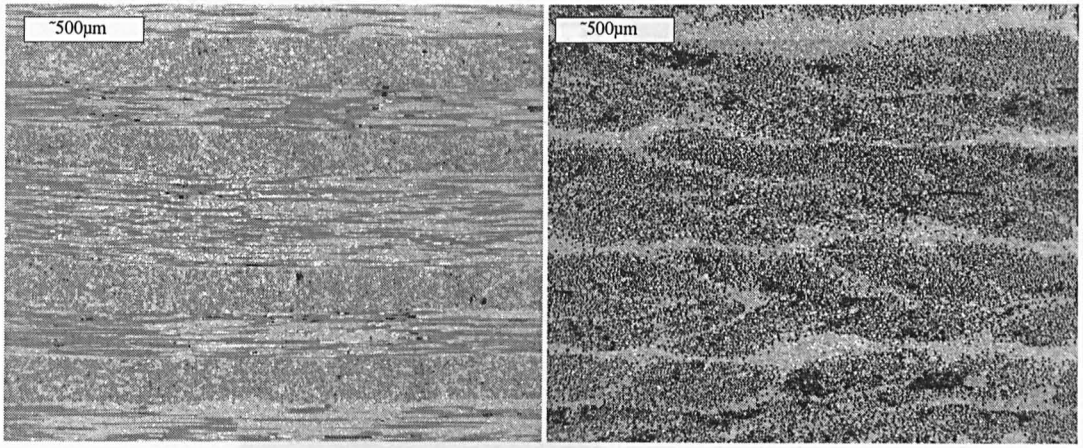

Figure 3.4 Low magnification images of 0,90° and UD BMAS/Tyranno (Transverse section)

Higher magnification images displayed two major phases of light and dark contrast in BSE mode (Fig 3.5). The light phase was surrounded by an interconnected network of the darker phase. The back scattered electron (BSE) images suggested a large atomic number difference between the two. Minor quantities of a third discrete phase were also apparent. EDX analysis within the SEM of the phases present has shown the lighter contrast phase contains Ba, Al, Si and O (inset fig 3.5). The darker phase contains Mg but has no Ba. The small grain size of the BMAS matrix meant EDX analysis had to be conducted with care to avoid penetration of the beam into surrounding or underlying grains of a different phase. The excitation depth for a matrix of this density and 15kV operating voltage on the SEM was approximately 1μm so only the larger sized grains could be analysed. EDX of the fibre shows the silicon oxycarbide constitution. The small titanium content was also evident (insert, fig 3.5)

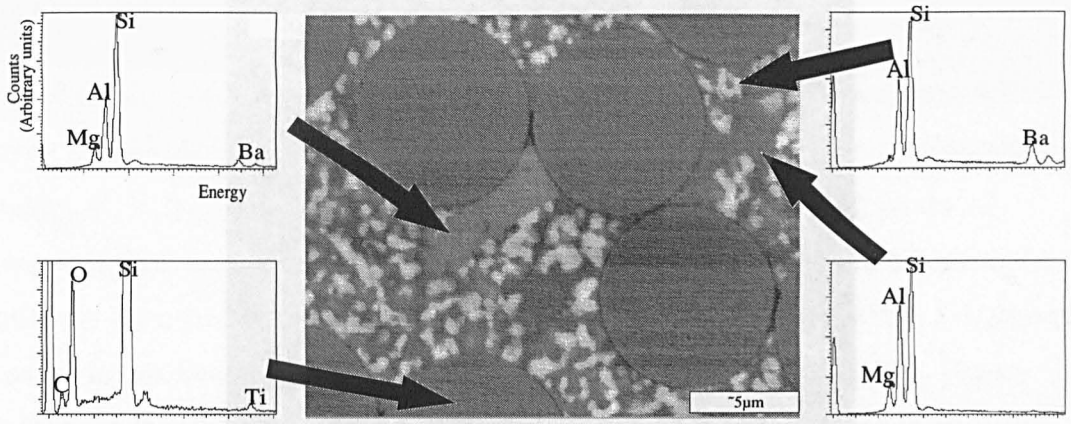

Figure 3.5 BSE image of BMAS/Tyranno ('NPP') showing the composition of the phases present and that of the fibre interior

The higher magnifications possible in the TEM revealed the matrix (tile NPP18) contained only two identifiable phases. However it was also possible to determine small quantities of residual glass at triple points.

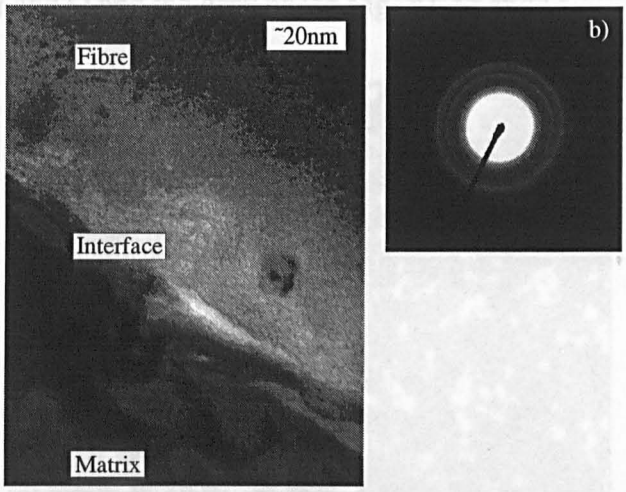

Figure 3.6 TEM image of interfacial region in BMAS/Tyranno

Selected area diffraction (SAD) patterns taken from the interior of the fibre showed diffuse rings indicative of β-SiC (insert b, fig 3.6). Within the fibre a structure could be seen which seemed to compare with the grain size of <3nm reported by Berger et al (1996). Toward the periphery of the Tyranno fibres there was a more electron transparent region in the form of a continuous band of approximately 30-50nm (fig 3.6). This zone has been shown to contain matrix elements which have diffused into the fibre during processing. This band ended at the fibre/matrix interface where a carbon rich layer was observed. SAD of this thin (~10-15nm) interface has shown the carbon was cryptocrystalline graphite (Plucknett et al, 1994, 1995).

The earlier BMAS/Tyranno appears similar to the NPP tiles (fig 3.7) but a third mid contrast phase is evident. This phase has been shown to contain Ba, Mg, Al Si and O.

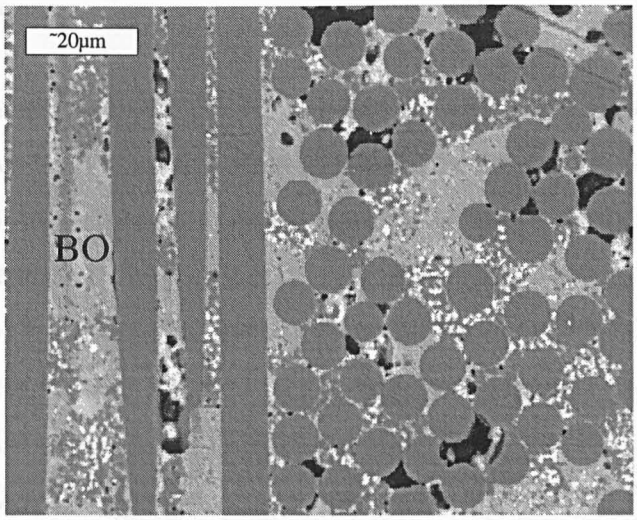

Figure 3.7 Micrograph showing how bariumosumilite (mid-grey phase) is accommodated in matrix of 'OBM' BMAS/Tyranno. Light and dark phases are celsian and cordierite respectively

The matrix only tiles showed three phases (fig 3.8). A major phase of mid grey contrast in the SEM has been shown to contain Ba, Mg, Al, Si and O, the light contrast phase contained Ba, Al, Si and O and the dark phase Mg, Al, Si and O.

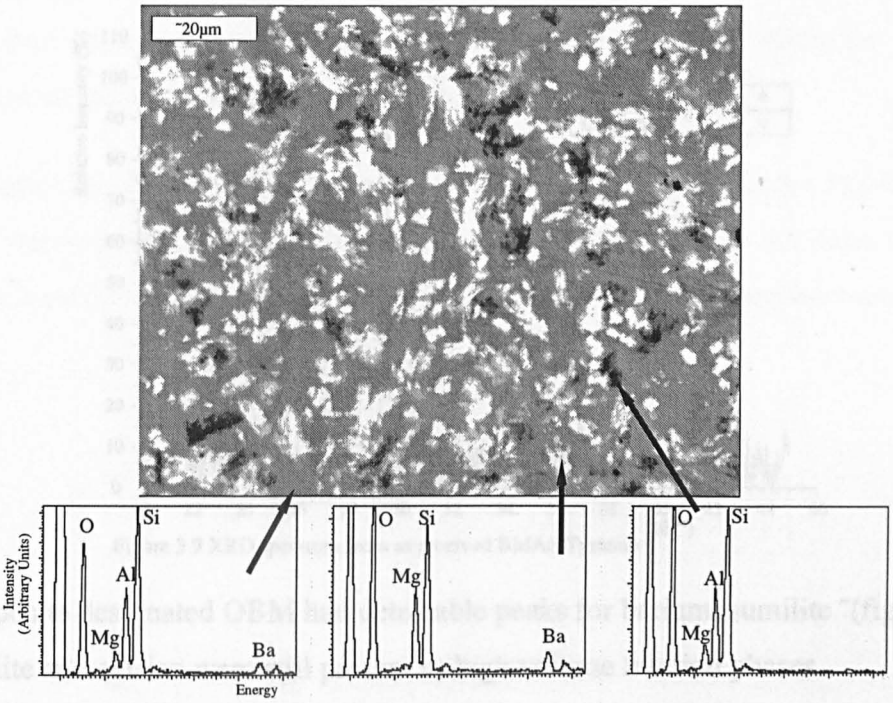

Figure 3.8 BMAS matrix material with EDX spectra for each phase

3.3.2 X-Ray Diffraction (XRD)

XRD studies on BMAS/Tyranno have been carried out to identify the crystalline phases present within the matrix. The equipment used was a Phillips PW 1130/00 and data capture was via an Archimedes personal computer. The data, though showing high noise levels, have not been averaged. Part of the reason for the poor signal to noise ratio is the limited amount of matrix material which is available to the incident X-Ray beam

due to obstruction by the near amorphous fibres.

Crystal phases present within the $BaO\text{-}MgO\text{-}Al_2O_3\text{-}SiO_2$ (BMAS) based composite matrix (fig 3.9) have been identified from X-ray diffraction traces. Bariumosumilite ($BaMg_2Al_6Si_9O_{30}$), was expected to be the main phase in the Harwell produced composite from the manufacturers assertions. However bariumosumilite could not be positively identified from the XRD spectra taken for the later tiles NPP5-18. It proved possible to positively identify the $BaO\text{-}Al_2O_3\text{-}SiO_2$ and $MgO\text{-}Al_2O_3\text{-}SiO_2$ phases observed in the SEM and TEM by EDX as indialite (hexagonal $Mg_2Al_4Si_5O_{18}$) and celsian ($BaAl_2Si_2O_8$). The small residual glass content was evident from the raised background at low 2θ angles synonymous with an amorphous phase. The occasional $Al_2O_3\text{-}SiO_2$ containing grains as seen by EDX in the SEM could not be discerned from the XRD spectrum implying either the quantities were too small to register or the phase was an aluminosilicate glass.

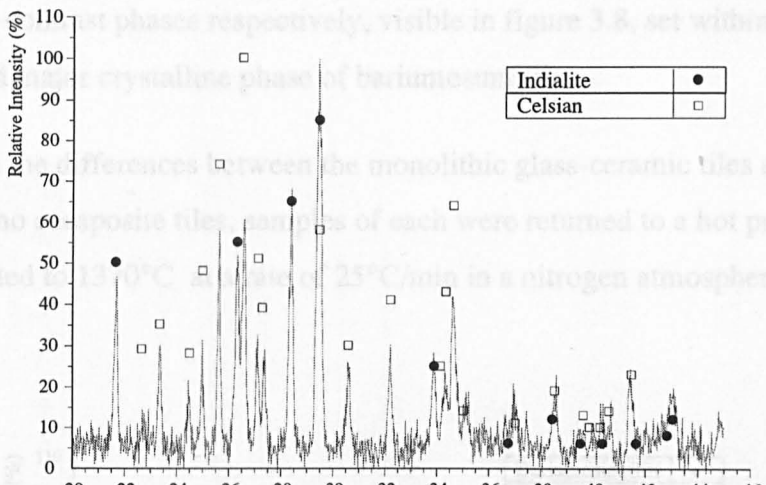

Figure 3.9 XRD spectrum from as received BMAS/Tyranno

The composite designated OBM had detectable peaks for bariumosumilite ~(fig 3.10) but indialite and celsian were still present as high volume fraction phases.

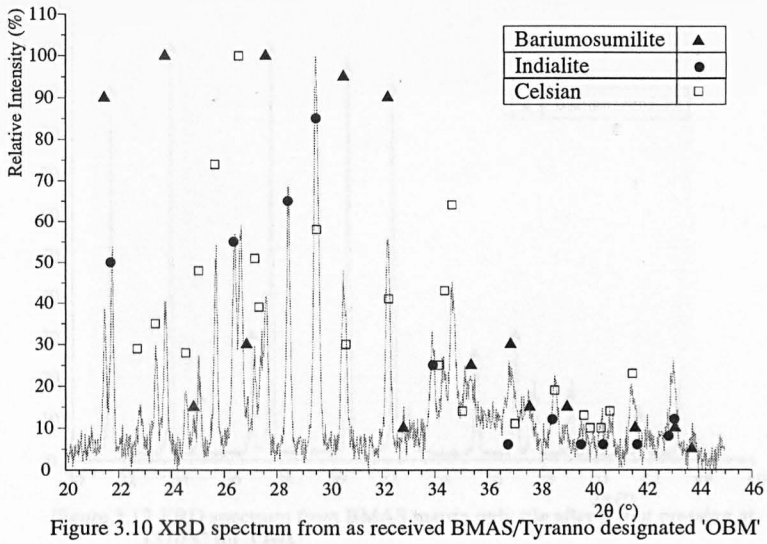

Figure 3.10 XRD spectrum from as received BMAS/Tyranno designated 'OBM'

The matrix only tile examined by XRD exhibited a spectrum which matched that of bariumosumilite (fig 3.11). The highest relative intensity peaks not attributable to this phase were identified as hexacelsian and either indialite or cordierite (orthorhombic $Mg_2Al_4Si_5O_{18}$). The hexacelsian and cordierite/indialite phases were present as the light and dark contrast phases respectively, visible in figure 3.8, set within the interconnected major crystalline phase of bariumosumilite.

To investigate the differences between the monolithic glass-ceramic tiles and the BMAS/Tyranno composite tiles, samples of each were returned to a hot press where they were heated to 1370°C at a rate of 25°C/min in a nitrogen atmosphere and held for 3 hours.

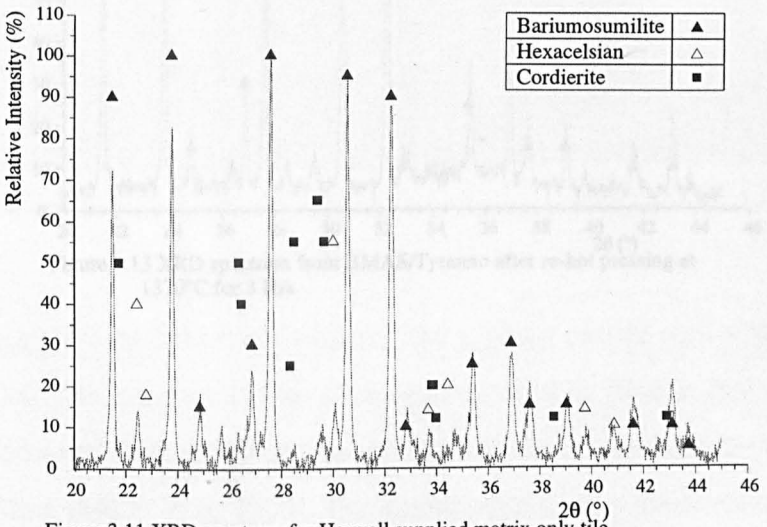

Figure 3.11 XRD spectrum for Harwell supplied matrix only tile

The spectrum for the re-hot pressed monolithic glass-ceramic is shown in fig 3.12. Bariumosumilite was the only identifiable crystalline phase.

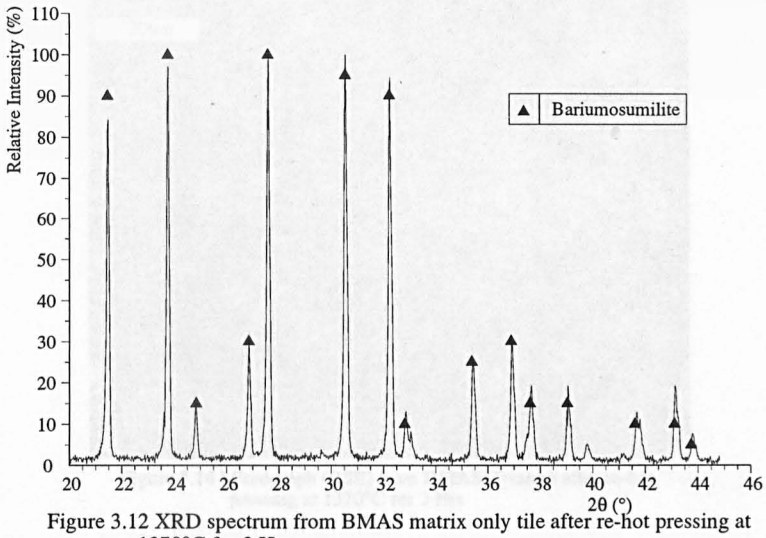

Figure 3.12 XRD spectrum from BMAS matrix only tile after re-hot pressing at 1370°C for 3 Hrs

The same re-hot pressing schedule was followed for the BMAS/Tyranno composite (tile NPP14). The major crystalline phase evident from the XRD spectrum (fig 3.13) was bariumosumilite. Small peaks were observed for cordierite/indialite and celsian at 2θ values of 26.55, 28.48 and ~29.5°. The relative intensity of these peaks was below 10%. However the change in the microstructure was also accompanied by the development of a lighter contrast band in the fibres (fig 3.14).

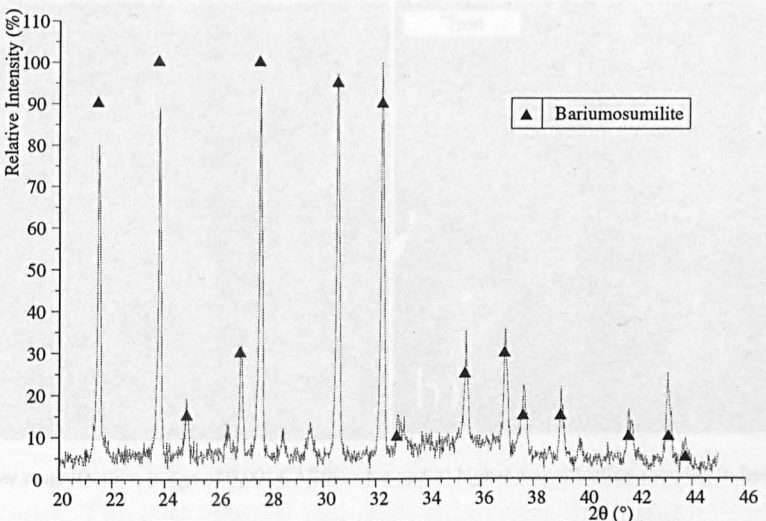

Figure 3.13 XRD spectrum from BMAS/Tyranno after re-hot pressing at 1370°C for 3 Hrs

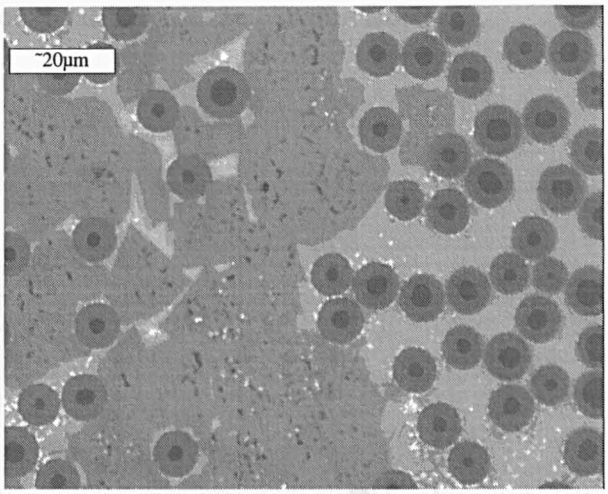

Figure 3.14 Micrograph (BSE) from BMAS/Tyranno after re-hot pressing at 1370°C for 3 Hrs

3.3.3 Characterization of Additional Systems

CAS/Nicalon

Low magnification micrographs of the CAS/Nicalon composite (fig 3.15) show that very little porosity was present. The large variation in the dimensions of the Nicalon fibres is evident. Higher magnification show individual matrix grains of anorthite with zirconia at the grain boundaries.

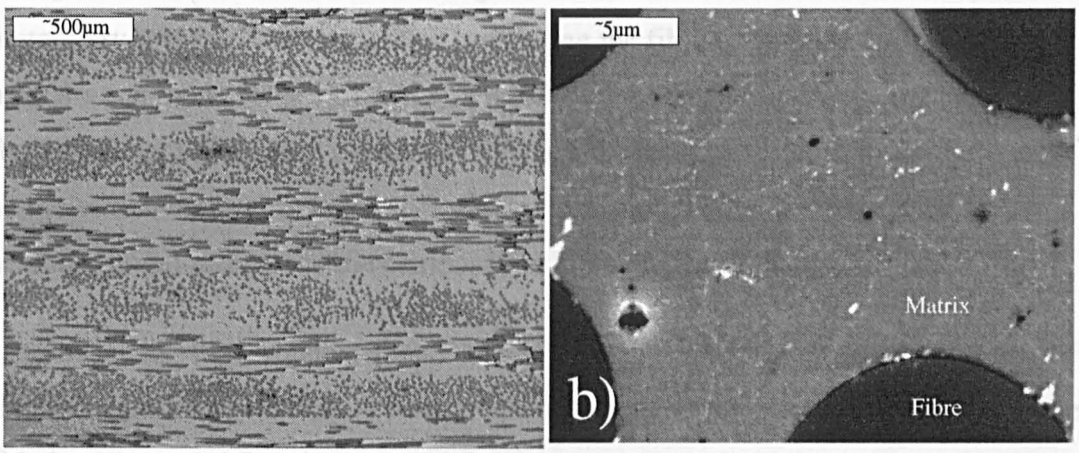

Figure 3.15 a) Low magnification image of 0,90° CAS/Nicalon and b) higher magnification showing individual grains of CAS

AS/Nicalon

The material supplied by Schott of Germany had a glassy matrix with a fibre volume fraction of ~40%. The interfacial shear stress as measured by fibre indent methods was 9-10MPa (Boccaccini et al, 1997) and the carbon enriched interfacial depth was assessed as ~30nm (Meier et al, 1995). The glassy matrix has a glass transition temperature of 745°C (Boccaccini et al, 1997). XRD of the polished composite shows the amorphous matrix but with a 'hump' in the spectrum (fig 3.16) which can be

attributed to the nanocrystallinity of the Nicalon fibres.

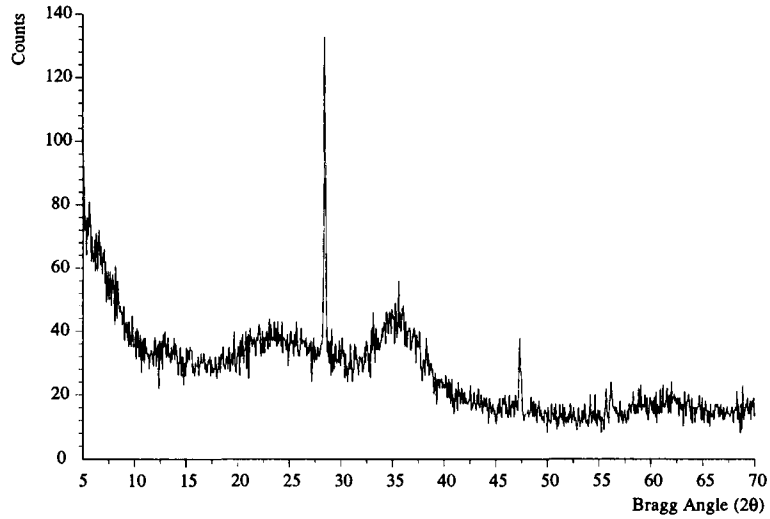

Figure 3.16 X-Ray spectrum of AS/Nicalon. Peaks correspond to Si standard Amorphous 'humps' can be observed for the Nicalon fibres

3.3.4 Thermal Expansion

The relative thermal expansion of the matrix and fibres plays an important role in the residual stress state of the composite after processing and cooling down. The stress condition at the interface affects the degree of fibre clamping and in turn the debonded sliding resistance. To evaluate the composite residual stress state in BMAS/Tyranno dilatometry (Netzch 402E) was used both along the fibre orientation and normal to it. From the equations given (3.1 and 3.2) it has been possible to estimate the matrix and fibre coefficient of thermal expansion (CTE) and hence the residual strain. Further to the use of dilatometry for thermal expansion the same facility has been used to assess the dimensional stability of the composite at high temperatures.

Dilatometry has been conducted on BMAS/Tyranno. UD BMAS/Tyranno was heated at a rate of 5°C/min to 1200°C. A standard sample holder correction was used as supplied with the dilatometer/logging system package. A two hour hold time was used before cooling at 5°C/min. The temperature was selected to give the highest possible temperature range and also to coincide with the high temperature mechanical testing programme. Both transverse and longitudinal coefficients of thermal expansion were determined to allow the thermal expansion coefficients of matrix and fibres to be fround from:

$$\alpha_c(parallel) = (\alpha_f V_f E_f + \alpha_m V_m E_m) \;/\; (E_f V_f + E_m V_m) \qquad (3.1)$$

A good approximation for the CTE normal to the fibres, ($\alpha_c(transverse)$), for high

volume fractions i.e. $V_f > 0.2$ to 0.3 is given by the linear mixture law:

$$\alpha_c(transverse) = (\alpha_f V_f + \alpha_m V_m) \tag{3.2}$$

where V_m and V_f are matrix and fibre volume fractions, E_m and E_f the matrix and fibre elastic moduli and α_m and α_f represent the matrix and fibre CTE. From these results it is possible to calculate the residual stress state in the axial direction for matrix, (3.3), and fibre, (3.4), from:

$$\sigma_m^R = (\alpha_f - \alpha_m) E_f V_f E_m \Delta T / E_c \tag{3.3}$$

$$\sigma_f^R = -\sigma_m^R V_m / V_f = (\alpha_m - \alpha_f) E_m V_m E_f \Delta T / E_c \tag{3.4}$$

where the symbols have the previous meaning and ΔT can be taken as the glass softening point (Beyerle et al, 1992b) or the glass ceraming temperature (Pryce and Smith, 1992) and is therefore negative in this instance. Negative values of stress represent residual compression.

Similarly the residual radial stress ($\sigma_c(radial)$) at the interface can be estimated from (Budiansky et al, 1988):

$$\sigma_c(radial) = -\frac{E_f V_m (\alpha_f - \alpha_m) \Delta T}{2\lambda(1-\nu)} \tag{3.5}$$

where

$$\lambda = 1 - \frac{(1-2\nu)}{2(1-\nu)}(1 - E_c/E_f) \tag{3.6}$$

The Poisson ratio (ν) is assumed to be the the same (=0.24) for fibre and matrix in both (3.5) and (3.6).

The thermal expansion in terms of strain and time are shown in figure 3.17. The CTE values were calculated from the extension immediately the target temperature was attained. Once at temperature the specimen elongation then reduced in the longitudinal orientation. In the transverse fibre direction the specimen dilated during the two hour hold time. Coupled to the above observations was a permanent deformation when cooled to room temperature. In the longitudinal direction the specimen had shrunk, conversely in the transverse orientation the specimen was longer than the initial length.

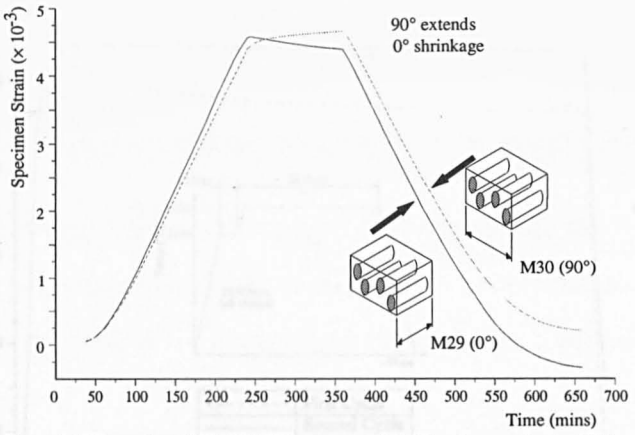

Figure 3.17 Expansion of UD BMAS/Tyranno parallel (0°) and perpendicular (90°) to the fibre orientation

The longitudinal and transverse CTE values were 3.88 and 3.75 × 10^{-6}/°C respectively. The fibre and matrix CTE as solved from (3.1) and (3.2) were:

$$\alpha_f = 3.56\times 10^{-6} / °C: \qquad \alpha_m = 2.77 \times 10^{-6} / °C$$

implying a misfit strain of ~9.5 × 10^{-4} at room temperature. From these values the residual stress states for matrix (3.3) and fibre (3.4) were calculated to be:

$$\sigma^R_m = -44.7MPa: \qquad \sigma^R_f = 82.9MPa$$

For the above calculations a temperature change of 1180°C was assumed, the elastic moduli E_f and E_m were taken as 170 and 98.4GPa respectively and V_f was taken from the manufacturer's data (Table 3.1).

Calculations of the radial stress at the interface from (3.5) give σ_c(radial) = 74.8MPa. These findings indicate the interface is under residual tension (i.e. there is no clamping of the fibre by the matrix) and the matrix is under longitudinal compression caused by the contraction of the fibres.

Further testing was conducted to assess the degree of shrinkage. A cycle with 20°C/min heating and cooling ramps was used. The first target temperature was 1100°C where an hour hold time was used. The second hold time was for 24 hours at 1200°C, the results can be viewed in figure 3.18.

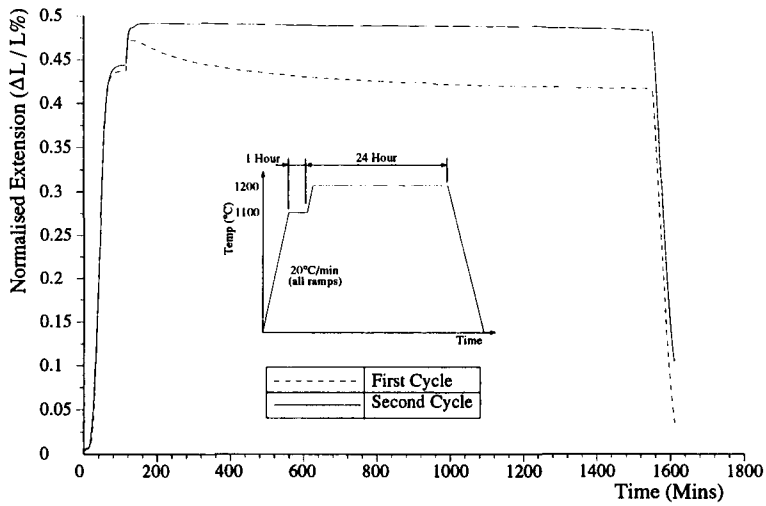

Figure 3.18 Thermal expansion results from two thermal cycles on the same specimen

No shrinkage was apparent during the 1100°C hold time for either cycle. At 1200°C shrinkage of 566×10^{-6} was observed but this figure was much lower on the second cycle at 97×10^{-6}. The thermal expansion on the second cycle was also slightly higher.

3.3.5 Interface Techniques

Specimens were prepared as for SEM observation with attention paid to the specimen depth (maximum permissible depth was 5mm). A novel indent system was used which was developed in-house (Daniel and Lewis, 1993; Lewis et al, 1993b). The small radius diamond was translated via an inchworm piezoelectric device (fig. 3.19). The entire assembly was located within the stage of a SEM (Cambridge Stereoscan 250 MkIII). Indent load and displacement were logged via an Archimedes personal computer while microprobe positioning was effected by monitoring the secondary electron image at TV scan rates. Data analysis for fibre push-in was by the Marshall and Oliver (1987) method (2.7).

For fibre push-out thin slices (200μm) of the respective composites were cut on the Capco diamond saw. These slices were then mounted on brass stubs with modelling wax for manual polishing. Once polished to a 1μm finish on both upper and lower faces the samples were carefully removed and individual slices of composite could be mounted on a sample holder with a suitable central slit. The slit enabled fibre push-out without impeding the emerging fibre. To prevent damage to the thin samples the depth was measured within the SEM after the push though testing was complete. Fibre push-out utilized the linear push-out model (Weihs and Nix, 1988).

$$\tau = \frac{P_m}{2\pi r h} \tag{3.7}$$

where P_m represents the load after debonding and h is the sample depth.

Samples tested in this way were the Corning CAS/Nicalon and the Harwell BMAS/ Tyranno (tile NPP18) composites. It has been possible to perform both fibre indent and fibre push-through experiments for comparison between the composite materials and the testing method used.

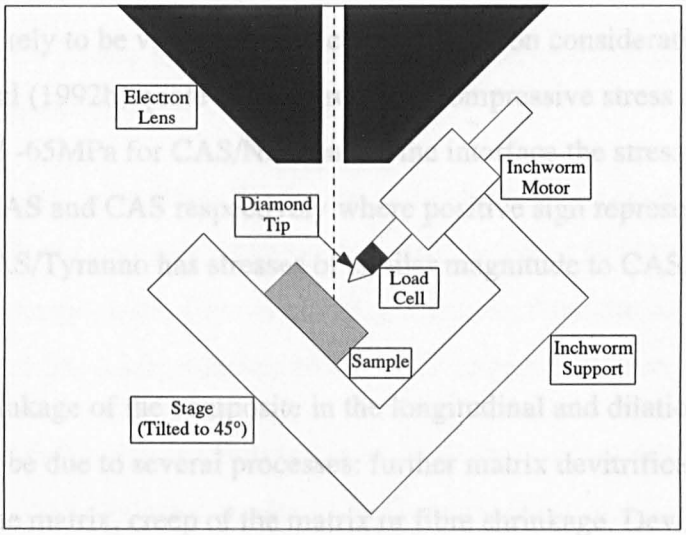

Figure 3.19 Schematic representation of the Warwick indent facility after Lewis

The results of the indentation and push-out tests conducted on the BMAS and CAS systems are presented in Table 3.2. They show BMAS/Tyranno has both the highest debond energy requirement and interfacial sliding stress. For both systems the interfacial shear stress measured by push-out is lower than the indent values.

Table 3.2 Results of fibre indent and push-out tests

	Indent		Push-out
Material	G_i (Jm^{-2})	τ (MPa)	τ (MPa)
BMAS/Tyranno	8±4.0	38±5	29±5
CAS/Nicalon	2.7±1.6	22±4	15±3

3.3.6 Discussion

The thermal expansion of the BMAS/Tyranno fulfils the ideal criterium set out by Evans and Marshall (1985) since the strain mismatch is small (i.e. less than 3×10^{-3}) and negative ($\alpha_f > \alpha_m$). Of the two most widely tested glass-ceramic composite systems this aligns BMAS/Tyranno with LAS rather than CAS. The figures quoted for residual stresses are subject to errors from residual glass viscosity and volume changes from crystallization and phase transformations.

From the radial tensile stress at the interface it can be seen that the debonded sliding resistance, τ, is likely to be very low from coulomb friction considerations, as with LAS. Beyerle et al (1992b) quote an axial residual compressive stress of 20MPa for LAS/Nicalon and -65MPa for CAS/Nicalon. At the interface the stresses were -50MPa and 89MPa for LAS and CAS respectively where positive sign represents compressive stress. Thus BMAS/Tyranno has stresses of similar magnitude to CAS/Nicalon but of opposite sign.

The apparent shrinkage of the composite in the longitudinal and dilation in transverse orientation could be due to several processes: further matrix devitrification, phase changes within the matrix, creep of the matrix or fibre shrinkage. Devitrification or phase transformations seem unlikely to result in a Poisson type contraction and expansion but crystallization peaks are present in the temperature range 1080-1140°C in DSC runs for BMAS glass (Lambrinou et al, 1996). However, both matrix creep and longitudinal fibre shrinkage could result in apparent longitudinal shrinkage and transverse expansion. The driving force for matrix creep could be provided by the residual tensile stress within the fibres. In turn this tensile stress could also be enhanced by fibre shrinkage. Fibre shrinkage has been seen previously for both early Nicalon fibres (Simon and Bunsell, 1984) and more recently for Tyranno fibres (Berger et al, 1996). Nicalon NLM202 also shows limited shrinkage but this is probably lower due to a stabilizing heat treatment (Bunsell, 1992). The reason for this shrinkage lies in the low density. The density suggests porosity is present. Lipowitz (1991) attributes a possible nanoscale porosity on the gas evolution phase during manufacture. When heated above the maximum pyrolysis temperature, likely to be 1100°C from the Yamura data ('above 800°C', Yamura et al, 1987; 'around 1000°C', Bunsell, 1992) densification increases the average pore size but reduces the pore volume fraction. Thus density increases along with the elastic modulus (Hochet et al, 1997): LoxM subjected

to 5hours at 1200°C in Argon displayed a modulus increment from 180 to 193GPa. The lower thermal expansion on the second cycle is consistent with this increase in the fibre elastic modulus. However crystallization of residual glass will also have the effect of reducing the measured CTE.

The figure for matrix expansion of 2.77×10^{-6} is slightly higher than both the constituent major phases of celsian and cordierite (celsian 2.29×10^{-6}/°C, cordierite $1.4\text{-}2.6 \times 10^{-6}$/°C). These compare to pure barium osumilite at $2.8\pm0.4 \times 10^{-6}$/°C (Winter at al, 1993a). Discrepancies may arise from residual glass present (the starting glass has a CTE of $4.8\pm0.4 \times 10^{-6}$/°C (Winter at al, 1995)). Similarly low quantities of the higher expansion phases hexacelsian (8×10^{-6}/°C) and quartz (~10×10^{-6}/°C) could also raise the apparent CTE.

Although no CTE data is available for Tyranno, that for Nicalon is often quoted between 3.1×10^{-6}/°C (Ishikawa, 1994) and slightly over 4×10^{-6}/°C (taken from graph of strain vs temperature: Lipowitz, 1991). Tyranno, from the current data, (3.56×10^{-6}/°C), appears to be closely matched to the CTE range for Nicalon.

The celsian and indialite phases identified from XRD studies for BMAS/Tyranno differ from those of the BMAS/Nicalon produced by Corning. Bleay and Scott (1992) report primarily bariumosumilite with minor quantities of hexacelsian (~20wt%) and mullite (~10wt%). The hexacelsian was believed to result from the high processing temperature of ~1500°C but can form easily from $BaAl_2Si_2O_8$- glass below 1590°C (Ochlschlegel et al, 1976). Table 3.3 details the matrix powder composition (Lambrinou et al, 1996) and that found in the as pressed composite from matrix rich regions between plies from tile NPP10.

Table 3.3 BMAS compositions

Oxide	Content (wt %) [1]	Content (wt %)[2]	Content (wt %)[3]	Content (wt %)[4]	Content (wt %)[5]
BaO	13.9±0.5	14.19	14.2	2.0	14.4
Al_2O_3	27.7±0.5	28.31	28.3	32.0	27.9
SiO_2	52.0±1.0	50.04	50.0	52.5	51.6
MgO	6.4±0.2	7.46	7.5	13.5	6.1

1 Powder composition from Lambrinou et al, (1996)
2 Stoichiometric bariumosumilite
3 Powder composition used by Winter et al, (1993)
4 Powder composition used by Chaim & Heuer, (1992)
5 Matrix EDX analysis on current composite

The limited quantity of the bariumosumilite phase is difficult to reconcile with the manufacturer's claims. Winter et al (1993) have produced isothermal crystallization sequences (fig 3.20a) at two different heating rates (25K/min and 5K/hour) on the glass

composition given in Table 3.3. They show a $MgAl_2SiO_4$ phase, with an h-quartz$_{ss}$ type structure, is the first crystallization product from 900-950°C for the fastest heating rate. This phase dissolved above 1050°C (fig 3.20a). Bariumosumilite is reported to form at temperatures as low as 900-1050°C and is the only crystallization product above 1150°C. The melt temperature of bariumosumilite has been reported as 1370°C (Winter et al, 1993a). Celsian and cordierite/indialite crystallize over a narrower range: 1000-1100°C and 1000-1150°C respectively (fig 3.20b) and are metastable within the BaO-MgO-Al_2O_3-SiO_2 bariumosumilite composition. However the transformation to bariumosumilite is slow. At the highest heating rate it was possible to produce a monophasic final glass-ceramic. Conversely the lower heating rate produced a more complicated structure consisting of celsian, hexacelsian and cordierite in addition to bariumosumilite.

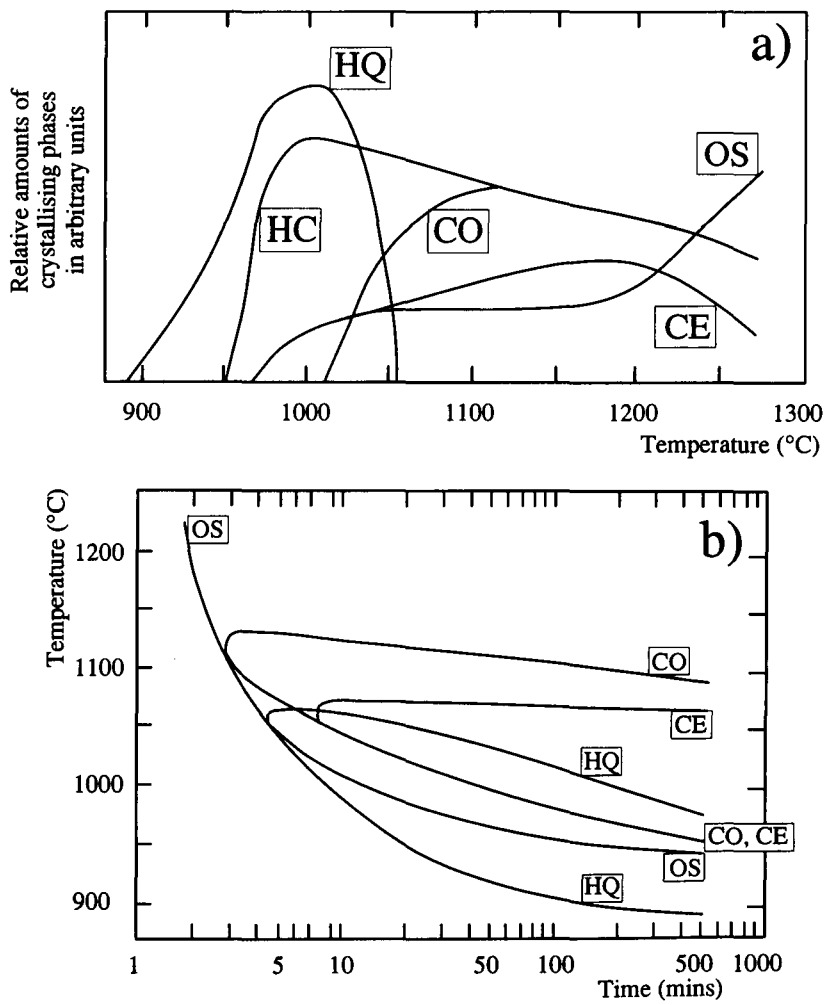

Figure 3.20 a) Crystallisation sequence of bariumosumilite glass heated at 5K/h and b) TTT diagram for Ba, Mg, Al, Si, O glass of stoichiometric bariumosumilite composition from isothermal crystallisation runs (after Winter et al, 1993) HC = hexacelsican, HQ = h-quartz$_{ss}$, OS = bariumosumilite, CE = celsian, CO = alpha-cordierite

The crystallization sequence becomes clearer from the TEM studies of Chaim and

Heuer (1992), who investigated a BaO doped magnesium aluminosilicate (see Table 3.3 for their composition). The h-quartz (or μ-cordierite) structure could not contain the Ba which was ejected to form a BaO rich interdentritic glassy phase (Chaim and Heuer, 1991). With increasing heat treatment temperatures (to 1200°C) the BaO concentration within the glassy phase reached 20wt%.

Lambrinou et al (1996) have used powder supplied by Harwell of nominally the same composition as the current composite matrix. They found Bariumosumilite was the main crystallization product for heat treatments within the 1100-1300°C temperature range investigated. Celsian and Cordierite were also identified. They found, however, that the number of bariumosumilite crystals decreased with the heat treatment temperature and the interconnectivity of the celsian and cordierite phases increased during isothermal exposure for 12 hour durations.

The phases identified here by XRD support the observations from both SEM and TEM where $BaO\text{-}Al_2O_3\text{-}SiO_2$ and $Mg\text{-}Al_2O_3\text{-}SiO_2$ containing phases were the main crystalline products. The crystallization studies by Winter et al (1993, 1995) do not clarify the 'ceraming' heat treatment which has indirectly been used on the composite material since no combination of temperature and heating rate appears to result in the formation of just indialite and celsian. The preferential crystallization of bariumosumilite above 1150°C indicates either the claimed 3 hour hold at 1350°C is insufficient for the 'sluggish' bariumosumilite growth or the material has not been held at such temperatures. The hot pressing temperature of 950°C would be sufficient to allow the crystallization of the hexagonal high-quartz phase leaving a barium rich glass. As the temperature is increased celsian and/or hexacelsian can grow. The high-quartz phase (μ-cordierite) presumably undergoes a polymorphic transformation at higher temperatures resulting in the stable β-cordierite polymorph. Below 1150°C celsian and cordierite crystallize more readily than bariumosumilite. With slow heating rates and a low 'ceraming' temperature barium osumilite must grow from the celsian and cordierite phases by solid state diffusion. It is only from temperatures approximating 1200°C and above that bariumosumilite becomes the dominant crystallizing phase.

The crystallization results for the pressureless sintering of the matrix only tiles probably differ from those of the BMAS/Tyranno composite as the temperature within a furnace can be more easily monitored. The quoted processing routine was more likely to have been followed closely with the ultimate temperature approximating 1350°C. However

the re-hot pressing carried out here has shown that a greater yield of bariumosumilite was possible with further heat treatment. The same schedule when used on the BMAS/ Tyranno composite saw bariumosumilite become the major phase, providing evidence the 'ceraming' did not reach such a high temperature. The decline in even the minor volume fraction of bariumosumilite in the tiles designated OBM and BNB with the new NPP tiles also coincided with an increase in the supplied dimensions of the composite tiles. This may have led to problems maintaining the temperature over the increased size of the hot pressing die and the lower yield in bariumosumilite. The higher temperature for re-hot pressing used here has however resulted in the diffusion of matrix elements into the fibres. The fibre ultimate strengths are expected to be weakened in this condition.

The fibre indent and push-out testing reveal CAS/Nicalon has a lower apparent debond energy and interfacial sliding stress than the BMAS/Tyranno. The BMAS/Tyranno indentation results compare to those reported by Plucknett et al (1994 and 1995) and Lewis et al (1993) at 36±6MPa and 25±7MPa respectively. No previous results have been reported for the push-out testing of this composite system.

The Corning CAS/Nicalon has been extensively studied. Lara-Curzio and Ferber (1994) have collated interfacial shear stress values for CAS/Nicalon obtained from different test methods and themselves contributed push-out values of 8.2-11.1MPa compared to the 15±3MPa found here. Indent data values reported here are slightly higher than the 10-19MPa found by Wang and Parvizi-Majidi, 1990.

The high values for the debond and interfacial shear stress for BMAS/Tyranno can be considered in relation to the thin carbon rich interface. Si-O bonds are known to be present at the interface in BMAS/Tyranno (Cain, 1995). Poor formation of the interface may imply these bonds bridge the carbon rich layer. A higher friction coefficient between fibre and matrix in the absence of the lubricating carbon may also be possible. Even if the C-layer was coherent, asperities could penetrate with a resulting higher friction coefficient. The roughness of the interface may allow mechanical interlocking which would have the result of increasing the force necessary to push the fibre relative to the matrix. Mackin et al (1993) performed push-though testing on a g-TiAl/Sapphire reinforced composite material with different depth and chemistry interlayers. They found low τ values for the thickest interfaces probably because the fracture propagation path did not mimic the underlying surface geometry.

Fibre surface roughness plays an important role in determining interfacial properties, especially when thin interfaces are present. Chawla et al, (1995), compared the surface roughness of Nicalon and Hi-Nicalon using atomic force microscopy. They concluded that small changes in the surface roughness of a fibre significantly affected the debonding and sliding properties between fibre and matrix, i.e. higher roughness amplitudes increased debonding and sliding stresses.

Another major consideration for the fine fibre diameter Tyranno fibres is the dependence of the interfacial shear stress on fibre diameter as reported by Daniel et al, (1997). They found that the fibre radius played a large role in the magnitude of the interfacial shear strength when measured by the fibre indentation test. They were able to test a wide range of fibre diameters in the CAS/Nicalon system. This was possible due to the large variation in the diameter of Nicalon fibres. Small diameter fibres exhibited apparently high values of τ due to a large contribution from radial Poisson expansion of the fibres. For small radius fibres (R=4μm) the apparent τ value was ~44MPa. This value reduced to 25MPa for larger diameters. A Poisson expansion during indent is believed to be the reason for the higher τ values over the push-out testing method (Daniel et al, 1997).

Interfacial sliding resistances have been reported for the Corning BMAS/Nicalon system. Bleay and Scott, (1992), found values of 3.5-4.4MPa for a Corning BMAS/ Nicalon composite in the as received state. Similar results were obtained by Mandell et al (1987) for BMAS/Nicalon at 5.5MPa.

However it must be acknowledged that Tyranno has been shown to produce a thinner interface under identical processing conditions in a borosilicate glass matrix (Murthy et al, 1990) due to the lower amount of free carbon and the formation of TiC precipitates.

3.4 Conclusions

The characterization studies reported within this chapter indicate the matrix for the BMAS/Tyranno composite is a mainly diphasic structure of indialite and celsian. The main phase claimed by the manufacturers was bariumosumilite. Despite the lack of bariumosumilite the matrix was shown to have a thermal expansion coefficient below that of the fibres. This indicates the interface was subject to residual tension and the matrix was under residual compression. At 1200°C the composite was shown to be dimensionally unstable, a characteristic attributed to fibre shrinkage. This suggested the composite was not ceramed at a temperature of 1200°C or over.

The matrix only tiles supplied by the same company consisted of bariumosumilite as the major phase. However small amounts of hexacelsian and cordierite/indialite could also be distinguished. The evidence suggests either incorporation of the Tyranno fibres inhibits bariumosumilite nucleation and growth or the composite was not 'ceramed' at a high enough temperature, unlike the matrix only material which was heat treated in a separate furnace. The reasons for this are outside the remit of this thesis but the large dimensions of the tiles supplied (220x220x2.2mm) could lead to large temperature differentials across the hot zone with low temperatures at the tile to be pressed.

A thin carbon rich interface of only 10-15nm was observed in the BMAS/Tyranno composite. The poor development of the interface has been suggested as the cause of the high interfacial shear stress when measured by fibre indent and push-out test conducted within a scanning electron microscope. Other researchers have found the carbon rich interface can be enhanced in depth by up to 100% during short term exposure (1 hour) at 1100-1200°C (Cain, 1995). Subsequent re-hot pressing of the matrix only material and the composite has shown exposure to elevated temperatures can lead to near monophasic bariumosumilite. Therefore it is proposed closer control of the ceraming temperature would have led to a higher bariumosumilite yield and lower interfacial shear strength through development of a thicker carbon interphase between fibre and matrix. However this must be tempered with possible lower fibre strengths due to inward diffusion of matrix elements into the fibres at higher processing temperatures. Thus the lower processing temperature has inadvertently resulted in higher fibre strength being retained. The following chapters will demonstrate the effects the high fibre strength but limited interfacial development have on composite properties.

Chapter 4 Room Temperature Mechanical Properties

To characterize the mechanical properties both flexural and tensile testing modes have been utilized. Monotonic testing was complemented by cyclic loading to assess the damage state and also the interfacial shear stress which can be evaluated from hysteresis loop widths (Kotil et al, 1990), matrix crack spacing (Aveston and Kelly, 1973) and fibre pull-out lengths (Prewo and Brennan, 1982). The notch sensitivity of both UD and 0,90° BMAS/Tyranno was also probed.

4.1 Flexure Testing

Room temperature flexure tests were conducted for several of the different BMAS/ Tyranno plates at an actuator displacement rate of 0.2mm/min.

Typical UD and 0,90° flexural stress strain curves for BMAS/Tyranno tiles NPP5, 7, 11 and 14 are illustrated in figure 4.1. Figure 4.2 shows the result of a flexural test from an early BMAS/Tyranno tile designated BNB1 along with a test from tile NPP5.

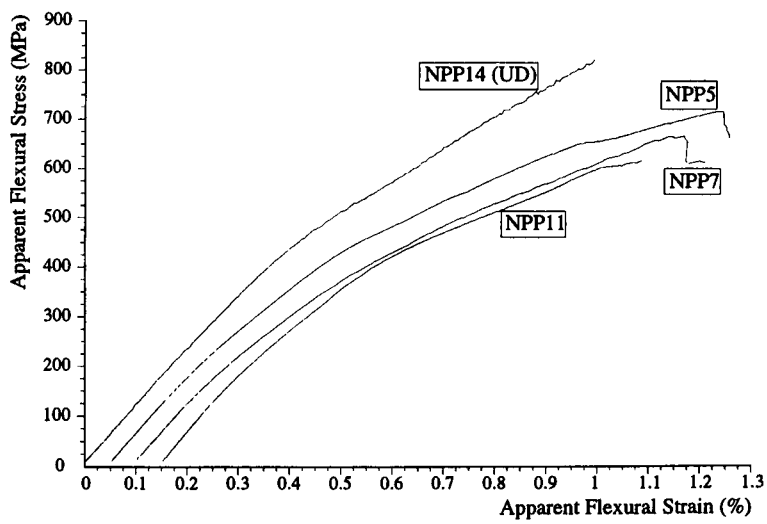

Figure 4.1 Flexural stress-strain plots of three BMAS/Tyranno 0,90° and one UD (offset for clarity)

The plots of figure 4.1 show an initial linear region. For the 0,90° specimens a deviation from linearity occurs at approximately 130MPa, a second pseudo-linear section then extends to ~300MPa. The maximum flexural strengths are all in excess of 600MPa but some scatter is evident. The UD flexure tests show only one major deviation from linearity between 290 and 340MPa but small decrements in the elastic modulus are evident from as low as 120MPa. The strain to failure for all the room

temperature tests (UD and 0,90°) are similar, within the range: $0.87 < \varepsilon_f < 1.18$, the UD material assuming the lower values within this range.

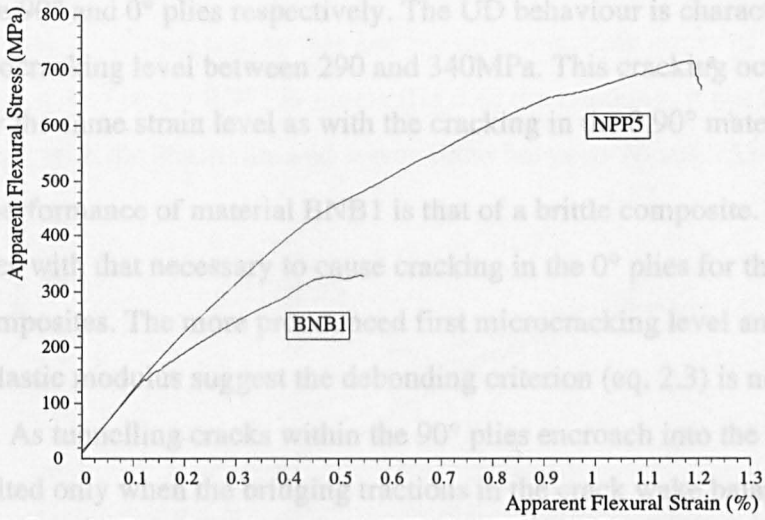

Figure 4.2 Flexural stress-strain plots for 0,90° tiles NPP5 and BNB1

The contrast between BNB1 and NPP5 material is marked, (fig 4.2). The initial elastic modulus is similar at 110GPa as is the first non-linearity stress at approximately 130MPa but at this stress the BNB1 shows an obvious strain step rather than a gradual transition. Above this stress the apparent elastic modulus and the ultimate strength of BNB1 is lower. The strain at failure for BNB1 is coincident with the second strain non-linearity for the NPP5 specimen.

The fracture surfaces were also different with fewer energy absorbing features apparent for the BNB composites (fig 4.3) than with the NPP composite (see fig 4.8). Fibres bridged the fractured tensile surface of the failed sample in the NPP composite. In the BNB material the initial fracture was planar with no noticeable fibre pull-out.

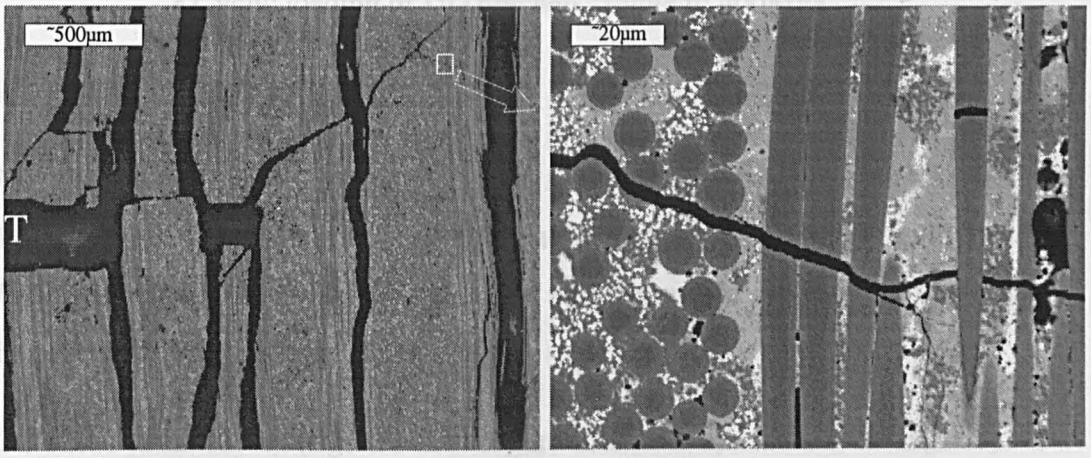

Figure 4.3 Brittle room temperature fracture of 'BNB' material during flexural testing. Note how cracks propagate through the fibres in both orientations. The tensile face is represented by 'T'

Flexural stress-strain plots of specimens from tiles NPP5, 7, 11 and 14 (fig 4.1) all show 'ductile' failure behaviour. The deviations from linear in the stress strain plots for the cross ply laminates was approximately 130 and 300MPa. These correspond to cracking in the 90° and 0° plies respectively. The UD behaviour is characterized by only one microcracking level between 290 and 340MPa. This cracking occurs at approximately the same strain level as with the cracking in the 0,90° material.

The flexural performance of material BNB1 is that of a brittle composite. The failure strain coincides with that necessary to cause cracking in the 0° plies for the 'ductile' NPP 0,90° composites. The more pronounced first microcracking level and greater reduction in elastic modulus suggest the debonding criterion (eq. 2.3) is not met at all of the interfaces. As tunnelling cracks within the 90° plies encroach into the 0° plies progress is halted only when the bridging tractions in the crack wake balance the stress intensity at the crack tip. The elastic modulus is therefore reduced due to the longer crack lengths and fewer intact fibres. At the strain level necessary for 0° ply cracking more fibre failures occur until the intact fibres cannot sustain the applied stress.

4.2 Tensile Testing

Room temperature tensile testing in air of BMAS/Tyranno consisted of:

- Monotonic testing of UD and 0,90° at four different rates
- Incremental cyclic testing of UD and 0,90°
- Cyclic testing with a prolonged hold at 250MPa for 0,90°
- Monotonic testing of notched 0,90°
- Monotonic testing of notched UD
- Cyclic loading of UD notched sample to 400MPa

4.2.1 Monotonic Testing

Four different cross head speeds were used in the tensile testing of both UD and 0,90° BMAS/Tyranno. The specimens were taken from plates NPP7 (0,90°) and NPP17 (UD). The cross head speeds of 0.02, 0.2, 2 and 20mm/min relate to test durations of the order of 5 hours to under 10 seconds.

The stress-strain curves (figs 4.4 and 4.6) are similar to other GCMCs (e.g. Beyerle et al 1990a, 1990b, Mah et al, 1985a, Prewo and Brennan, 1986) which display

microcracking initially in the 90° plies for cross-ply lay-ups followed by 0° ply cracking at a higher applied stress.

The elastic modulus did not seem to be affected by the rate of testing (fig 4.5). However there is a correlation between testing rate and the microcracking stress of the 0° plies (inset table, Fig. 4.4). For the 0,90° laminate (fig 4.6) the cracking of the 90° plies did not seem to vary with the strain rate and seems fixed between 70 and 75MPa.

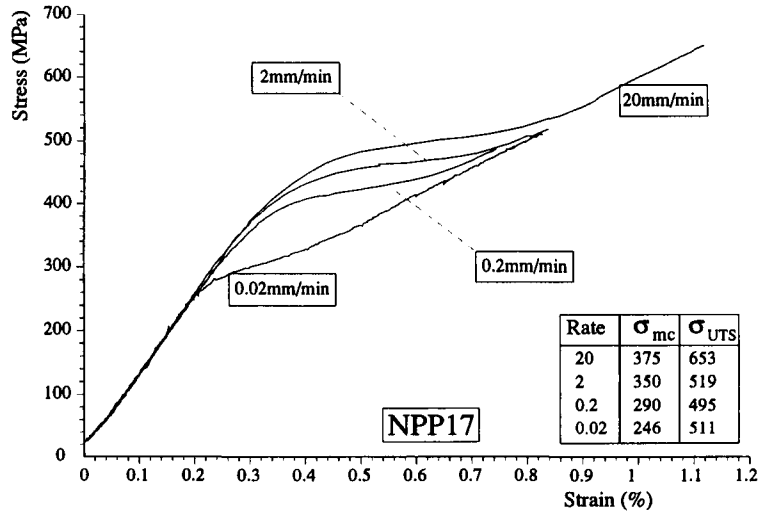

Figure 4.4 Tensile stress-strain curves for four different testing rates. Table (inset) shows the corresponding matrix cracking stresses and ultimate strengths

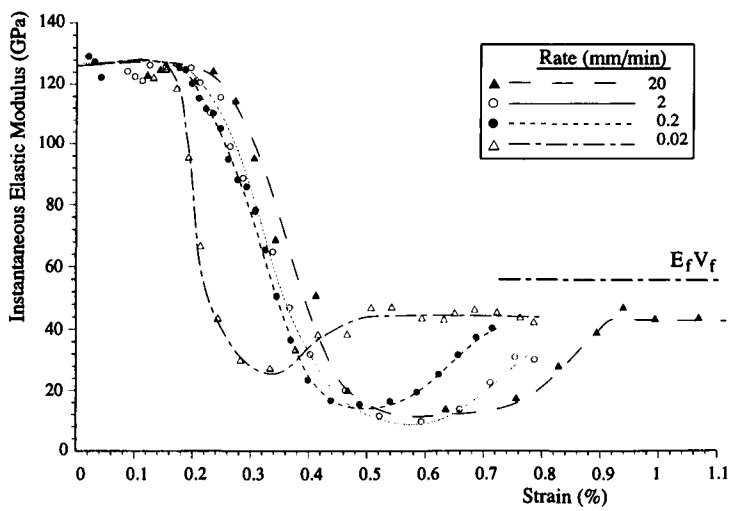

Figure 4.5 Variation in instantaneous modulus during loading at four different testing rates for UD BMAS/Tyranno

The ultimate strength also seems to have increased with the testing rate but this cannot be considered conclusive due to the limited number of tests. The instantaneous elastic modulus decreases after microcracking in the 0° plies and tends toward a second constant modulus (fig 4.5). The 0,90° BMAS/Tyranno material, unlike the UD, shows a marked final decrease in this elastic modulus near the ultimate failure stress (fig 4.7). The modulus from the slower testing rates for both fibre architectures tend to this

second elastic modulus at a lower stress and strain than with the higher testing rate, i.e. the microcracking takes place over a larger stress and strain range than the slower testing rates. Neither of the composite configurations has a final modulus close to that expected for the fibres oriented in the loading direction alone. The UD final modulus of 45.5GPa compares to 56.1GPa from E_fV_f considerations and the 0,90° modulus of 23.5GPa is similarly lower than the 33.0GPa given by the formula $E_fV_f / 2$.

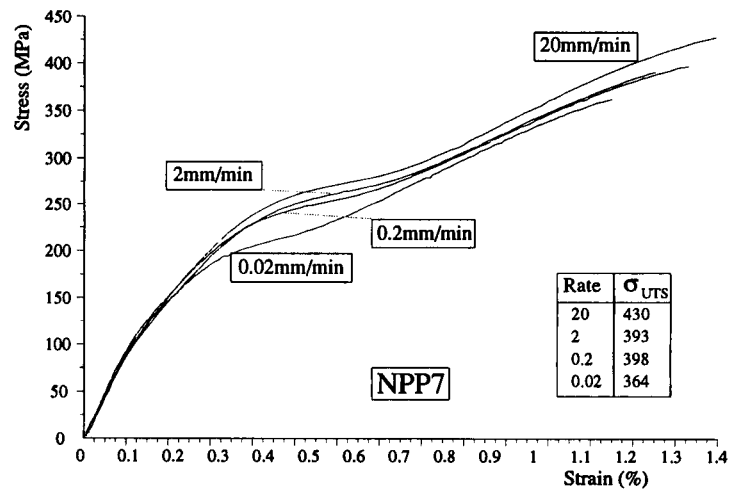

Figure 4.6 Tensile stress-strain curves for 0,90° BMAS/Tyranno at four different testing rates. Table (inset) shows the variation of strength.

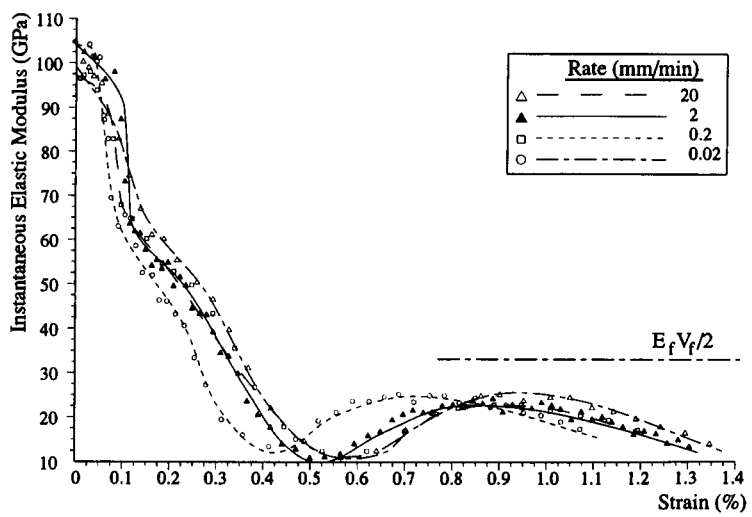

Figure 4.7 Elastic modulus evolution during tensile loading of 0,90° BMAS/Tyranno at different testing rates

Low magnification images of the fracture faces in the 0,90° BMAS/Tyranno (fig 4.8) show the pull-out.

Fracture of the UD BMAS/Tyranno was not of the expected form for purely tensile loading, i.e. fracture did not initiate from a dominant crack and propagate across the specimen normal to the aligned fibres. Instead crack initiation was from the change in sample section located at the point where the flared section for gripping met the parallel

gauge section. Propagation invariably transpired by longitudinal splitting such that fracture split the sample into two tapered segments (fig 4.9).

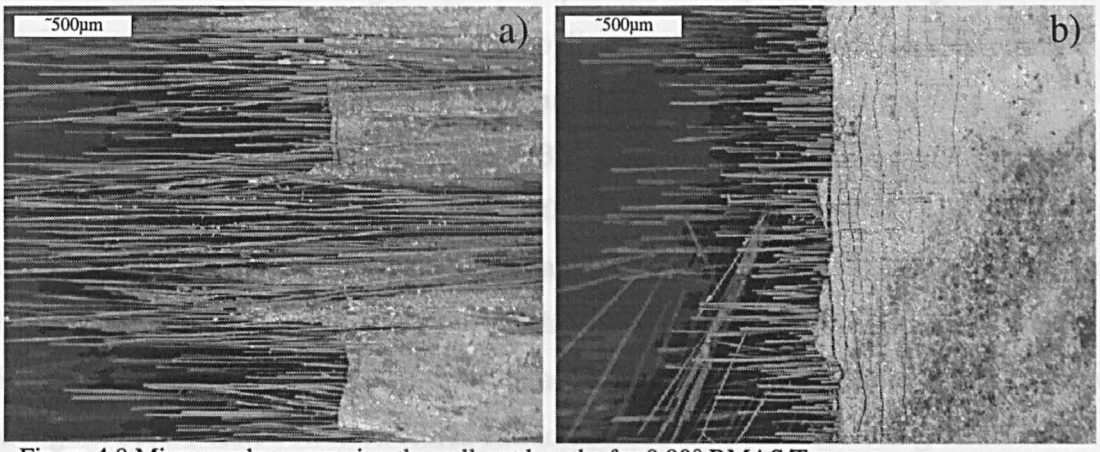

Figure 4.8 Micrographs comparing the pull-out lengths for 0,90° BMAS/Tyranno at cross head speeds of a) 0.02 and b) 20mm/min

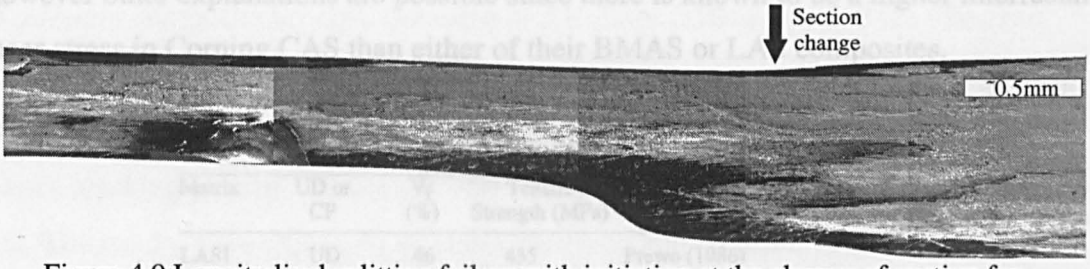

Figure 4.9 Longitudinal splitting failure with initiation at the change of section for tensile tested UD BMAS/Tyranno. Note pull-out at the change in section

For tile NPP17 (UD) the microcrack spacing as measured by acetate replication of the stressed composite was 31±6µm. The NPP7 [0,90°] tile had a 0° crack spacing of 27±6µm, 90° ply crack density of 181±12µm and a spacing of 378±19µm in the double thickness central 90/90° ply. A single ply thickness was approximately 235µm.

The stress-strain curves of figures 4.4 and 4.6 display the characteristic deviations from linearity with 90 and 0° ply cracking and with substantially reduced elastic moduli once crack saturation is reached. However the assertion that the final linear modulus prior to failure is lower due to variations in τ and fibre failure (Evans, 1994) seems at odds with the cyclic behaviour which will be elaborated in section 4.3. The ultimate tensile strengths are excellent when compared to CAS/Nicalon especially considering the reduced fibre volume fraction for the UD BMAS/Tyranno (V_f=0.33) and the final fracture mode of the UD composite. Table 4.1 has a selection of ultimate strengths for LAS, CAS and BMAS matrix composites. The lower strengths of CAS/Nicalon and the

early BMAS/Nicalon quoted could be due to the high temperatures used for fabrication. The AEA Harwell produced BMAS/Tyranno was hot pressed at a temperature no higher than 950°C but was apparently 'ceramed' at 1350°C (Churchman-Davies, 1996). CAS and BMAS from Corning has been hot pressed at temperatures as high as 1500°C (Brennan et al, 1986). A European patent application for BMAS/Nicalon by Corning provides an example of a typical hot press run where a maximum temperature of 1500°C was chosen (Brennan et al, 1984). Bonney and Cooper (1990) investigated CAS/Nicalon which was hot pressed at 1250 to 1450°C. LAS is known to be hot pressed between 1250 and 1300°C (Chaim and Heuer, 1987). Thus CAS is processed at the highest temperature and it may be that these high processing temperatures cause fibre weakening by diffusion of matrix elements into the fibre and hence low composite strengths. Prewo tested Nicalon fibres extracted from LAS matrices using dilute HF acid and found strengths of ~1500MPa: a strength degradation of ~800MPa.

However other explanations are possible since there is known to be a higher interfacial shear stress in Corning CAS than either of their BMAS or LAS composites.

Table 4.1 Selected values for BMC ultimate strengths from the literature

Matrix	UD or CP	V_f (%)	Tensile Strength (MPa)	Reference
LASI	UD	46	455	Prewo (1986)
LASII	UD	46	664	Prewo (1986)
LASIII	UD	44	680	Prewo (1986)
LASIII	UD	50	790	Jansson and Leckie (1992)
CAS	UD	25	350-500	Sorenson and Holmes (1996)
CAS	UD	41	420	Walter and Ravichandran (1995)
CAS	UD	37	444	Corning
CAS	UD	37	430±30	Beyerle et al (1992a)
CAS	UD	37	330	Bleay et al (1992)
CAS	UD	37	334	Harris et al (1992)
CAS	CP	37	210	Bleay et al (1992)
CAS	CP	37	194	Corning
CAS	CP	37	210	Harris et al (1992)
CAS	CP	38	230±20	Beyerle et al (1992b)
BMAS	UD	N/Q	416-500	Kim and Katz (1988)

N/Q = not quoted

The initial linear portion of both the UD and 0,90° can be used to solve for E_m and E_f by the rule of mixtures where the modulus of a transverse ply is taken as that of the matrix alone. This approach yields E_m= 98.4GPa and E_f =170GPa. The value for E_f compares to 171GPa given by Fischbach et al (1988) and is within the range given by Pysher et al (1989) at 140-170 but is slightly below the 180GPa reported by Berger et al (1995). The matrix elastic modulus appears similar to that reported for CAS (97-100GPa) and above that reported for LAS (85GPa).

Several authors have investigated the strain rate sensitivity or static fatigue of GCMCs under room temperature conditions, e.g. Vaidya and Chawla (1994), Spearing et al (1994) Karandikar and Chou (1993), Sorenson and Holmes (1996) and Martin et al (1995). Vaidya and Chawla found increasing the strain rate enhanced catastrophic failure of PRD-166 fibre reinforced borosilicate glass. Strain rates of 8×10^{-4} to 0.08/ min were used. They found the monolithic glass was *stronger* at lower strain rates due to macroscopic crack branching. Similarly the composite strength was found to be higher with *lower* strain rates. Spearing et al (1994) subjected CAS/Nicalon to static loading and found cracking developed at stresses below that normally expected for matrix cracking and higher crack densities. The findings were attributed to stress corrosion cracking of the matrix; they used this as the basis of a subcritical crack growth model. Karandikar and Chou (1993) observed that crack growth in CAS/ Nicalon was environmentally driven depending on the maximum load and time. The crack densities were similar between static fatigue and cyclic fatigue tests for a variety of different composite lay-ups. Sorenson and Holmes (1996) reported the effects of loading rate on UD CAS/Nicalon. They found that the strength and the microcracking threshold both increase with the loading rate. The average fibre pull-out lengths and matrix cracking saturation densities were found to decrease with increasing loading rate. The results were explained by stress corrosion and an increase in the interfacial shear strength with loading rate. Martin et al (1995) tested 0,90° CAS/Nicalon at four strain rates from 0.0005 to 20/s. The pull-out lengths were found to decrease with increases in strain rate except for the fastest rate. The mean crack spacing was found to contradict the trend of larger spacings with higher strain rates observed by Sorenson and Holmes. These crack spacings ranged from 202.6μm at the lowest strain rate to 163.6μm for Martin et al (1995) and compare to 100 to 180μm respectively as measured by Sorenson and Holmes (1996). The apparent disparity may point to the difficulty in measuring crack spacings with no applied load. Many researchers have observed total crack closure upon load removal (as with a broken specimen). Of these Beyerle et al (1992b) and Marshall and Evans (1985) provide example micrographs of the same area under load and without: the cracks disappear and this therefore leaves a question mark as to the validity of crack spacing measurements under no load situations. Kim and Katz (1988) noted in a BMAS/Nicalon system that crack closure in flexure occurred at stresses below 85% of the peak load. This problem is likely to be exacerbated in systems where the axial matrix residual stress is compressive as crack closure is likely to be more pronounced. For this reason the matrix crack spacing has not been studied

from broken specimens.

The apparent increase in the 0° ply matrix cracking threshold and the ultimate strength show that in common with CAS/Nicalon the current composite system is highly strain rate sensitive.

The tensile stress/strain curves of the 0,90° and UD composites can be compared with respect to the fibre volume fraction aligned in the loading direction (Prewo et al, 1989) by the assumption $\sigma_{0,90^\circ} = \sigma_{UD}(V_f^{0,90^\circ}/2)/(V_f^{UD})$. A very close correlation can be attained after saturation cracking in the 0° plies has occurred (fig 4.10). This shows the matrix becomes less of a contributory factor to the stress/strain performance at high strains. However the strength of the 0,90° composite is always higher than would be expected from considering the volume fraction of fibres aligned in the loading direction and the UD strength results. This can be seen by comparing the maximum strains attained in the plots of figures 4.4 and 4.6. The 0,90° composite is clearly able to withstand a greater strain and therefore extracts greater strengthening from the aligned fibres. Thus the delamination splitting which originates at the sample section change is responsible for reducing the ultimate strain capability of the UD composite. Although not highlighted this can be observed for CAS/Nicalon, e.g. Beyerle et al, (1992a,b) $\sigma^{0,90}$=230 and σ^{UD}=430 and Harris et al, (1992) $\sigma^{0,90}$=210MPa and σ^{UD}=334MPa.

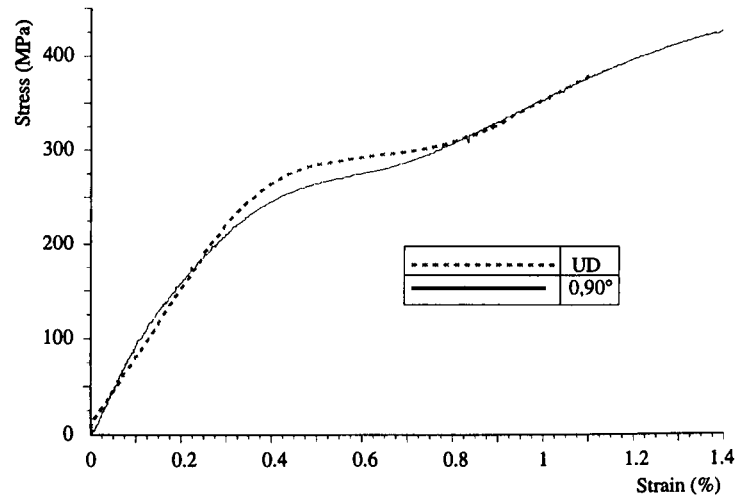

Figure 4.10 Tensile stress-strain curves. 0,90° normal scale, UD scaled according to fibre volume fraction aligned in loading direction

Assuming the same interfacial shear strengths and fibre ultimate strengths for the UD and 0,90° BMAS composites simple arithmetic suggests the UD BMAS/Tyranno failure stress should be as high as 747MPa at the highest rate and 632MPa at the lowest testing rate from aligned volume fraction and fibre strength considerations from the

0,90° results. Such a simple approach can be supported by the model for ultimate composite strength (σ_u) proposed by Curtin (1991):

$$\sigma_u = V_f \sigma_c \left(\frac{2}{m+2}\right)^{1/(m+1)} \frac{m+1}{m+2} \tag{4.1}$$

where m is the Weibull modulus of the fibres and σ_c is the characteristic fibre strength. The above calculation holds if we assume σ_c and m are the same in both composites. The premature failure of UD BMAS/Tyranno explains why no deviation is evident in the elastic modulus in the final stages of testing unlike the 0,90° material where marked deviations associated with statistically distributed fibre failures contribute to the ultimate strength through their ability to sustain stress by load transfer via the shear stress across the interface. The failure mode suggests the UD BMAS/Tyranno is sensitive to defects such as notches whereas the 0,90° is not. This presumption will be tested later in this chapter.

We can further utilize equation 4.1 above and substitute approximate values for the fibre Weibull modulus to obtain an approximate value for the characteristic fibre strength σ_c. For an ultimate strength of 400MPa for 0,90° BMAS/Tyranno and large m values, σ_c approximates to ~2.1GPa. However to obtain realistic values for m and σ_c we can utilize the graph produced below (figure 4.11). If no fibre degradation is assumed during manufacture the fibre strength of ~2.5GPa yields m = 18. Fischbach et al (1988) suggest σ_c > 2.75GPa for as received Tyranno and m = 7.3. This strength is a high value compared to that quoted for single Tyranno fibres tested by Berger et al, (1995) and Pysher et al (1989). With this m value the strength of the fibres within the composite comes out as 2.83GPa. For such a high strength we must assume the fibres have undergone no chemical or mechanical damage during manufacture.

The above fibre characteristic strength can also be used to evaluate the average fibre pull-out length, *h*:

$$h = \lambda(m) r \sigma_c \,/\, 4\tau \tag{4.2}$$

where λ(m) approximates to unity for m > 3 (Beyerle et al, 1992a). Therefore we can expect average pull-out lengths of the order of 200μm to 100μm for τ=15-30MPa.

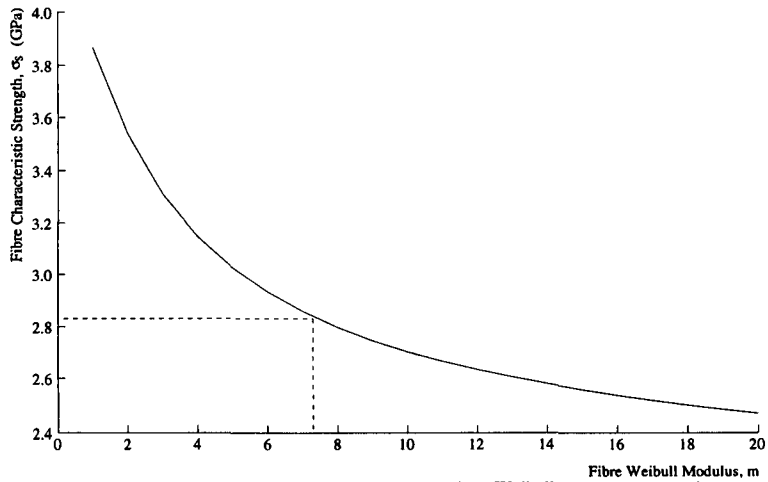

Figure 4.11 Dependence of fibre characteristic strength on Weibull modulus. Composite strengt of 400MPa assumed for 0,90° BMAS/Tyranno (NPP7)

Such a prediction should be considered in conjunction with figure 4.8 where the fibre pull-out lengths are far in excess of this value suggesting a much lower value for τ prevails. For τ = 5MPa the average pull-out length prediction becomes 600μm.

4.2.2 Models for τ Evaluation

To estimate values of the interfacial shear stress we can employ models by Aveston, Cooper and Kelly, (1971) and Zok and Spearing (1992). ACK provide two means of calculating τ: via the matrix crack initiation (mci) stress, (σ_{mc}), and the matrix crack spacing (mcs) at saturation, d_s. These equations are given below:

$$\frac{\sigma_{mc}}{E_c} = \left(\frac{6\tau\Gamma_m E_f V_f^2}{E_c E_m^2 R V_m}\right)^{1/3} - \frac{q}{E_m} \tag{4.3}$$

$$\tau = \frac{1.34 V_m r \sigma_{mu}}{2 V_f d_s} \tag{4.4}$$

The results from the monotonic tensile testing shows σ_{mc} varies with the testing rate. The results displayed in Table 4.2 use the upper and lower mci stresses. For the matrix crack spacing calculations a matrix ultimate strength is necessary (σ_u). This value is taken as 100-150MPa. The results table quotes values for both stresses. In the initial ACK paper the saturation spacing was stated to lie between x and 2x, the load transfer length. Kimber and Keer, (1982), found this spacing was 1.3376 × x, which is included in (4.4) above.

Zok and Spearing (1992) suggest a different saturation crack spacing method:

$$\frac{d_s}{r} = \chi\left[\frac{\Gamma_m V_m^2 E_f E_m}{V_f \tau^2 E_c r}\right]^{1/3} \tag{4.5}$$

where χ is a crack evolution coefficient which they suggest might be 1.6.

Table 4.2 Results of interfacial shear stress evaluation

Model		Γ_m (J/m^2)	τ (MPa)
ACK mci	σ_{mc}= 375MPa	25	18.7
		20	23.4
	σ_{mc}= 245MPa	25	4.0
		20	5.0
ACK mcs	σ_u = 150MPa		25.8
	σ_u = 100MPa		17.2
Zok &		25	90.9
Spearing		20	101.7

The values of τ given above vary considerably for the different models used. Closest approximations to the values obtained in chapter 3 by direct measurement methods are obtained for the highest matrix fracture strength with the ACK mcs method. A similar result was observed for the ACK mci method for the highest σ_{mc} level. The model proposed by Zok and Spearing (1992) gave excessively high values for τ which will be disregarded.

The above calculations are only valid for small debond energy (SDE) materials and it is likely the BMAS/Tyranno tested here fits into the large debond energy (LDE) category of composite due, in part, to the limited development of the interface. A LDE at the interface may lead to closer matrix crack spacing than that developed in a SDE material. Since, in the Zok and Spearing model τ is directly proportional to $d_s^{-3/2}$, smaller crack spacing data would increase the apparent sliding stress. A value of 20-25J/m^2 for the matrix fracture energy has been prescribed by Evans (1993): researchers have used Γ_m values for CAS of 6Jm^{-2} (Pryce and Smith, 1992) to 80Jm^{-2} (Kim and Pagano, 1991).

4.2.3 Tensile v Flexure

The first inflection of the stress strain curve for both tensile and flexural testing of cross-ply BMAS/Tyranno relates to microcracking in the 90° plies. However the first cracking level differs by as much as 55MPa for the different testing methods. This can be explained by the ply thickness, sampled volume and stress levels in the various plies.

In a tensile test the whole of the gauge section is subjected to the same stress, cracking commences in the thickest 90° ply (the 90/90° central ply) as the cracking stress in a 90° ply is proportional to the ply thickness. In a flexural test the stress experienced by the central ply is minimal (10% of tensile and compression surface stress prior to matrix cracking in the current $[0.90°]_{4s}$ BMAS/Tyranno). Therefore the first ply to crack is the thinner 90° ply nearest the tensile surface. The maximum stress in this ply is only 80% of the stress at the specimen surface. The final factor is the much lower sampled volume than in a tensile test. The outer ply orientation also favours a higher than expected flexural elastic modulus (flexural E_c of 119 compares to tensile 112GPa).

The UD composite on the other hand shows much closer accord between the two testing methods when comparing both elastic modulus (flexural 120GPa against tensile 122GPa) and initial cracking stress (290-340MPa against 290-350 for the intermediate testing rates) due to the greater uniformity of the fibre orientation.

4.3 Load Cycling

To complement the monotonic tensile testing a series of cyclic loading experiments have been performed on UD and 0,90° BMAS/Tyranno. Damage evolution has been assessed through elastic modulus decrements, matrix cracking and hysteresis loop width evaluation.

4.3.1 Incremental Cycling

Load cycling increments of either 25 or 50MPa have been employed. Crack evolution was observed by acetate surface replication. The cyclic stress- strain plots for 0,90° and UD BMAS/Tyranno can be viewed in figures 4.12 and 4.13 respectively. During cycling, damage became manifest as a reduction in the loading and unloading elastic modulus (Figure 4.14). A loading cycle, subsequent to the microcracking threshold stress, can be typified by three sections (Fig. 4.15): (i) an initial elastic modulus within 5% of the uncracked composite modulus (122GPa), see table 4.3; (ii) an ostensibly constant elastic modulus to the previous maximum applied stress, and; (iii) a damage development zone above the previous applied maximum stress. The relative proportion of these sections changes with the maximum applied stress. At low stresses (ii) and (iii) only are evident. When high stresses are applied region (iii) is not discernible.

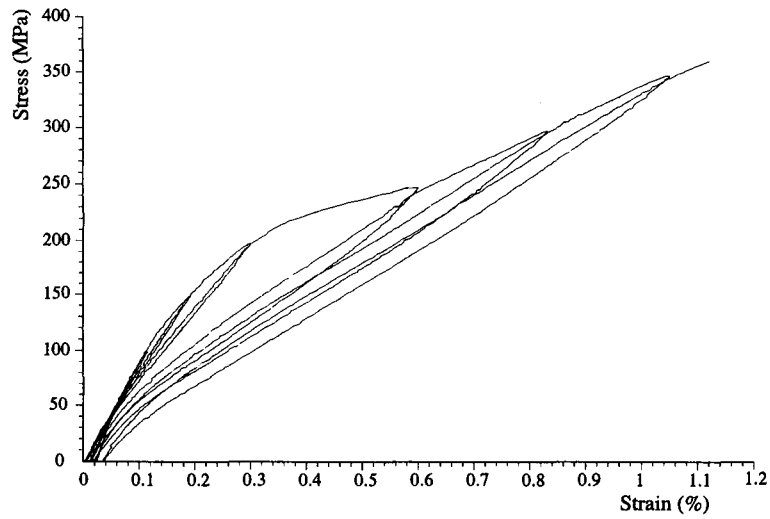

Figure 4.12 Incremental cycling of 0,90° BMAS/Tyranno (NPP7)

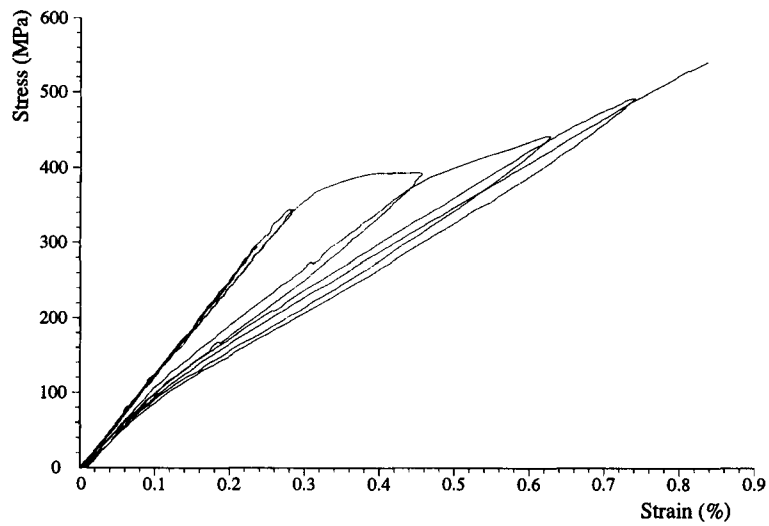

Figure 4.13 Incremental cyclic loading of UD BMAS/Tyranno (NPP17)

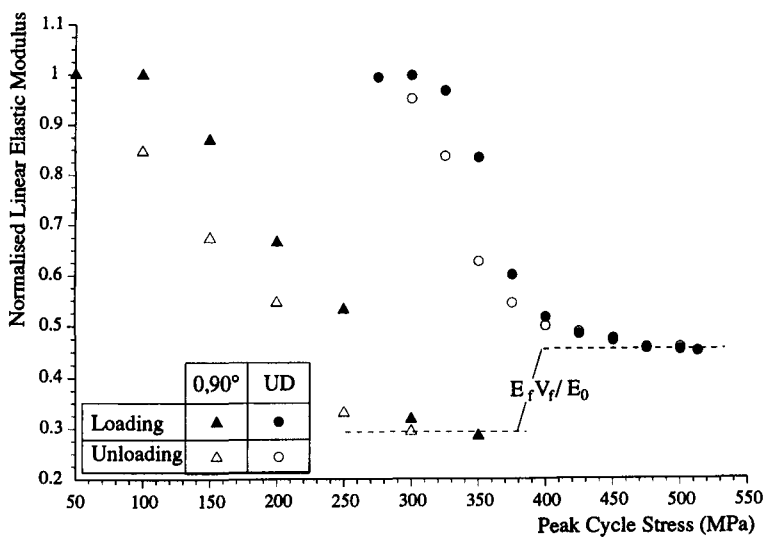

Figure 4.14 Normalised linear elastic moduli from incremental cyclic loading for 0,90° and UD BMAS/Tyranno

Table 4.3 Loading and unloading moduli from cycling of UD BMAS/Tyranno

Peak Stress, σ_p (MPa)	Loading		Unloading	
	$E_{0\text{-}30}$	E_{lin}	$E_{\sigma_p\text{-}30}$	E_{lin}
300	123.5	123.0	125.0	125.2
325	122.0	122.8	126.0	120.9
350	122.5	109.5	116.3	106.9
375	126.0	73.8	95.6	77.1
400	120.5	63.5	77.7	66.9
425	116.0	59.4	80.4	61.4
450	125.0	57.8	75.0	59.9
475	122.0	56.1	76.3	58.3
500	118.4	55.6	78.5	56.2
513	116.9	55.3	n/a	n/a

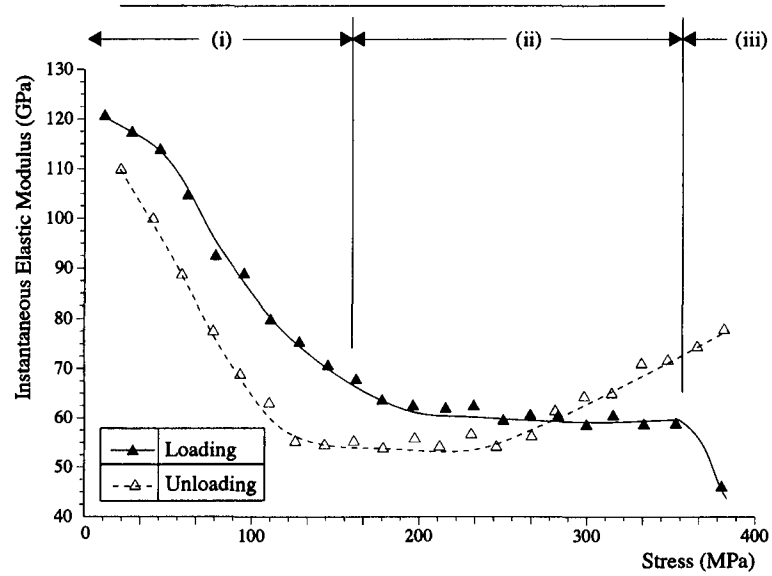

Figure 4.15 Instantaneous elastic modulus for loading and reloading to 400MPa for UD BMAS/Tyranno

The elastic loading moduli of figure 4.14 are obtained from region (ii) (fig 4.15) in all cases. Unloading moduli are taken from the minima as in figure 4.15. The loading elastic modulus seems to decrease linearly between 100 and 300MPa for the 0,90° composite but is not linear for the UD. A similar result was seen for CAS/Nicalon by Domergue et al (1996). Both BMAS/Tyranno composites' moduli reach a plateau level as their respective ultimate strengths are approached. This level is due to the stiffness of the fibres in the loading orientation (i.e. E_fV_f for UD and $E_fV_f/2$ for 0,90°).

The modulus apparent from the unloading cycle (fig 4.15) is initially high when the load is being removed but this succumbs to a linear region similar to (ii) above. Whereupon the modulus again increases at low stresses but not to the same magnitude as during loading.

During cyclic loading upon removal of the load most of the strain was recovered (fig 4.16). For the UD BMAS/Tyranno a small permanent strain was introduced once matrix microcracking was initiated. This level of permanent strain was maintained until a peak applied stress in excess of 450MPa was applied at which point the remnant strain increased fourfold. The 0,90° BMAS/Tyranno showed a gradual increase in the permanent strain to 300MPa but it seemed to increase above this peak stress. The permanent strain reaches a similar level for the UD and 0,90° lay-ups.

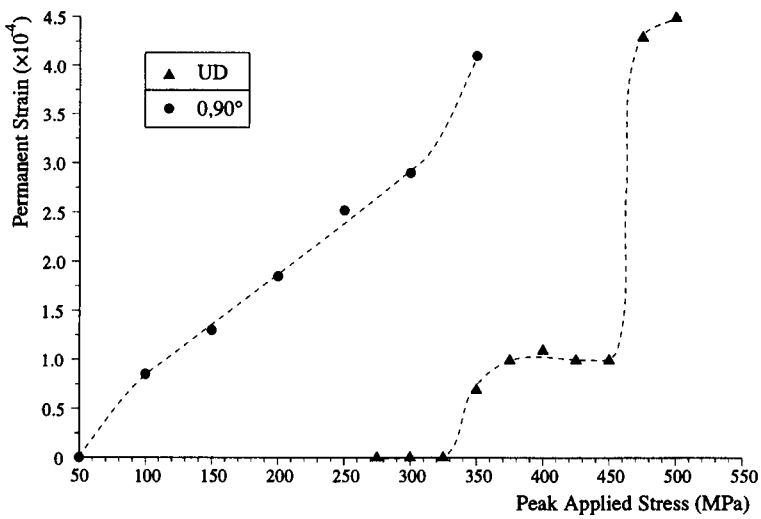

Figure 4.16 Evolution of permanent strain upon removal of the applied stress during incremental cyclic loading of both UD and 0,90° BMAS/Tyranno

The maximum hysteresis loop widths measured at half the cycle peak stress (Fig. 4.17) increase with the applied stress (fig 4.18) and reach a plateau level from approximately 400MPa for the UD lay-up. The 0,90° loops do not obtain to a plateau level.

If the hold time at the cycle peak stress was brief then on subsequent reloading further damage could be observed by inflections of the stress-strain graph prior to the previous peak stress being reached (fig 4.19 with ×2 enlargement).

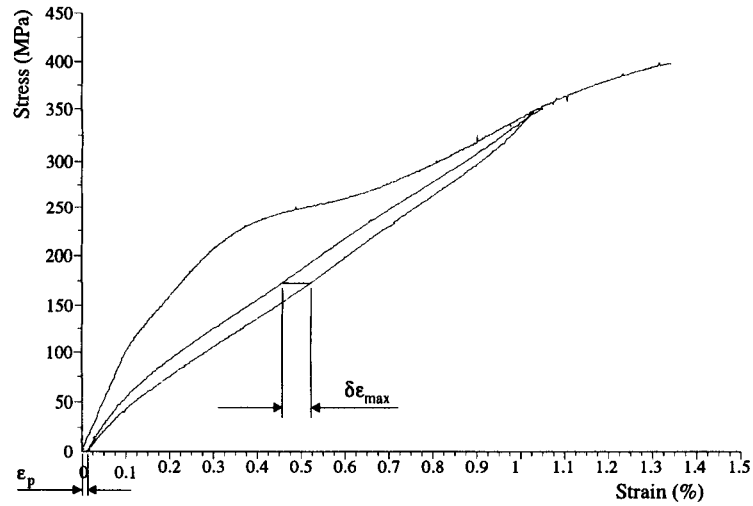

Figure 4.17 Loading/Unloading cycle for hysteresis loop width measurement, $\delta\varepsilon_{max}$, and permanent strain, ε_p

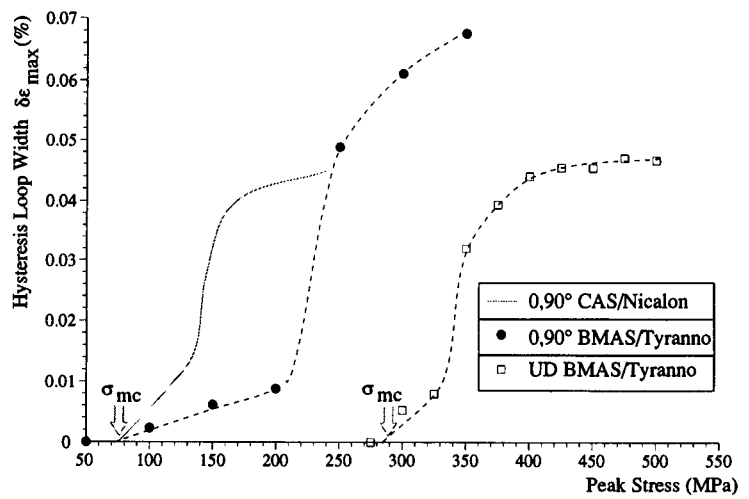

Figure 4.18 Hysteresis loop widths from 0,90° CAS/Nicalon (Domergue et al, 1996) and UD and 0,90° BMAS/Tyranno

The elastic modulus measured during cycling only falls below that expected from the fibre contribution, ($E_f V_{f\{\text{in loading orientation}\}}$), near the composite ultimate tensile strength (UTS) for both fibre architectures (fig 4.14). The saturation microcracking level has been identified as ~400MPa but the matrix contribution to the linear elastic modulus is present until stresses above 475MPa. This implies that at least some of the interface is still bonded above 400MPa. The linear elastic modulus for LAS/Nicalon also seems to tend to $E_f V_f$ during cycling (Prewo and Brennan, 1986). Similar results for CAS/ Nicalon are not available in the literature as the unloading modulus is always higher than $E_f V_f$ (e.g. Domergue et al, 1996; Cady et al, 1995; Beyerle et al, 1992b). A possible explanation lies in the more stable debonding for interfaces subjected to residual compression (Evans, 1990).

The loop widths are used in this instance for two purposes: to predict the interfacial

shear stress and provide a means of estimating the 90° ply cracking stress. These will be dealt with in a later section.

A stress-strain curve can be assembled from the increments from successive cycles (fig 4.20). This plot is compared to the 0.2mm/min cross head speed monotonic tests. There seems to be only a small difference at the 0° ply microcracking stresses. This is probably due to the hold times during the cyclic tests where time dependent deformation was observed.

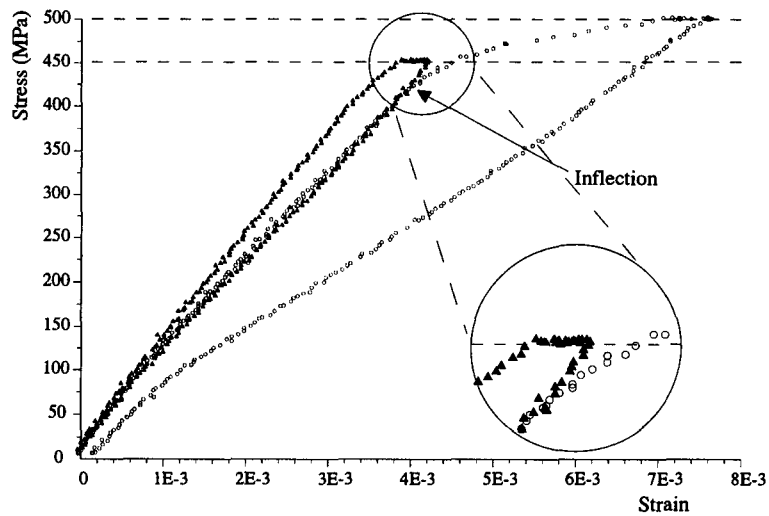

Figure 4.19 Two loops from an incremental cyclic test. Note inflection below previous peak stress and damage sustained during unlod/load cycle

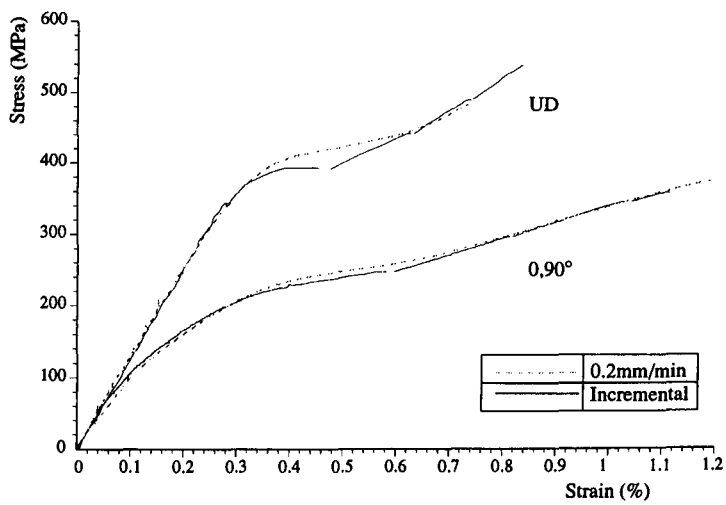

Figure 4.20 Incremental and monotonic (0.2mm/min) stress/strain behaviour compared for UD and 0,90° BMAS/Tyranno

Two factors can be identified to explain the elastic moduli disparity between loading and unloading at low stresses (where crack closure is prevalent) and at the peak stress (table 4.3). From the two hysteresis loops of figure 4.19 several observations can be made: some damage mechanism is operating during the hold time (note the strain increase while at 450MPa), and damage initiates on the second cycle before the

previous peak stress (450MPa) was reached resulting in an increased strain when loaded to 450MPa the second time. Clearly the damage is still evolving during the relatively short hold time at stress so it is not inconceivable that further cracking can occur during the initial unloading. Strain increments during this phase of unloading would appear to increase the unloading elastic modulus. With lower applied stress the cracking is able to stabilise and reach the plateau level seen in figure 4.13. The second contributory factor to the elastic moduli disparities could be due to a variation in τ. Thomas et al (1993) proposed the static coefficient of friction is much greater than the dynamic. Such a finding has also been observed in indent and push-though testing by Daniel et al (1997). Hence when the loading is interrupted or reversed the static coefficient of friction dominates. As more of the interface slides the friction decreases to the dynamic coefficient of friction.

The permanent strain offset can be used to evaluate the residual stress state for composite systems where $\alpha_m > \alpha_f$ (Vaggagini et al, 1995). For the UD BMAS/Tyranno where $\alpha_m < \alpha_f$, the permanent strain is very much lower and only becomes appreciable above 450MPa. The small offset strain above 325MPa can be associated with bulk matrix cracking. The exact cause is not known but may be from fibres broken during manufacture or fibre or ply straightening. The large increase above 450MPa can only be the result of either matrix fragments inhibiting crack closure and thus inducing a permanent strain or the loss of stored fibre elastic energy due to fibre fracture or lateral offset between closing crack faces resulting in poor fracture surface mating.

A value for the fibre residual stress state can be obtained simply by calculating the y-axis intercept for the linear region of the unloading portion of the stress-strain curve. This intercept obtains to a plateau level for the UD BMAS/Tyranno at ~25MPa. If we consider this is a composite stress and that the matrix is fully decoupled from the fibres, i.e. the fibres assume all of the load, then residual fibre stress, σ_f = y-Intercept/V_f. The value of ~75MPa compares to that calculated from the residual strain found in chapter 3 from thermal expansion measurements of 82.9MPa. The result is not expected to be exact but provides a useful approximate measure of the fibre stress once the matrix crack saturation level is reached. The result is also subject to errors from fibre failures and the simple calculations used in the residual stress calculations of chapter 3. Similar findings are apparent with the cyclic testing of 0,90° BMAS/Tyranno.

The linear increase in ε_p for the 0,90° composite is due to the release of residual stress

from the 90° plies. The large increase above 300MPa is probably due to fibre failures.

4.3.2 Cyclic test with prolonged hold

Cross-ply BMAS/Tyranno has been subjected to a prolonged hold time at 250MPa. The cyclic loading employed three minute hold times at all stresses except 250MPa where a 24hour hold time was used. After the 24hour hold the incremental cycling was continued to failure.

During the three minute hold times a time dependent deformation was seen for all except the 50MPa maximum applied stress (Table 4.4). During the 24hour hold period an additional strain of ~0.2% was observed. Unlike the previous cyclic tests, on each subsequent loading it appeared no extra damage was introduced as the same strain was attained at the previous maximum stress, i.e. during a reload the stress strain plot passed through the previous maximum stress/strain point (fig 4.21).

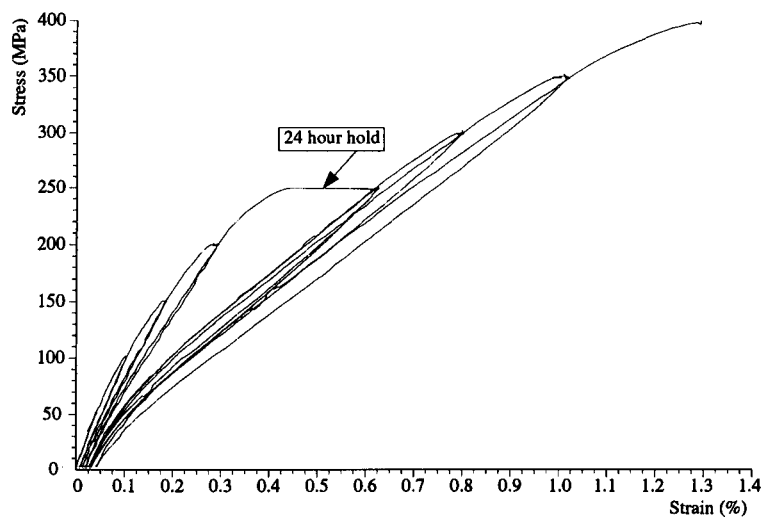

Figure 4.21 Results of incremental cycling with hold times of three minutes. Hold tin at 250MPa was 24hours. BMAS/Tyanno 0,90° tile NPP7

Table 4.4 Time dependent strain increments for 0,90° BMAS/Tyranno with 3 minute hold times and 24hours a 250MPa

Max. Stress (MPa)	Strain 2 $\times 10^{-3}$	Strain 1 $\times 10^{-3}$	Strain Diff. $\times 10^{-3}$
50	0.701	0.701	0
100	1.324	1.284	0.04
150	2.154	2.025	0.129
200	3.211	3.063	0.148
250*	6.540	4.624	1.916
300	8.277	8.124	0.153
350	10.450	10.230	0.22

* 24 hour hold time

Cracking of 90° plies in BMCs is considered to occur almost instantaneously (Xia et al, 1993, Karandikar and Chou, 1993). This can be seen in the very small increase in strain at 100MPa which is above the 90° ply cracking threshold. Time dependent damage is induced at all the other peak stresses. The time dependent extension could be due to matrix crack growth due to stress corrosion cracking (SCC) by diffusion of water molecules at crack tips reducing the matrix fracture toughness in the presence of moisture (Weiderhorn, 1967; Michalske and Freiman, 1983). As an alternative to reductions in the matrix fracture energy it is proposed time dependent debonding of the interface would have the same effect by decoupling the fibre and matrix blocks with a subsequent increase in composite strain. Bonding susceptible to SCC by water molecules is known to exist at the interface in BMAS/Tyranno (Cain, 1995) where Si-O bonds at the interface were observed by electron energy loss spectroscopy (EELS). It is suggested the interface contains less of these bonds than the matrix but in the presence of a debond crack front and an additional driving force from the residual tension believed to exist at the interface the effects of breaking these bonds would have a correspondingly greater effect on the composite strain accumulation.

4.4 Notch Testing

Notch sensitivity is an important factor for these composites since applications will require the joining of components. Mechanical connectors such as rivets and bolts should not act as catastrophic failure initiators. Notches of various depths were cut into samples of larger nominal width (5mm) for tensile testing.

4.4.1 Notch sensitivity of Cross Ply BMAS/Tyranno

Notch depths were chosen to give notch to width ratios of 0 (normal tensile test), 0.05,

0.01, 0.2 and 0.3. These ratios correspond to notches of 0.25, 0.5, 1 and 1.5mm cut into either side of the 0,90° tensile specimens cut from tile NPP10. The apparent extension over 25mm was recorded. However it is acknowledged these readings do not relate to the strain as the extension is concentrated in the notched zone.

Unfortunately it has only proved possible to test one specimen at each notch depth to width ratio so no statistically valid conclusions can be drawn. SEM of the fracture surfaces (Fig 4.22) shows cracks emanating from the notch root and either traversing the specimen directly or deviating across the 0° plies at an obtuse angle before reorienting normal to the 0° fibre direction.

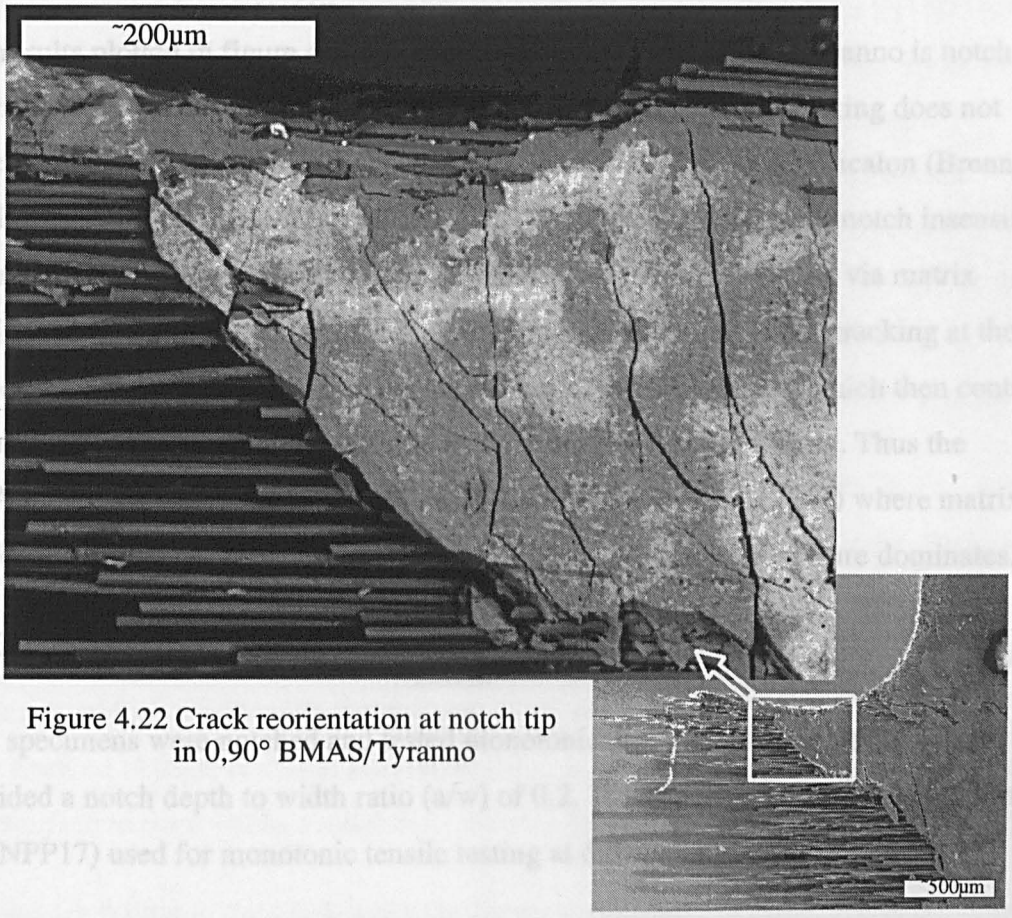

Figure 4.22 Crack reorientation at notch tip in 0,90° BMAS/Tyranno

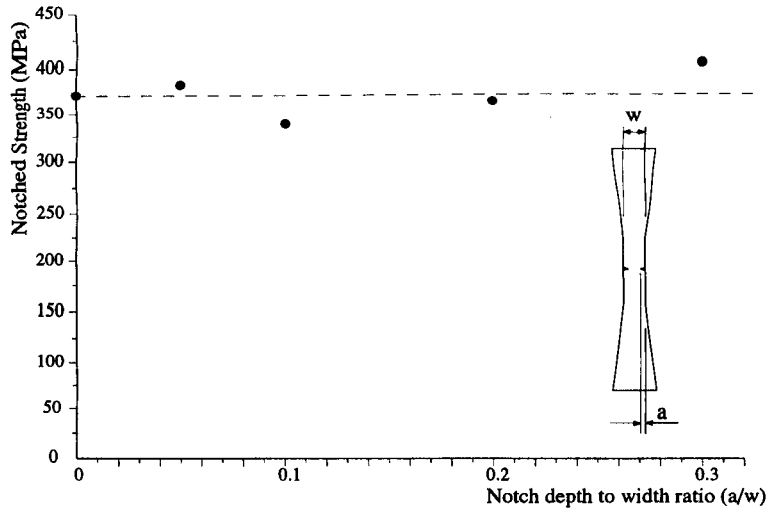

Figure 4.23 Effects of notch depth to width ratio on the tensile strength of 0,90° BMAS/Tyranno at room temperature

The results plotted in figure 4.23 appear to show the 0,90° BMAS/Tyranno is notch insensitive under the testing conditions. That is, the matrix microcracking does not affect the failure strength. CAS/Nicalon (Cady et al 1995) and LAS/Nicalon (Brennan and Prewo, 1982) with 0,90° architecture have both been shown to be notch insensitive. The relief of stress concentrations is effected by a stress redistribution via matrix cracking. In this way the notch is effectively blunted by matrix microcracking at the root of the notch. The matrix microcracking leaves the fibres intact which then control the ultimate strength as with standard tensile testing of these materials. Thus the BMAS/Tyranno is a 'Type II' material according to Evans et al, (1993) where matrix microcracking precedes failure as opposed to 'Type I' where fibre failure dominates.

4.4.2 Notch testing of UD BMAS/Tyranno

Two specimens were notched and tested monotonically. The notch depth of 1mm provided a notch depth to width ratio (a/w) of 0.2. The specimens were from the same tile (NPP17) used for monotonic tensile testing at different strain rates earlier.

The two notched specimens tested failed at 398 and 385MPa at a loading rate of ~5MPa/s which is much lower than the strength at even the lowest testing rate. Using the extensometer to observe gross matrix microcracking by non-linearity within its 25mm span, cracking seemed to start at 220-230MPa from which point the stress/ extension curve showed a rapid increase in extension for small increases in applied load. The fracture was unlike the 0,90° notched samples. Failure seemed to initiate at the notch root and propagate at an oblique angle to the fibres. This process occurred from both the notches but in opposite directions. The fracture faces showed very little

pull-out but concentrations of 'pulled-out' fibres could be observed at the notch root and at points where the crack orientation reversed (fig 4.24).

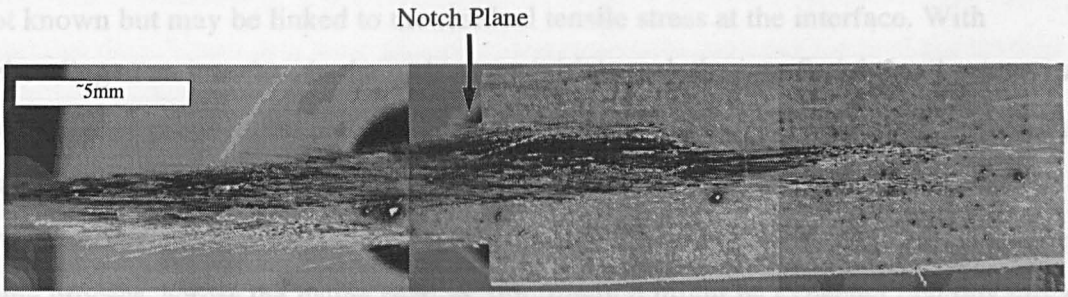

Figure 4.24 One half of a failure during notch testing of UD BMAS/Tyranno
The other half of the sample was identical

From the strengths realized by the previous tensile testing it appears the UD BMAS/ Tyranno is notch sensitive, this contrasts with the apparent notch insensitivity of the 0,90° tests above. The sub 400MPa notched strengths compare to a minimum unnotched UTS of 511MPa at a very much lower testing rate (~5hours to failure compared to ~80s for the notched specimens). The low ultimate strength is only marginally above the matrix cracking threshold which varies between 246 and 375MPa depending on testing rate. Brennan and Prewo (1982) found a UD LAS/Nicalon, equivalent to the 0,90° composite mentioned above, displayed 'slight' notch sensitivity.

The mixed mode crack opening at the crack front seems to promote fibre failure with negligible pull-out. It is not known whether these fibre failures occur in the crack path or wake. If the fibre failure takes place in the crack path the implication is that debonding does not occur when the matrix crack approaches at an oblique angle. Such a finding would be at odds with the analysis of He and Hutchinson (1989) who, from their work on oblique cracks at interfaces, calculated a lower impingment angle relaxed the interface to fibre fracture toughness criterion to values over 0.25 (see eq 2.3).

If fibres are failing in the crack wake the suggestion is that the additional debonding in the crack wake described by Charalambides and Evans (1989) is not occurring.

The apparent failure pattern is that of a crack which initiates at the root of the notch. As with the propagation of cracks in the 0,90° BMAS/Tyranno the shear between the stressed and unstressed sections results in a crack approximately parallel to the fibres. In the 0,90° composite further crack growth sees a realignment of the crack normal to the 0° fibres. In the UD composite the crack does not become realigned and seems to become unstable ultimately causing the premature failure such that initial

microcracking and failure are not discrete events. We can therefore infer that in this composite system the 90° plies play an important role in deviating the crack path to pass normal to the 0° fibres. The reason for the crack instability in the UD composite is not known but may be linked to the residual tensile stress at the interface. With debonding at an interface in the path of the initial crack the interfacial tensile stress may form an easy propagation path which is not present in composites where $\alpha_m > \alpha_f$. The crack path will then orient parallel to the fibres. With a 0,90° ply arrangement the propagation route is restricted by the 90° plies which will encourage the crack, by the same process, across the gauge section. Intuitively it might be expected that this process will force the crack, in the worst case, to traverse the sample at 45° until coalescence occurs with a similar crack emanating from the other notch.

In addition to the above explanation bending moments may affect the fracture behaviour. These may be introduced by the non-symmetrical crack formation and propagation from the notches or be present from specimen misalignment, inaccurate machining of specimens or even application of the extensometer. These bending moments can all be minimized but cannot be totally eradicated. It could be that UD specimens are more susceptible to such strains. Such susceptibility may stem from an inability to reorient a propagating crack in the absence of the transverse fibres as suggested above. To have such a large effect on the composite strength the fibres in the crack path or wake must fail. Thus transverse shear across the fibres introduced from the bending moment could be the cause.

A single sample with smaller notches has also been tested but with a prolonged hold at 400MPa. The 0.5mm notches represented a depth to width ratio of 0.1. Failure occurred during this prolonged hold after 18minutes. The strength therefore appears higher than the results above which could indicate the depth of the notch effects the strength adversely.

4.5 Interfacial Properties from Cyclic Loading

Researchers at the University of California, Santa Barbara (Vaggagini et al, 1995, Domergue et al, 1995 and Domergue at al, 1996) have developed a methodology for evaluating composite constituent properties from hysteresis measurements. In the proceeding section these methods will be applied to the unidirectional BMAS/Tyranno composite system. The model assumes Poisson ratios for composite, fibre and matrix

are the same. Also type II boundary conditions apply where reinforcement is unidirectional within a matrix divided into a double periodic hexagonal arrangement.

From the cyclic loading of tile NPP17 it was possible to obtain instantaneous elastic modulus data. These data were plotted as the reciprocal modulus (termed the inverse tangent modulus, ITM) against instantaneous stress for both loading (fig 4.25) and unloading (fig 4.26) conditions.

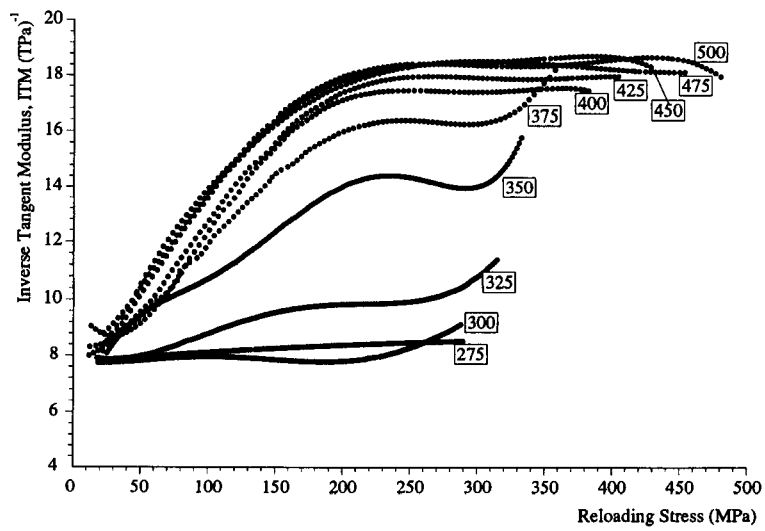

Figure 4.25 Inverse tangent moduli during reloading of UD BMAS/Tyranno
Peak Stresses (MPa) are indicated

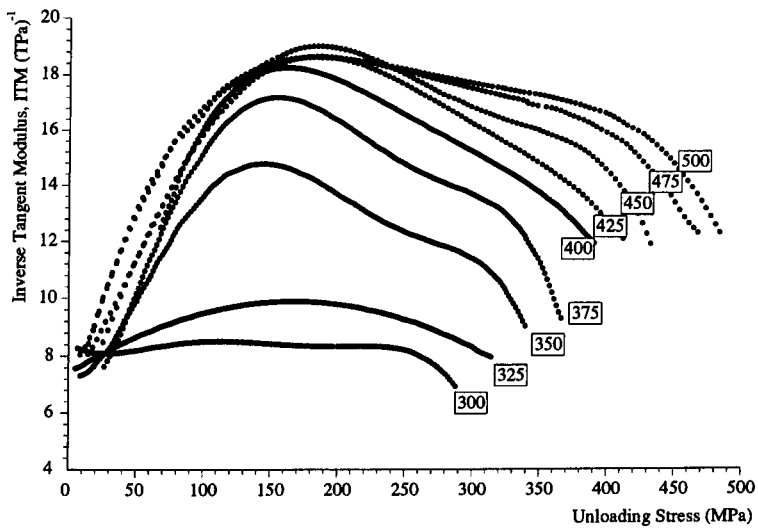

Figure 4.26 Inverse tangent moduli during unloading of UD BMAS/Tyranno
Peak stresses (MPa) are indicated

From the data reported in Chapter 3 and obtained by fibre indent and push-out testing the debond energy was found to be high. Schematic forms for ITM are presented for large debond energy materials in figure 4.27 (Domergue et al, 1995). As with the LDE SiC/Nicalon system studied by Domergue et al, (1995) the schematic tangent moduli of figure 4.27 are not exactly like the results depicted in figures 4.25 and 4.26. However the BMAS/Tyranno studied here gives reload and unload ITM which are very similar to

their SiC/Nicalon results.

The inelastic strain index, £, can be obtained from the initial slope of the ITM during loading and unloading. This represents the reverse sliding at the interface. At a transition stress, either σ_{tr} or σ_{tu} for reloading and unloading respectively, the reverse sliding at the interface is arrested at the bonded interface. The 'debond' stress, σ_i, can be obtained from the formulae given on figure 4.27 at the transition stresses, where σ_p represents the peak stress.

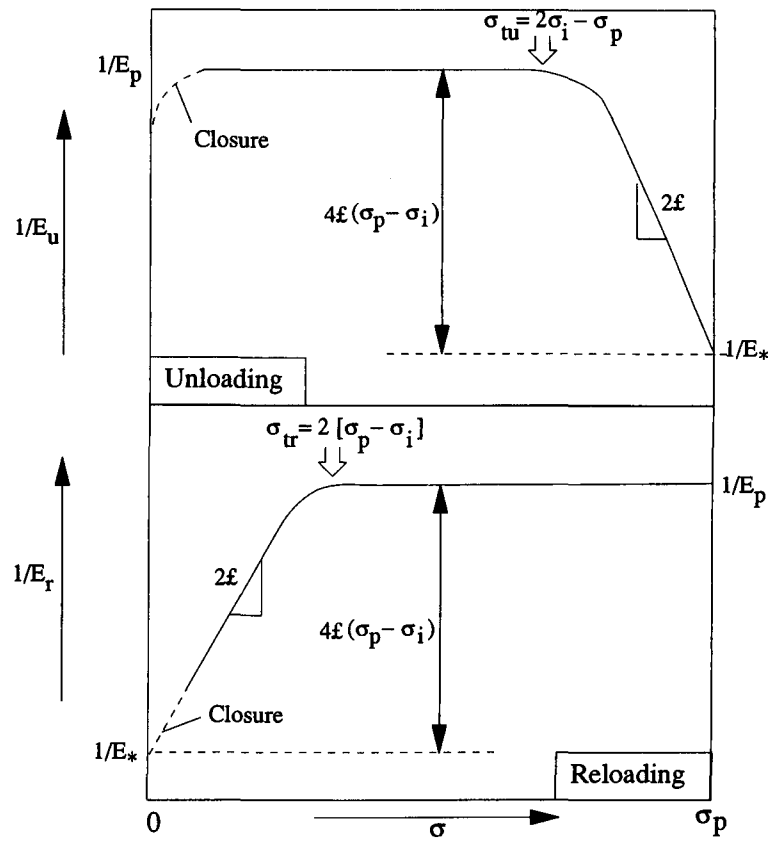

Figure 4.27 Schematic forms of ITM for LDE materials

The data of figure 4.25 indicate that the composite under investigation here has a LDE. This can be seen from the loading ITM curves where, after an initial linear region with slope 2£, a plateau is reached. For SDE materials no constant modulus is attained during loading hence no plateau level is evident in an inverse tangent plot. As with Domergue et al, (1995), and their studies on CAS/Nicalon and SiC/Nicalon the greatest data fidelity with the fibre indent methods was achieved during reloading.

Taking the initial slope provided values for £. These data are presented in figure 4.28. The following equation was used to obtain a value range for τ (plotted on fig 4.28):

$$£ = \frac{b_2(1 - a_1 V_f)^2 R}{4V_f^2 \tau E_m d} \tag{4.6}$$

where b_2 and a_1 are coefficients proposed by Hutchinson and Jensen, (1990):

$$b_2 = \frac{(1+\nu)E_m\{2(1-\nu)^2 E_f + (1-2\nu)[1-\nu+V_f(1+\nu)](E_m - E_f)\}}{(1-\nu)E_f[(1+\nu)E^* + (1-\nu)E_m]} \tag{4.7}$$

and $a_1 = E_f/E_c$. E*as used above is given by:

$$E^* = V_m E_f + V_f E_m \qquad (sic) \tag{4.8}$$

The crack spacing, d, was obtained from a linear interpolation between the values corresponding to matrix crack initiation, σ_{mc}, and saturation, σ_s (Domergue et al, 1995). These thresholds were found from estimates from the monotonic tensile testing and are validated from figure 4.28 where £ > 0 and £ saturation levels are similar to σ_{mc} and σ_s values of 290MPa 400MPa respectively.

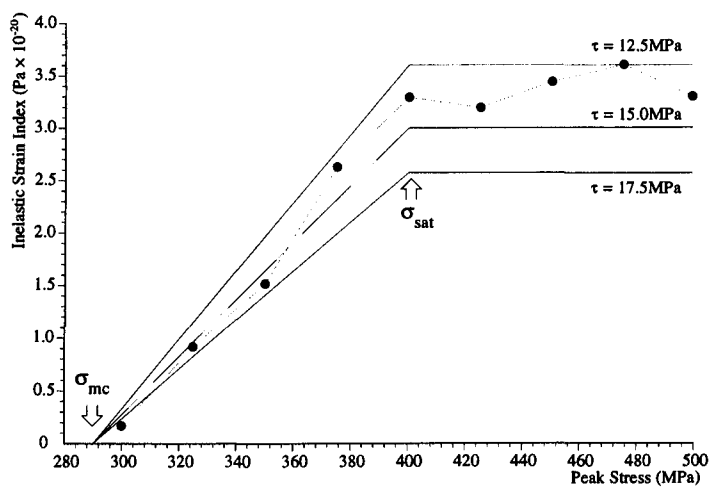

Figure 4.28 Inelastic strain index dependence on peak applied stress. Possible fits for the interfacial shear stress are shown for τ values of 12.5, 15.0 and 17.5MPa

The debond energy, Γ_i, has been estimated from σ_i, obtained from the reloading transition stress, from the following:

$$\Gamma_i = \frac{R}{E_m}[(\sigma_i + \sigma^T)c_1]^2 \tag{4.9}$$

where Hutchinson and Jensen provide c_1 as:

$$c_1 = \frac{(1 - V_f a_1)(b_2 + b_3)^{1/2}}{2V_f} \tag{4.10}$$

and b_3 as:

$$b_3 = \frac{V_f(1+\nu)\{V_m(1+\nu)(1-2\nu)(E_f - E_m) + 2(1-\nu)^2 Em\}}{(1-\nu)V_m[(1+\nu)E^* + (1-\nu)E_m]} \tag{4.11}$$

σ^T is the misfit stress calculated from the misfit strain (see Chapter 3) by:

$$\sigma^T = q_m E_c / E_m \tag{4.12}$$

In this instance the residual matrix stress, q_m, of -44.7MPa was used, as found in chapter 3, leading to a misfit stress of 56.1MPa. This approach gave debond energies of 1.2Jm^{-2} to 2.6Jm^{-2} before saturation.

The magnitude of τ can also be calculated from hysteresis loop widths. The data presented in fig 4.18 has been used. For LDE composites £ can be obtained by:

$$£ = \delta\varepsilon_{max} / 4\sigma_p^2(1 - \sigma_i/\sigma_p)^2 \tag{4.13}$$

when $0.75 < \sigma_i / \sigma_p < 1$. At $\sigma_p/2$ the maximum hysteresis loop width ($\delta\varepsilon_{max}$) occurs. The values of £ with σ_p are plotted in figure 4.29.

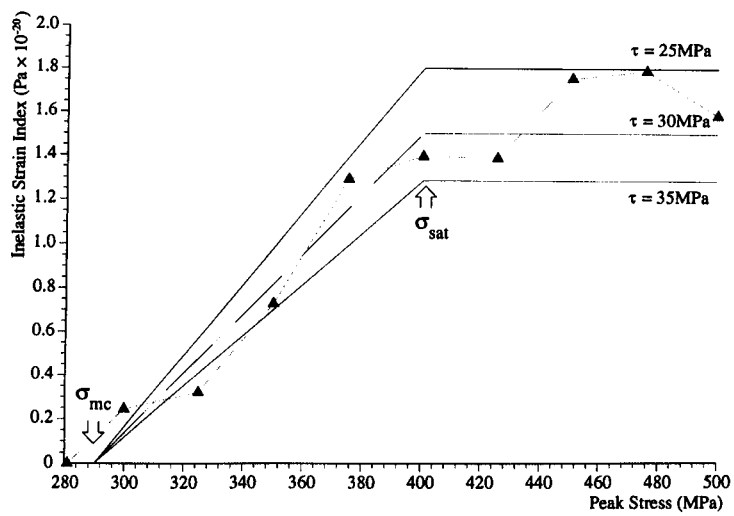

Figure 4.29 Inelastic strain index derived from hysteresis loop widths plotted against peak applied stress. Possible fits for the interfacial shear stress are shown for τ values of 25, 30 and 35MPa

The interfacial shear stress calculated by the two methods presented here varies by approximately 15MPa. The 15MPa from the initial loading slope of the ITM and the 30MPa by hysteresis loop measurements both depend on the 'debond' stress and hence

the measurement of the transition stress, σ_{tu} or σ_{tr}. These stresses could not be determined accurately since the unloading graph (fig 4.26) is not as well defined as the schematic diagram (fig 4.27) and the reloading is subject to distortion from the release of compression within the matrix. Such an effect would be to increase £ during reloading as the loading slope of the ITM curve would be higher. Thus for composites where high residual stresses exist the data from the ITM curve must be considered with care and are likely to underestimate τ.

Of the two shear stress values the hysteresis loop width value of ~30MPa is closest to that found by direct measurement methods in chapter 3. The push-out value of 29MPa may be deemed more accurate than the indent since the data are not subject to such large Poisson expansion effects as with indent testing. The loop width measurements are taken at half the peak applied stress. Thus, for all the stress ranges, the loop width measurements are taken above the maximum crack closure stress of ~150MPa, as observed in the maximum ITM of figure 4.26.

The exact definitions of σ_{tu} and σ_{tr} are also open to debate since the theory presented by Domergue et al (1995) indicates the plateau stress should be used. However in the companion paper, Vaggagini et al, 1995, a stress constructed from the intersection of the 2£ slope and the plateau stress is used. Since this represented the practical application of the models this has been applied in this study. When the plateau stress is used the 'debond' stress is increased and results such as the debond energy become exceptionally high.

4.6 Conclusions

Within the period of this project the mechanical properties of the supplied composites have improved. Failure has been characterized by transverse ply cracking from 70-75MPa in the 0,90° composite with 0° ply cracking occurring at higher stresses. In UD composites this 0° ply cracking was found to vary with the testing rate. The 0,90° composite displayed a strength increment with increases in the testing rate. The UD seemed to reflect this correlation too but ultimate strengths were reduced (compared to the 0,90° BMAS/Tyranno) due to improper failure caused by unstable crack growth roughly parallel to the fibres.

The 0,90° composite displayed high ultimate strengths which seemed to imply that little or no mechanical or chemical damage to the fibres occurred during composite

manufacture. This was believed to be the result of the low processing temperature used as identified in chapter 3.

Ahe introduction of artificial defects in the form of notches of different depths seemed to have no effect on the ultimate strength of 0,90° BMAS/Tyranno. However in UD BMAS/Tyranno the unstable crack growth described above appeared to initiate at a lower stress with the notch present. From the limited number of tests possible the depth of the notch seemed to adversely effect the ultimate strength i.e. the UD composite was highly notch sensitive to the extent that matrix cracking and composite failure were no longer discrete events.

The higher relative strengths found with the 0,90° BMAS/Tyranno were suggested to stem from its notch insensitivity. This property must have been imparted by the 90° plies. It was suggested that the driving force for unstable crack growth in the UD composite was the residual tensile stress at the interface. Cracks which initiated at the change in section between the gauge length and the gripped area presumably had a longitudinal orientation which could not be reoriented to traverse the section. Notch sensitivity was also impaired by the same process where the shear stress between high and low stressed regions led to longitudinal crack formation which could not be corrected across the gauge section.

Various models have been employed in an attempt to evaluate τ from the matrix cracking stress, saturation matrix crack spacing and cyclic loading measurements. Of these models closest agreement with the direct measurement methods of chapter 3 were attained with hysteresis loop widths measured from the cyclic loading data.

Cyclic loading has indicated matrix cracking occurs for long periods after the peak stress is attained. This suggests that environmentally driven crack growth takes place. It was suggested stress corrosion cracking at the interface was the cause where water presence ensured the breaking of Si-O bonds known to reside there.

A certain inconsistency emerged between the τ value and the average pull-out lengths. For the length of pull-out encountered here it was estimated that $\tau<5$MPa. This value compared to the range of values found of 15-40MPa by the various methods employed in this and the previous chapter.

Chapter 5 Elevated Temperature Mechanical Behaviour

It is important to assess the mechanical performance of GMCs and GCMCs at elevated temperatures in aerobic environments as these represent particularly aggressive conditions under which the composites are intended to operate. Within this chapter the mechanical performance over relatively short periods is addressed: time dependent properties will be reported in a later chapter.

5.1 Flexure Testing at Elevated Temperatures for 0,90 BMAS/Tyranno

The effects of an oxidising atmosphere on 0,90° BMAS/Tyranno have been assessed by flexural testing from room temperature to 1300°C. A maximum of 3 tests was conducted at any one temperature, however only single tests were performed at some temperatures. Specimens for this investigation have been taken from the original BMAS/Tyranno (OBM), tile NPP5, NPP7 and 11 and the poor quality BNB1. Additionally results are given for Pilkington's UD MAS/Nicalon and Corning's CAS/ Nicalon (0,90°). Problems with tile manufacture and availability respectively allowed only limited tests to be performed for the last two systems.

The effects of elevated temperatures on the flexural strength can be seen in figure 5.1 for tiles NPP5, 7, 11, the original BMAS/Tyranno ('OBM') and 'BNB1' at a testing rate of 0.5mm/min (actuator displacement rate, ADR). The volume fractions for NPP7 and 11 are identical and give very similar results at temperatures where both have been tested (room temperature (see table 3.1) and 1100°C) and are therefore joined in figure 5.1. Similar results to those shown in figure 5.1 (tile NPP5) have subsequently been reported for tensile testing of the same tile (Sutherland et al, 1995).

The flexural strength decreased with temperature for all the tiles tested above a threshold temperature. For NPP5, 7 and 11 this was over approximately 450°C but seems to be higher for OBM and in excess of 700°C for BNB1 from the limited number of tests conducted. Associated with the strength degradation was a decrease in the level of pull-out. As a result, fracture faces at the lowest strength temperature (1000°C) were flat and featureless (fig 5.2). At temperatures in excess of 1000°C the strength degradation was not as severe for all the BMAS/Tyranno tiles tested.

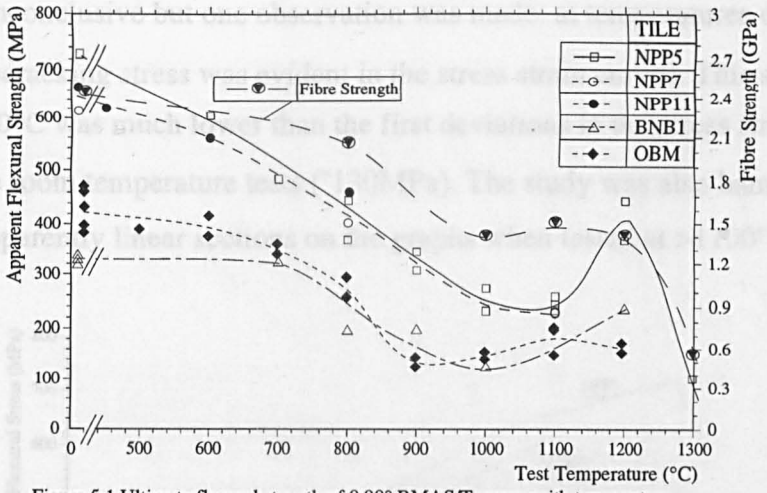

Figure 5.1 Ultimate flexural stength of 0,90° BMAS/Tyranno with temperature
Also included are the strengths of Tyranno in air after Pysher et al (1989)

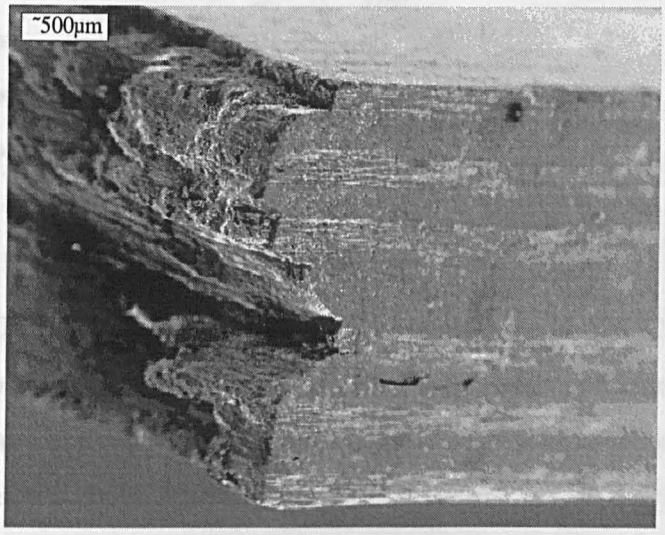

Figure 5.2 Brittle failure of 0,90° BMAS/Tyranno (NPP) from flexural testing at 1000°C in air

The flexural strengths of NPP5, 7 and 11 specimens across the temperature range all exceeded the first microcracking stress of ~130MPa observable at room temperature. Between room temperature and 800°C failure was characterised by a progressive truncation of the pseudo-linear extension following cracking in the 0° ply (fig 5.3). Above this temperature no second microcracking inflection was evident up to and including 1100°C, i.e. ultimate failure and 0° ply cracking appear to be coincident. The ultimate flexural strength decreased gradually during this temperature interval. Above 1100°C a much greater proportion of the room temperature flexural strength was retained. This strength improvement accompanied a disproportionate increase in the strain to failure, i.e. the apparent elastic modulus decreased rapidly (fig 5.5). The highest test temperature of 1300°C resulted in no fracture, just deformation of the test-piece around the contact rollers. Attempts have been made to measure the microcracking stresses by examining all stress strain curves below 200MPa. These

results were inconclusive but one observation was made: at temperatures over 800°C a definite microcracking stress was evident in the stress strain curves. This stress of ~60MPa at 900°C was much lower than the first deviations in the stress strain graph plotted for the room temperature tests (~130MPa). The study was also hampered by a lack of any apparently linear sections on the graphs when tested at >1100°C.

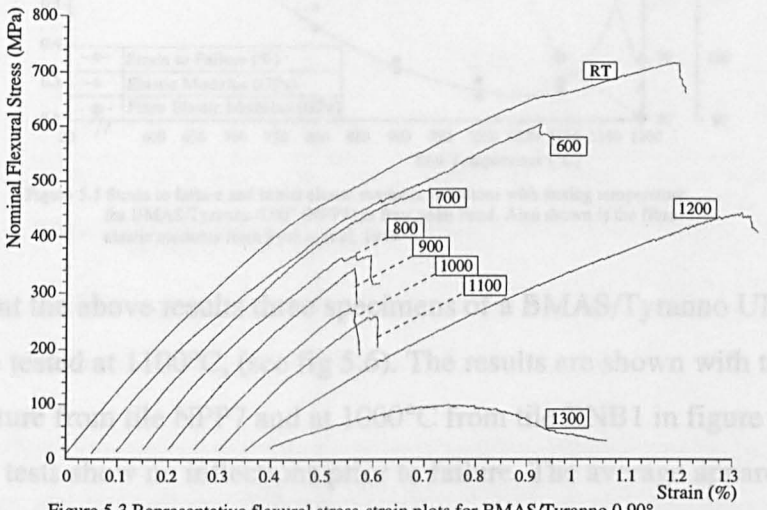

Figure 5.3 Representative flexural stress-strain plots for BMAS/Tyranno 0,90° (Tile NPP5)

The failure of BNB1 BMAS/Tyranno at room temperature and 700°C was similar to the intermediate temperature (800 to 1100°C) results of the 'NPP' specimens with regard to the premature failure at the nominal second microcracking stress (0° ply cracking level). At temperatures above 700°C up to 1000°C failure occurred prior to the expected 0° ply cracking stress. The lowest strength results of all material tested originate from tile BNB1 at 1000°C where 90° ply cracking and failure were coincident at 122MPa (fig 5.7). A fracture face of a BNB sample is shown in figure 5.4.

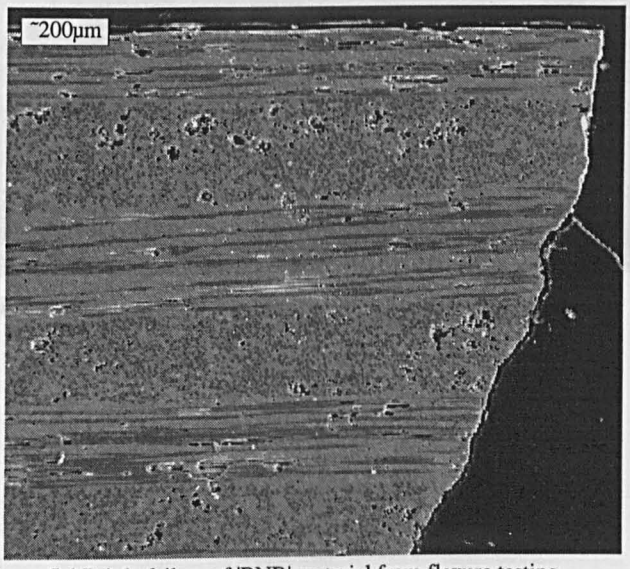

Figure 5.4 Brittle failure of 'BNB' material from flexure testing at 1000°C in air. Note the poor quality evident as matrix voids

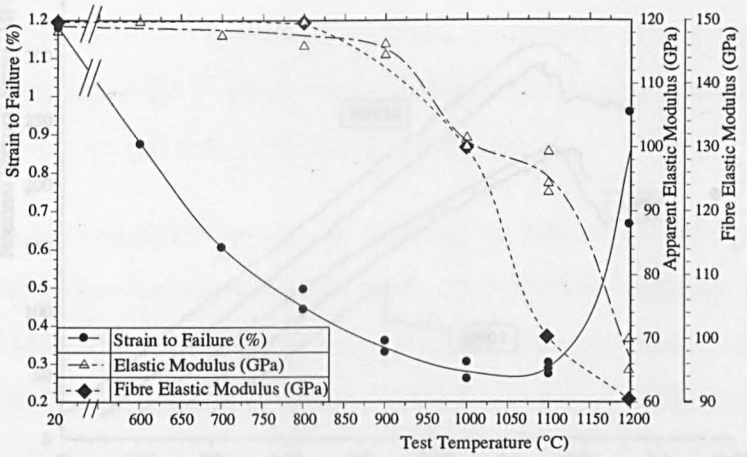

Figure 5.5 Strain to failure and initial elastic modulus variations with testing temperature for BMAS/Tyranno 0,90° (NPP5) in four point bend. Also shown is the fibre elastic modulus from Pysher et al, 1989

To complement the above results three specimens of a BMAS/Tyranno UD tile (NPP14) were tested at 1100°C, (see fig 5.6). The results are shown with tests at the same temperature from tile NPP7 and at 1000°C from tile BNB1 in figure 5.7. The unidirectional tests show no inflections prior to failure. The average apparent flexural strength of the UD samples was 301MPa compared to 230MPa for NPP7 at 1100°C. The room temperature flexural strength of tile NPP14 was found to be 805MPa (average of 3 tests) with inflections in the flexural stress-strain plot at 290 to 340MPa.

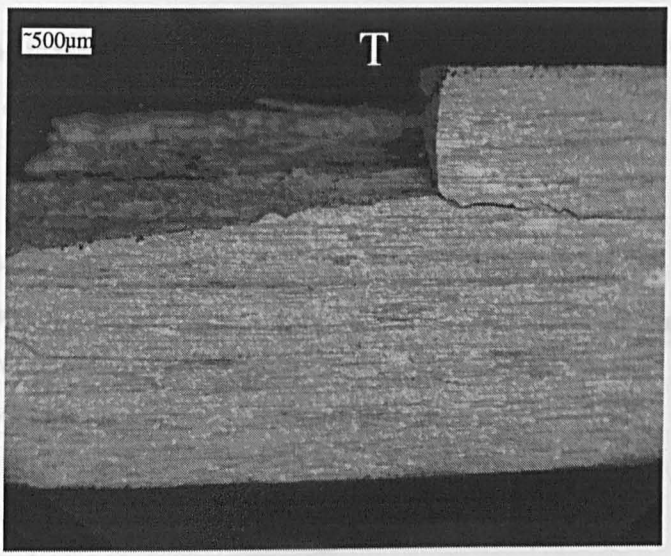

Figure 5.6 Micrograph showing brittle failure of UD BMAS/Tyranno at 1100°C. 'T' denotes the tensile face

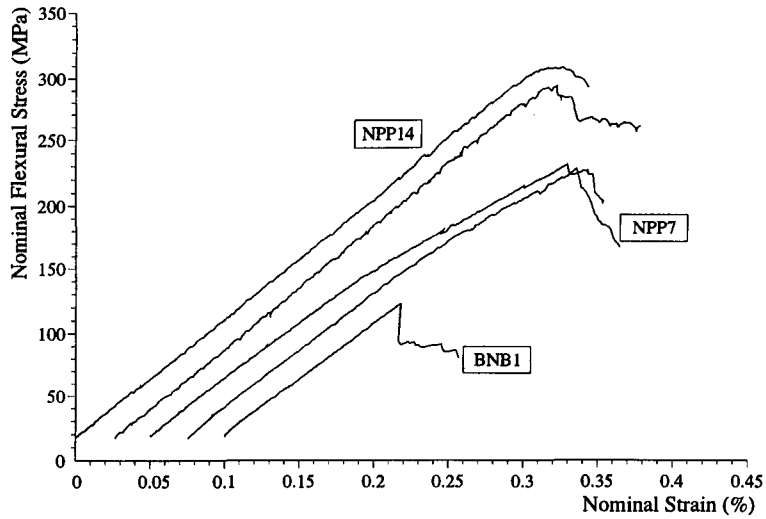

Figure 5.7 Nominal flexural strengths of NPP7 (0,90°), NPP14 (UD) at 1100°C and BNB1 (0,90°) at 1000°C

Limited testing of other systems has taken place, these systems are Pilkington's MAS/ Nicalon (UD) 'JG6' and Corning's CAS/Nicalon 0,90° (fig 5.8).

The UD MAS/Nicalon, unlike the other composite tiles and systems, actually increased its apparent flexural strength to 700°C but mirrored the intermediate temperature strength decline of tiles NPP5, 7 & 11 and OBM. Greater strength retention occurred above 900°C as opposed to 1000°C in BMAS/Tyranno and dropped off sooner (1200°C v 1300°C).

The CAS/Nicalon system shows the same flexural strength trends as 'NPP' BMAS/ Tyranno with the exception that the strength retention upswing was not as dramatic at 1200°C.

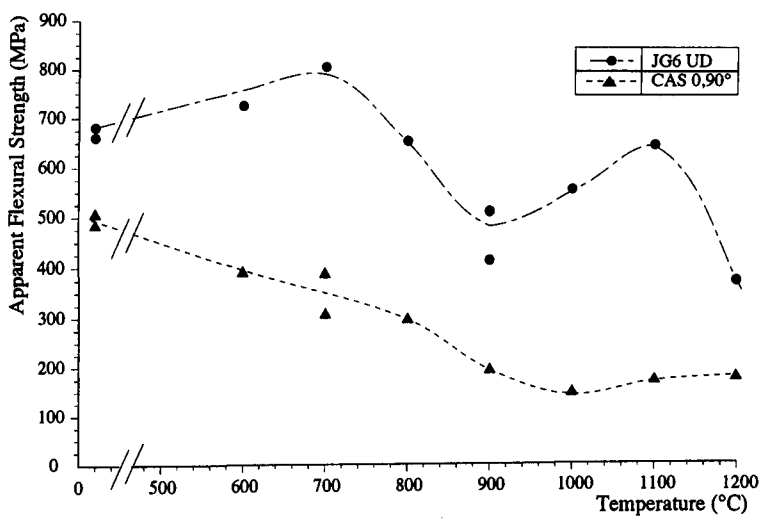

Figure 5.8 Apparent flexural strengths of Pilkington's 'JG6' MAS/Nicalon (UD) and Corning's CAS/Nicalon (0,90°) in air to 1200°C

In the previous chapter BMAS/Tyranno was seen to follow the failure behaviour of a

typical 0,90° BMC. That is, an initial linear extension which concluded with cracking in the 90° ply subjected to the highest stress. Further extension also appeared linear until cracking initiated in the 0° plies. Again a further pseudo-linear section of lower modulus preceded fibre and therefore composite failure.

The degradation in strength of composites with carbon rich interphases and silicon carbide based fibres has been well documented within the literature (e.g. Stewart et al, 1987; Prewo, 1989). The culpability of oxygen for the degradation has also been demonstrated (Mah et al, 1985b). However, despite the identification of the form of the oxidation of the fibres and carbon rich interface with subsequent silica bridging, the sequence of these events requires some clarification. The following discussion of the BMAS/Tyranno composite will be assessed within the context of other glass-ceramic and ceramic composites.

For NPP5 the flexural stress-strain at low temperatures (<700°C) differs from the room temperature results only in the length of the final fibre dominated extension after 0° ply cracking (fig 5.3).

Similar strength loss has been obtained for CAS/Nicalon after heat treatments in air with flexural testing at room temperature (Pharaoh et al, 1993). The degradation in strength within this low temperature band was attributed by Pharaoh et al, (1993) to carbon removal at the interface precipitating a drop in the interfacial shear strength. It was hypothesised the supposed lower value for τ meant the additional stress in the fibre at a matrix crack required a longer distance to decay back to the lower far field stress where matrix and fibre share the load. The load transfer length, l, has been given by Marshall et al, (1985):

$$l = \frac{\sigma R E_m V_m}{2\tau E_c V_f} \tag{5.1}$$

It was postulated the longer transfer lengths sampled a greater fibre volume for flaws leading to a lower fibre, and therefore composite, failure stress. However the interfacial shear stress data (Pharaoh et al, 1993), as measured by the fibre push-down method, did not support such an hypothesis. The sliding stress was found to increase after ageing at all the temperatures tested (700-1200°C), (Pharaoh et al, 1993).

Similar heat treatment investigations have been conducted by Plucknett et al (1994, 1995) on BMAS/Tyranno, Bleay and Scott (1992) on BMAS/Nicalon and Thouless et

al (1989) on LAS/Nicalon (but only at 800°C).

Thouless et al found exposure to 800°C increased the sliding stress from ~2MPa in as received (AR) LAS/Nicalon to 30-40MPa after 4 and 8hours and up to 100-200MPa after 16hours. Plucknett et al (1994, 1995) found that with 100h heat treatments the interfacial shear stress increased from temperatures as low as 450°C (the minimum temperature investigated). However, after maximum debond and shear stress values at 700°C they found the sliding resistance of that at RT was retained within the interior of these higher temperature oxidized test samples. Bleay and Scott observed a similar result with BMAS/Nicalon after ageing for 60hours in air. Their strength minima and interfacial shear stress maxima occurred at 1000°C as opposed to the 700°C found by Plucknett et al. Surprisingly perhaps, Plucknett et al found the flexural strength was impaired only after exposure to temperatures greater than 450 °C and less than 1000°C, i.e. strength was retained after air exposure at low temperatures and high temperatures but not within the intermediate temperature band (600-800°C). When the sliding stresses are considered this result becomes even less clear: after exposure at 450°C the sliding stress had increased from 36±6MPa to 167±39MPa suggesting a strength reduction was likely. Conversely, after 800°C exposure a relatively low interfacial shear stress was retained (52±11MPa) but the strength was lower than the 450°C result. Bleay and Scott found the flexural strength in the BMAS/Nicalon system was retained to 800°C. At their next highest oxidation temperature of 1000°C the strength minima was observed. The strength retention of this system at 1200°C was also markedly lower.

The above low temperature flexural testing results can therefore be considered in relation to the interfacial carbon rich layer depth. Within the Harwell BMAS/Tyranno the interface has been demonstrated to have a depth of ~10-20nm. Within the Corning BMAS/Nicalon composite the depth is much greater at nearer 100nm. At temperatures where silica formation at the fibre is unlikely, but a carbon-oxygen reaction is possible, an increase of the interfacial shear stress can be envisaged for composites where the interface is thin in relation to the interfacial roughness (see fig. 5.9).

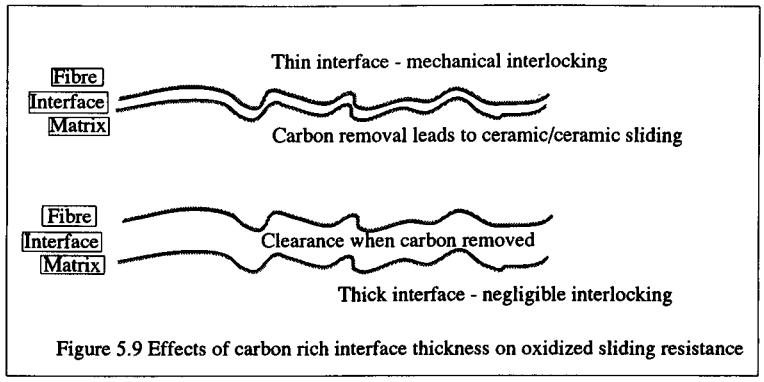

Figure 5.9 Effects of carbon rich interface thickness on oxidized sliding resistance

This is particularly relevant for the BMAS/Tyranno tested here. It has already been demonstrated the interfacial shear stress of the AR composite is surprisingly high considering the interfacial stress state and the carbon rich interface. The high values have been attributed to interfacial roughness and the limited depth of the interface. Sliding is therefore hindered by mechanical interference between asperities. With removal of the carbon layer this is exacerbated since the solid lubricant is removed. The sliding faces experience a large increase in the force necessary to cause sliding. Thouless et al (1989) found μ for carbon was 0.01 whereas for ceramic/ceramic sliding a 0.3 to 0.8 friction coefficient could be expected.

Generally, high sliding stresses are accompanied by correspondingly high debond energy requirements. However in the case of carbon removal but no silica formation composite integrity need not be impaired by the propagation of a crack since load transfer is possible to the fibre which, since it is not bonded to the matrix, does not fail in the crack path. The low temperature is also not expected to degrade the fibre strength and hence pre-oxidised strengths are retained. This demonstrates the importance of fibre properties on the composite strength.

However the above becomes irrelevant when the interfacial carbon layer is thick. In such instances removal of the interfacial carbon by oxidation results in a lower load transfer capability as demonstrated by Windisch et al (1997). In this investigation a SiC/Nicalon composite was oxidised at various temperatures in air with a carbon interfacial depth of ~1μm thick. Strength was found to diminish once the interface had been volatilised. This is in accordance with data presented by Droillard and Lamon (1996) who found SiC/Nicalon composites with weak interfacial shear stresses displayed lower strength and toughness. The reason for the lower strength could be the formation of a crack across the entire section over which fibres bridge. This would lead

to uniform stress in the bridging fibres across the section, i.e. a dry bundle. The difference in strengths between a dry and an impregnated fibre bundle has been amply demonstrated by Lamon (1988). He found Nicalon dry fibre bundles exhibited an average strength of 1301MPa and individual fibres an average of 1566MPa. These figures compared to an impregnated bundle strength of 2564MPa.

At higher temperatures (>600°C) even AR fibres succumb to oxidation (see Tyranno fibre strengths tested in air superimposed onto figure 5.1 (Pysher at al, 1989)). However contradictory data exist within the literature for the strength of as received Tyranno and Nicalon in air which has been shown to deteriorate very little below 800°C by some researchers, (Pysher et al, 1989), but degrades at temperatures as low as 600°C by others (Berger et al, 1996; Rigdon et al, 1990). Similarly, Kim and Moorhead (1991) found oxidation heat treatments caused rapid fibre degradation (less than 1 hour) at the lowest exposure temperature tested (800°C), so presumably fibre damage was also possible below this temperature. In contrast Ishikawa et al (1987), working at Nippon Carbon Co., reported no degradation at 800°C below exposure times of 10hours. Mah et al, (1984), explained the fibre weakening due to the reaction of the free carbon within the fibre with oxygen. The escaping oxidation product (CO) was believed to leave a hole behind which, with ongoing oxidation, formed a deep notch and consequently lowered fibre strength.

At temperatures above 700°C passivation of the fibre surfaces is known to occur (e.g. Huger et al, 1993). The silica so formed is associated with a volume increase of 80% over the unoxidised fibre substrate (Bischoff et al, 1989). At high temperatures the rate of silica formation can cause bridging or 'pinching' between the fibre and the matrix (Brennan, 1986) even within the time frame of a 'standard' mechanical test (Stewart et al, 1987).

Bridging leads to very high debonding resistance with the outcome that, for heat treated specimens, matrix cracks propagate through the fibres. This is an important distinction between heat treatments in oxidizing atmospheres with post exposure testing at room temperature and the testing at elevated temperature. In this instance it has proved possible to model the amount of interface that is lost (depth of recession) to the atmosphere by oxidation (Fillipuzzi and Naslain, 1994 and Eckel et al, 1995). The model of Fillipuzzi and Naslain can also be used to predict the time of closure of surface pores (i.e. the annulus left after carbon volatilization) by silica formation on

both fibre and matrix (both nominally SiC). Huger et al (1993) have provided a means of estimating the time for matrix/fibre bridging at different temperatures by TGA analysis of as received Nicalon fibres. From their analysis they predict the evolution of the depth of silica. With knowledge of the carbon thickness at the interface, closure times can be calculated. However Huger et al (1993) have studied AR *Nicalon* fibres and, as mentioned, evidence exists which suggests fibres within a composite may oxidise more rapidly. Despite this at 1100°C closure of an annular gap of 15nm (the approximate interface depth for BMAS/Tyranno) is predicted to take approximately thirty seconds. The same data at 900°C predict a closure time of the order of 6 minutes. For a greater carbon interfacial depth (30nm) Cooper and Chyung (1987) observed full 'bridging' in less than one minute at 900°C. Therefore with more rapid oxidation of as processed fibres the time span necessary must be assumed to be considerably shorter.

Thus, composite strength loss at intermediate temperatures can be explained by either fibre strength degradation and/or fibre bridging due to rapid silica formation. The time dependency is clear for both mechanisms. Both of these phenomena, the depth of silica formation and the fibre strength loss, depend upon the temperature and time of exposure. Also, with sealing of the composite surface ensured by the pre-heat treatment, neither process occurs until breach of the integrity of the matrix. Therefore it is the relative speed of these reactions (fibre strength degradation and silica bridging) which remains under debate.

Examination of fracture surfaces from intermediate temperature testing reveals very low pull-out lengths. This evidence does not clarify the issue since both high interfacial shear stresses and local strength loss of the fibre at the crack would reduce the pull-out. It seems likely the two processes act in union. As the silica forms at the fibre surface and the interfacial shear stress increases, the stress within the fibre at the crack exceeds the fibre strength and failure results leading to an increase in the stress in the neighbouring fibres. The tractions in the crack wake are reduced by such failures so crack extension is necessary. As the new fibres are exposed the process continues.

The bridging tractions in the fibre (p) have been related to the crack opening displacement (u) by Thouless and Evans (1988):

$$p(u) = \left(V_f^2 V_m \frac{4\tau E_f E_m u}{R E_c} \right)^{1/2} \qquad (5.2)$$

In this instance τ is time dependent during oxidation, further crack opening displacements would cause large increases in the bridging traction, p, of these fibres. If a tenfold increase in τ from the silica formation is assumed (e.g. see the oxidation studies of Plucknett et al, 1994, 1995) the nominal stress in the bridging fibre would increase by a factor of over 3 according to the above equation for the same crack opening. The maximum bridging traction is limited by the fibre strength which is in turn reduced by oxidising atmospheres at high temperature. Consequently fibres fail in the crack wake. In this way there is a failure mode transition from noncatastrophic to catastrophic where only one crack is necessary to promote composite failure. A subtle difference exists between embrittlement from oxidizing heat treatments and embrittlement during testing at high temperature. Where oxidation by piped diffusion along the interface allows silica bridging very planar fracture surfaces result. When fibre fracture takes place in the crack extremely small pull-out lengths of the order of crack opening displacements can be seen (fig 5.10).

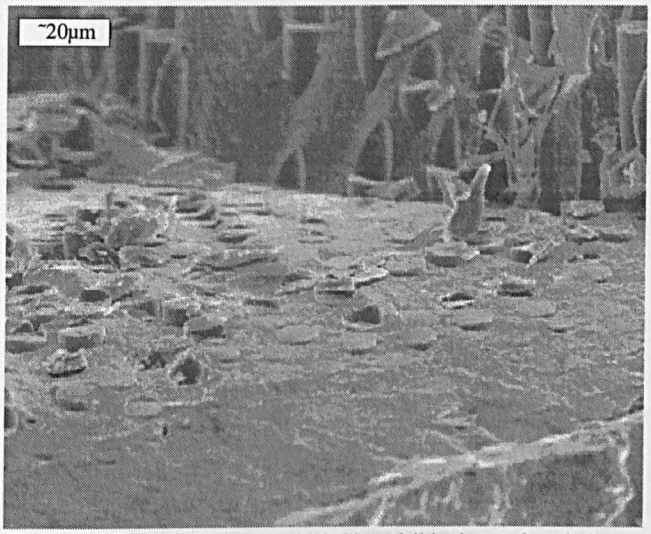

Figure 5.10 Transition zone in which fibres fail in the crack path due to strong bonding in the near surface region, deeper into the sample fibres display short pull-out lengths

To increase the sliding stress significantly in the crack wake it is not necessary to fully bridge the matrix and the fibre. With carbon removal the fibres are free to touch the matrix at periodic locations. At these points any oxidation of the fibre surface will lead to formation of silica ligaments with the silicate matrix. Thus strength loss is possible at any temperature where the fibres are known to develop a silica skin. Intimate contact between fibre and matrix is not as frequent in systems where the oxidised carbon rich interface was thick. In the BMAS/Tyranno composite the frequent mechanical interference would lead to a great many of these ligaments forming whenever oxygen penetrated through matrix cracks at elevated temperatures and the two silica rich

components contacted. This explains the onset of strength loss at lower temperatures than, for example, the LAS/Nicalon system (Stewart et al, 1986) and BMAS/Nicalon (Bleay and Scott, 1992) as both have thicker carbon interfacial depths. These silica bridges can be thought of as spot welding of the matrix and fibre along the length of the oxidized interface. As such the 'welding' can occur at any temperature where silica forms at the fibre surface. This argument also goes some way to explaining the relatively high strength of UD MAS/Nicalon over UD BMAS/Nicalon at 1100°C. Kumar and Knowles (1996) have shown the interfacial carbon in MAS/Nicalon is up to 200nm thick. Clearly fibre matrix 'welding' will take longer in the MAS/Nicalon and the spacing of the 'spot welds' will, at least initially, be further apart. Figure 5.11 schematically shows the effects of oxidation on both thick and thin interface types. For the same degree of fibre oxidation the degree of bonding is clearly greater for the thin interface material. The small degree of bonding for the larger interface composite may allow the possibility of debonding or fracture of the silica ligament without fibre fracture.

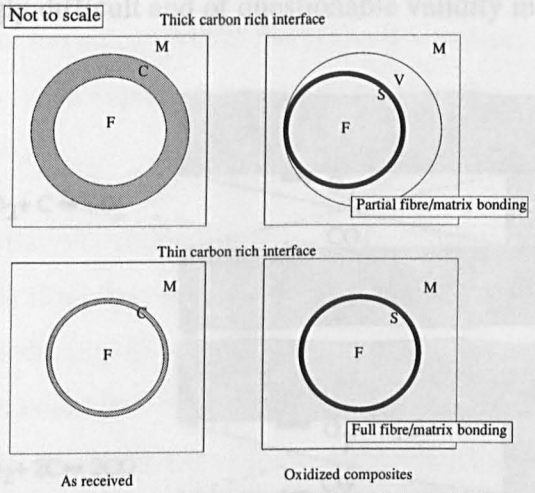

Figure 5.11 Schematic of the effects of carbon oxidation and silica formation for two different interfacial thicknesses. M=matrix, C=carbon, F=fibre, S=silica and V=void

The oxidation degradation of this class of materials has been modelled recently by Evans et al (1996). No attempt was made to model the piped diffusion at exposed fibre surfaces. The modelling was based on fibre strength degradation from differing oxygen partial pressures within a bridged crack. The strength was related to the depth of the silica layer formed on the fibre surface which was believed to act as a surface flaw, thus the thicker the layer the lower the strength. Oxygen ingress was only expected after the first matrix cracking stress. Two conditions were modelled: i) simultaneous weakening and failure of bridging fibres at a surface crack by oxidation with subsequent crack

propagation and ii) Sequential failure of individual fibres from the exposed surface from progressive fibre degradation. The former case relies on rapid gas flow within the crack, the latter on oxygen and gaseous oxidation product concentration gradients within the crack as depicted by Eckel et al, (1995), fig 5.12. Although the possibility of modifications to the interface are acknowledged, the paper made no attempt to model such effects.

The development of an apparently lower matrix microcracking stress at temperatures above 800°C may be due to several factors. At such temperatures the matrix cracking of the 90° plies may not be arrested as effectively at the boundary between the 0° and 90° plies. Two explanations exist for this lower efficiency: a reduction in the compressive stress in the 0° plies as the temperature increases so the resistance to crack propagation is reduced, and the failure of fibres in the 0° plies; the result of oxidation weakening. The measurement of the matrix cracking level of UD BMAS/Tyranno is likely to have proven viable if the same series of tests was conducted as with the 0,90° composites. However the inconclusive cracking thresholds in the 90° plies make quantification of 0° ply cracking exceedingly difficult and of questionable validity in the 0,90° composites.

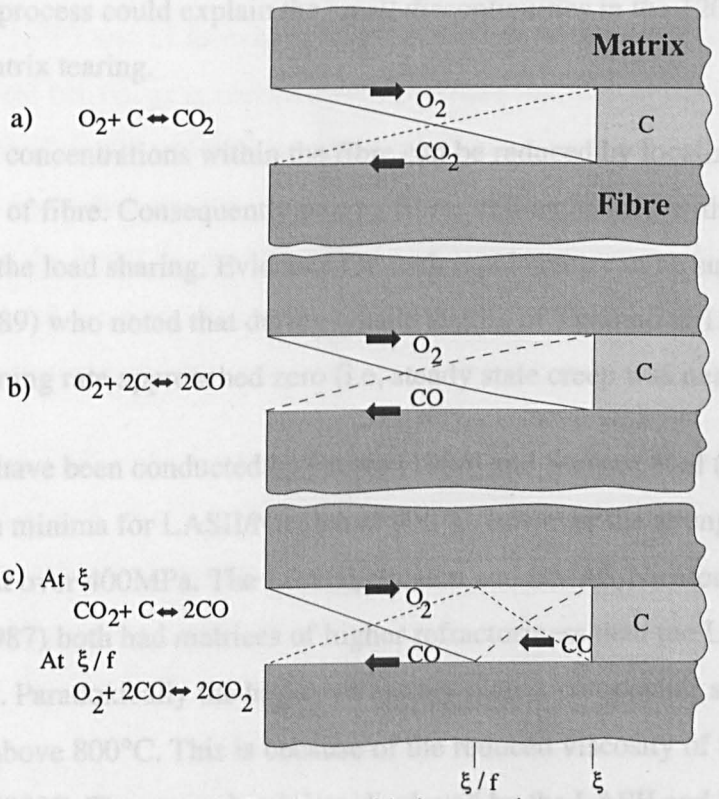

Figure 5.12 Possible oxidation reaction sequences (after Eckel et al, 1995)

Within the highest temperature band the greater strength retention of 0,90° BMAS/ Tyranno at 1200°C and MAS/Nicalon at 1100°C could be due to three mechanisms:

extensive matrix deformation which excludes oxygen from the interface and fibres, shear yielding of the matrix, or extensive plastic deformation of the fibres due to creep.

At such a high temperature the matrix is able to flow at the selected testing rate. This time dependent deformation of the matrix means the matrix stress remains low and additional loading is assumed by the fibres. This protection lasts until fibres fail within the matrix. Similar results have been reported by Gadkaree, (1994), who has used a potassium borosilicate glass to dope barium stuffed cordierite for high temperature use where he claims the glassy phase blunts cracks thus protecting the interface from oxygen ingress. This procedure is now used as part of Corning's 'Oxidation Protection System'.

In the intermediate temperature band, stress concentration in the fibres in the crack wake was suggested to promote their early failure. However at 1200°C the matrix shears easily. If matrix cracking (or tearing) were to occur and chemical bonding at the interfaces result after carbon removal, the fibre stress would not necessarily increase sufficiently to cause fibre failure. Fibre stress would be kept low by localized shear yielding of the matrix or the silica layer at the bridged interface, analogous to frictional sliding. Such a process could explain the small discontinuities in the 1200°C curve of figure 5.3 as matrix tearing.

Similarly stress concentrations within the fibre can be reduced by localized creep of the stressed section of fibre. Consequently nearby fibres still embedded within the matrix would assist in the load sharing. Evidence for such rapid creep can be supplied by Pysher et al (1989) who noted that during tensile testing of Tyranno at 1200-1400°C 'the work-hardening rate approached zero (i.e, steady state creep was nearly achieved)'.

Similar studies have been conducted by Prewo (1986) and Stewart et al (1987). Prewo found a strength minima for LASII/Nicalon at 800°C, however the strength was still relatively high at over 400MPa. The LASIII/Nicalon and BMAS/Nicalon tested by Stewart et al (1987) both had matrices of higher refractoriness than the LASII matrix tested by Prewo. Paradoxically the higher refractory matrix composites showed lower bend strengths above 800°C. This is because of the reduced viscosity of the LASII/ Nicalon above 800°C. The strength minima displayed by the LASII and BMAS composites coincided with the BMAS/Tyranno tested here at 1000°C.

The rapidity of the oxidation mechanisms is also seen in the BNB1 data. The lowest

strength of this composite shows the matrix cracking stress in the 90° plies controls the properties at 1000°C (figure 5.7) as opposed to the 0° ply cracking for all the other tiles tested (including NPP14; the UD tile). Composite BNB1 is not completely dense and has residual porosity (fig 5.4), thus oxidation can attack the interface during warm up to test temperature and during testing prior to matrix cracking via the interconnected pores. With oxidised interfaces cracking of the 90° plies can extend through the pre-oxidised 0° plies due to high interfacial sliding resistances. Oxidation may also be more rapid due to the argument constructed previously: the limited formation of the carbon rich interface from the incorrect processing will enable very rapid bonding between fibre and matrix by silica formation.

5.2 Strain Rate Effects

To investigate the speed of the oxidation reactions discussed above, various strain rates were tried at elevated temperatures in the flexural testing mode (4-point).

5.2.1 Flexural Strain Rate Testing of BMAS/Tyranno

The temperatures investigated were 450, 600, 800, 950 and 1100°C. BMAS/Tyranno 0,90° from tiles NPP7 and 11 have been tested and are reported as if one tile was used, i.e. the mechanical behaviour is assumed the same for both tiles. The testing rates of 100, 25, 5, 0.5, 0.05, 0.005 and 0.001mm/min relate to actuator displacement rates (ADRs) and are equivalent to strain rates of 0.64, 0.16, .016, 1.6×10^{-3}, 1.6×10^{-4} and 3.2×10^{-5}/min in the initial linear region. The approximate times to failure ranged from less than one second to several hours. Due to the limited material supply at the time of testing, each data point represents one test under each temperature and strain rate.

The effects of strain rate at high temperatures on the flexural strength are displayed in two formats in figures 5.13 and 5.14. Strain rate effects have been seen at temperatures as low as 450°C where the strength is seen to be lower for the slower strain rate. The flexural stress-strain plots are ostensibly the same up to the lower failure stress (fig 5.15a).

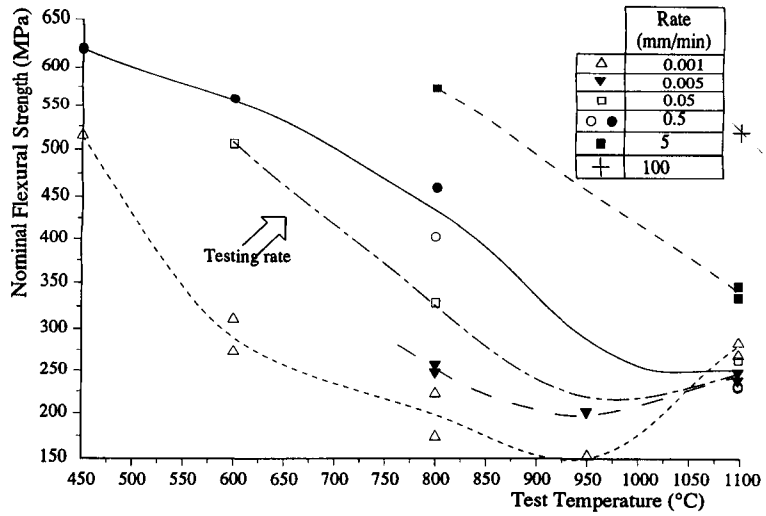

Figure 5.13 Effect of testing rate on the nominal flexural strength of 0,90 BMAS/Tyranno in air.

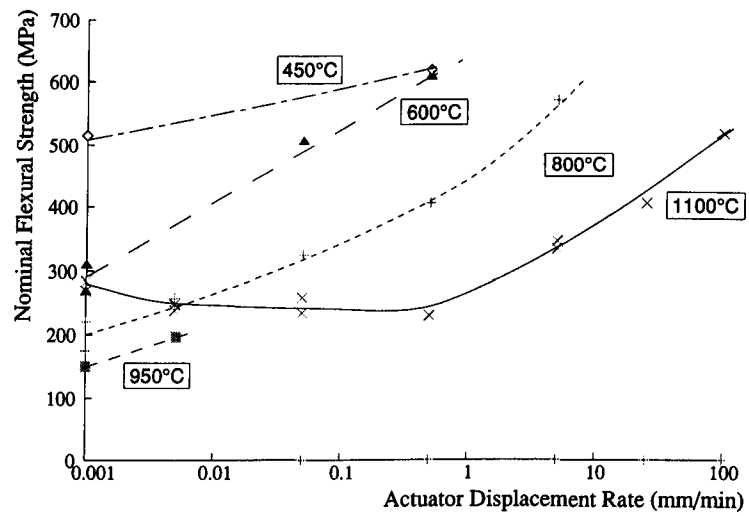

Figure 5.14 Effects of testing rate on nominal flexural strength of 0,90 BMAS/Tyranno in air

At 600°C the reduction in strength with lower testing rates is more pronounced with a strength of under 300MPa at the slowest testing rate (figs 5.13 & 5.14). The strength at 0.5mm/min was double this at nearly 600MPa. From the plot of figure 5.14 it does not appear this represents the lowest failure stress for this temperature, i.e. lower testing rates may reveal a lower flexural strength. The 0.05mm/min curve mimics that of the 0.5mm/min curve but fails at a lower stress (fig 5.15b), as with the 450°C results, but failure at the lowest ADR (0.001) is characterized by a drop in the apparent elastic modulus prior to failure.

Similar results were apparent for the testing regime at 800°C with two important differences: i) the degradation initiated at higher testing rates and ii) the strength minimum was lower. At 800°C lower strengths than at 600°C were revealed at each of the rates tested (fig 5.15c). The strength only exceeded 500MPa at the fastest rate used

at this temperature (5mm/min). At an ADR of 0.005 and 0.001mm/min a modulus drop prior to failure was evident. Again it appears lower strength would be possible at lower testing rates.

Although only three tests were performed at 950°C, a lower strength was found at a stress which has been shown to be only marginally higher than the first microcracking level in room temperature testing, (fig 5.15d). The lowest two strengths were displayed at this temperature.

At 1100°C the minimum strength was higher than the minimum found at 800 and 950°C (fig 5.15e). A retention of a greater proportion of the room temperature strength was apparent at the lowest testing rates. Near room temperatures strengths were only attained at the very highest testing rates. At this testing temperature a reduction in the initial elastic modulus was found for all the testing rates. Fracture faces from the highest and lowest testing rates at this temperature are compared in figure 5.16.

When strengths in excess of 450MPa were observed the failure was accompanied by fibre pull out at all testing rates. This was not the case for specimens which failed at 300MPa and under.

Thus it appears the effect of reducing the strain rate is to project the strength minimum down the temperature scale.

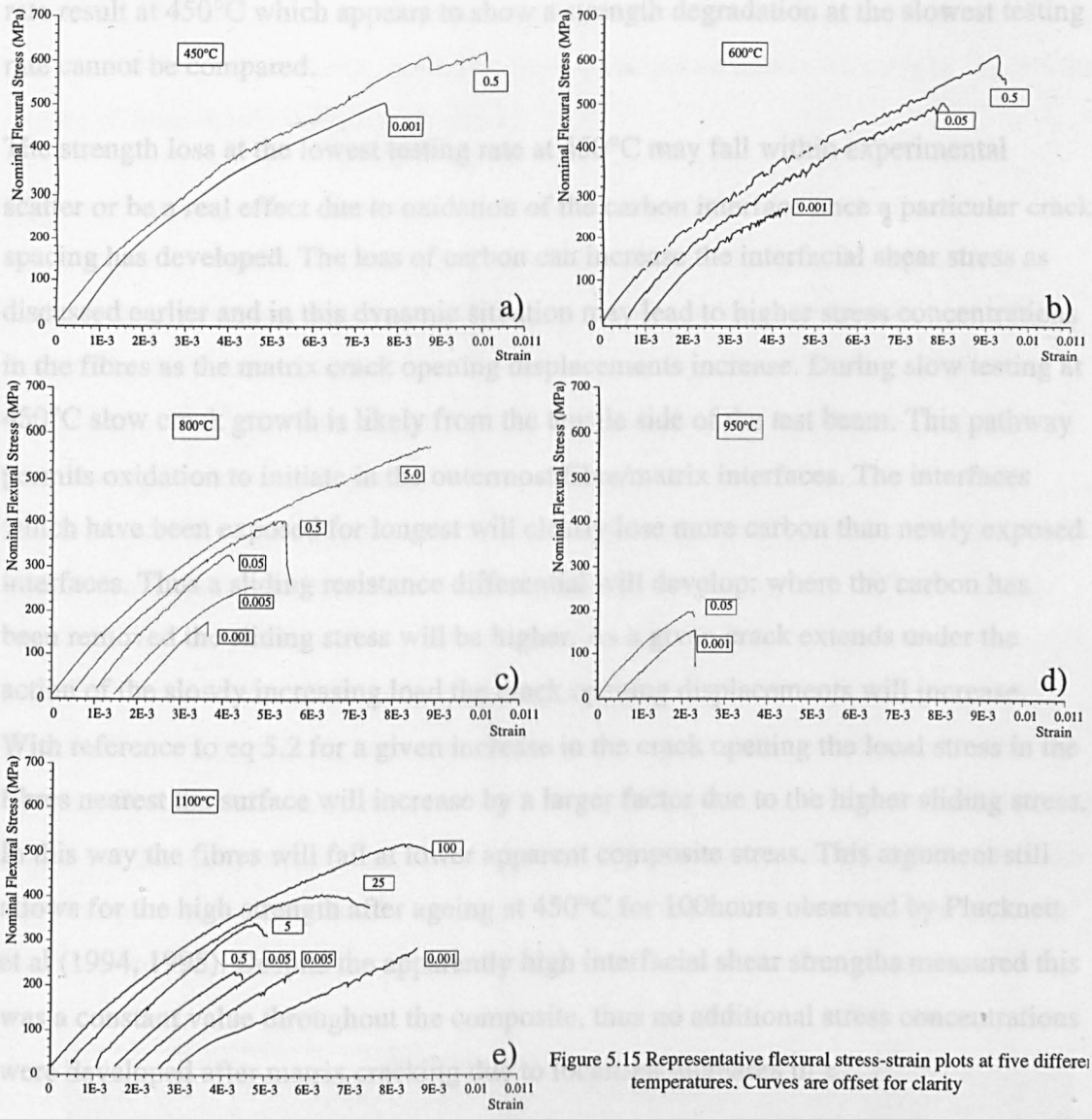

Figure 5.15 Representative flexural stress-strain plots at five differe temperatures. Curves are offset for clarity

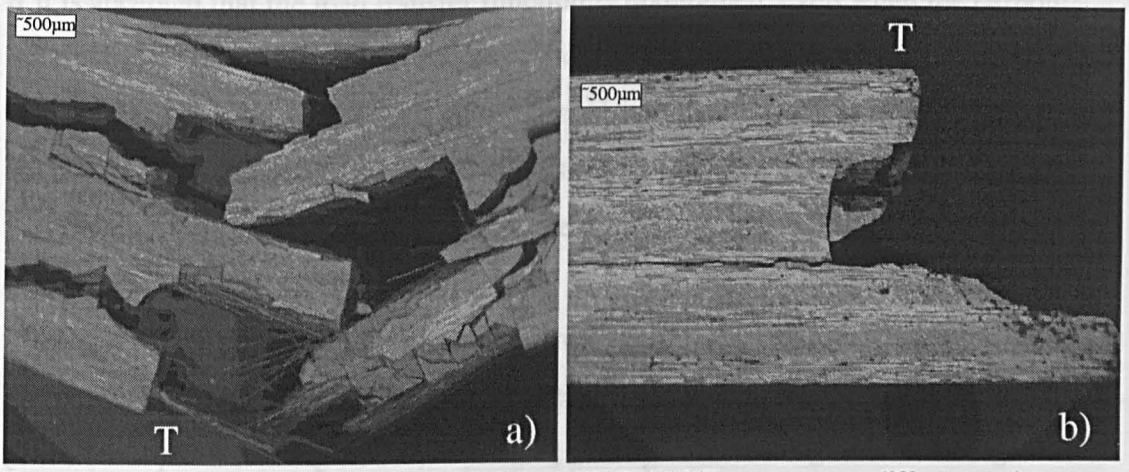

Figure 5.16 Comparison of fracture at 1100°C for 0,90° BMAS/Tyranno at two different testing rates. Actuator displacement rates of a) 100mm/min b) 0.001mm/min. 'T' denotes tensile face

5.2.2 Discussion

Unfortunately it was not possible to perform the tests at room temperature so the strain

rate result at 450°C which appears to show a strength degradation at the slowest testing rate cannot be compared.

The strength loss at the lowest testing rate at 450°C may fall within experimental scatter or be a real effect due to oxidation of the carbon interface once a particular crack spacing has developed. The loss of carbon can increase the interfacial shear stress as discussed earlier and in this dynamic situation may lead to higher stress concentrations in the fibres as the matrix crack opening displacements increase. During slow testing at 450°C slow crack growth is likely from the tensile side of the test beam. This pathway permits oxidation to initiate in the outermost fibre/matrix interfaces. The interfaces which have been exposed for longest will clearly lose more carbon than newly exposed interfaces. Thus a sliding resistance differential will develop: where the carbon has been removed the sliding stress will be higher. As a given crack extends under the action of the slowly increasing load the crack opening displacements will increase. With reference to eq 5.2 for a given increase in the crack opening the local stress in the fibres nearest the surface will increase by a larger factor due to the higher sliding stress. In this way the fibres will fail at lower apparent composite stress. This argument still allows for the high strength after ageing at 450°C for 100hours observed by Plucknett et al (1994, 1995). Despite the apparently high interfacial shear strengths measured this was a constant value throughout the composite, thus no additional stress concentrations were developed after matrix cracking due to localised increases in τ.

If it is accepted that the load transfer function is maintained, even when the carbon interface has been oxidised in this composite, then we can make certain observations from the flexural stress/strain graphs of figure 15a-e. Reductions in modulus after matrix cracking can be due to two mechanisms: loss of load transfer function or fibre failures. In turn this latter mechanism can be due to two effects: fibre weakening or higher τ values from silica bridging leading to greatly increased local stress within the fibre. If we now draw upon the study of fibre strength when tested in an oxidising atmosphere by Pysher et al (1989) we can tentatively reject fibre strength loss at 600°C, (this data is plotted on figure 5.2). Pysher et al only observed significant strength loss above 800°C. If the fibre strength loss of pristine, as received, fibres is accepted as representative of as processed fibres then the lower strength observed at 600°C can only be attributed to formation of silica ligaments. As mentioned earlier these ligaments are not required to fill the annulus left by the oxidised carbon; it is sufficient to bond only

where the fibre and matrix are in intimate contact. Clearly with longer oxidation exposure and the opportunity created by the microcracked matrix for oxygen ingress the degree of fibre-matrix bonding increases.

The above argument can also be proposed for testing at 800°C with the process occurring more rapidly. This, coupled with fibre strength loss grossly impairs high temperature performance until, at 950°C the process is so rapid composite strength is dictated by the first oxygen ingress afforded by cracking of the 90° plies. This stress equated to 130MPa at room temperature. It becomes clear the cracks can propagate from these plies into the 0° plies. the large opening displacements and continuous nature of the 90° tunnelling cracks providing easy oxygen and gaseous oxidation product pathways. Such behaviour is exemplified in the micrograph of figure 5.17 in which 0,90° BMAS/Tyranno was tensile tested at 800°C. Failure is seen to spread from both the exposed outer surfaces and the tunnelling crack oxidation pathways provided after the first microcracking stress level. The degradation zone evolution can be traced by the pull-out trends. In the centre of each 0° ply pull-out soon subsides into flat planar regions at the composite surface and the region of ply bordering the 90° plies. Once the zone has propagated sufficiently into the 0° plies the applied stress cannot be borne by the intact regions with resultant fast fracture and pull-out of the fast fracture surfaces.

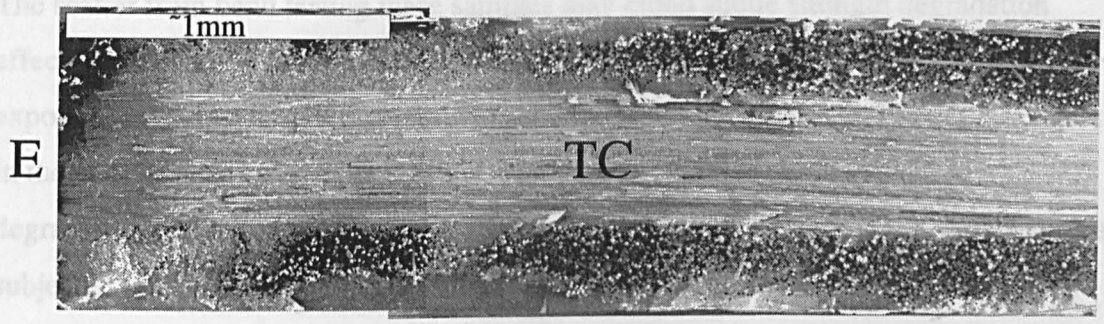

Figure 5.17 Tensile fracture face of 0,90° BMAS/Tyranno tested at 800°C in air
E=Exposed exterior surface, TC=plane of tunnelling crack

At 1100°C the strength retained at the lowest testing rate could suggest either delayed oxygen ingress or an ability to tolerate oxidized interfaces by reduced stress concentrations in the fibres. The slower strain rates appear to allow creep to reduce the stress concentrations in the fibres or exclusion of the oxidizing atmosphere. Both of these effects were discussed earlier for the standard rate testing at 1200°C.

5.3 Heat Treatment of UD BMAS/Tyranno

So far the effects of oxygen on BMAS/Tyranno have been considered through easy oxidation pathways: exposed fibre surfaces, 0° ply matrix microcracks and 90° ply tunnelling cracks. With reference to fig 2.7 a more insidious oxidation route with implications for composite lifetimes must be addressed. The oxidation mechanism occurs even when matrix integrity is preserved and pre-heat treatments have sealed the fibre surfaces. The oxidation route is through matrix diffusion. To investigate the degradation caused by this mechanism and demonstrate the efficacy of the one hour at 1100°C pre heat treatment of BMAS/Tyranno, heat treatments of flexure test specimens have been assessed. The coupons were of nominal 3x3x50mm dimensions and exposure was in still air at 1200°C for periods of up to 240 hours. The material used was from UD tile NPP14. It was expected the easiest way to clarify the depth into the composite over which strong chemical bonding applied was to examine the fracture surfaces after 3-point bend testing at room temperature. Where fibres protruded, the interfacial shear stress was to be presumed low, where no pull-out was evident the planar surfaces were to be taken as an indication of high fibre/matrix bonding.

5.3.1 Results and Observations

The scatter from bend testing these samples may cloud subtle strength degradation effects. It is conceivable there may have been a drop in strength after the 24 hour exposure but the as received composite exhibited both the highest and lowest strengths in the three samples tested. This effect remains unquantified. While the strength degradation was not obvious, the formation of an oxidised surface region was. Samples subjected to the heat treatment for 72 and 240 hours were examined by SEM after polishing. The 72 hour sample had a surface region of ~60μm where the fibres were partially consumed (fig 5.20a). The previously diphasic matrix also appeared to show regions of greater phase uniformity. In this layer large areas of light and dark contrast were seen. Probing these showed the lighter contrast phase consisted of Ba, Si, Al and O whereas the darker phase had all of these elements as well as Mg. Closer examination of the phase which contained Ba, Mg, Al, Si and O showed it too displayed two contrast levels. The darker phase tended to form in close proximity to the Ba-Al-Si-O phase and contained higher concentrations of Mg, Al and O than the lighter shade. This lighter shade phase in turn had higher levels of Si and O. The surface was also prone to bubbles which seemed to be approximately the same size as the fibres or smaller. Also

present as a scale at the surface was a layer which, when analysed, appeared to be rich in Ti with minor peaks for O, Al, and Si.

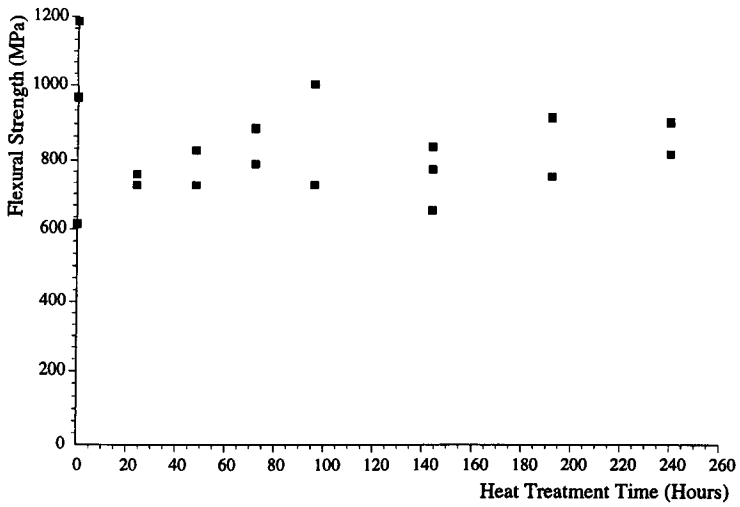

Figure 5.18 Effects of exposure to 1200°C in air on the room temperature flexural strength (3 point) of UD BMAS/Tyranno (tile NPP14) after one hour pre-heat treatment at 1100°C

Similar observations could be made for the longer heat treatment period, however the fibres within the surface region were more severely degraded and formation of a third phase was seen at the former site of the fibre (fig 5.20b). This phase was determined to contain Si and O. Despite the greater degradation to the fibres, the overall depth of the oxidation zone appeared to be similar for the two heat treatments examined (70μm versus 60μm, fig 5.20b). Though qualititative, the size of the bubbles within the surface region also appearred greater with the 240 hour heat treatment. A clear delineation was apparent within the 240hour samples in the form of a Mg-Al-Si-O phase concentration which formed parallel to the exposed surface. This line indicated the maximum extent of matrix phase modifications but not the limiting depth to which fibre degradation occurred.

XRD traces taken before and after exposure to 1200°C show only subtle differences.

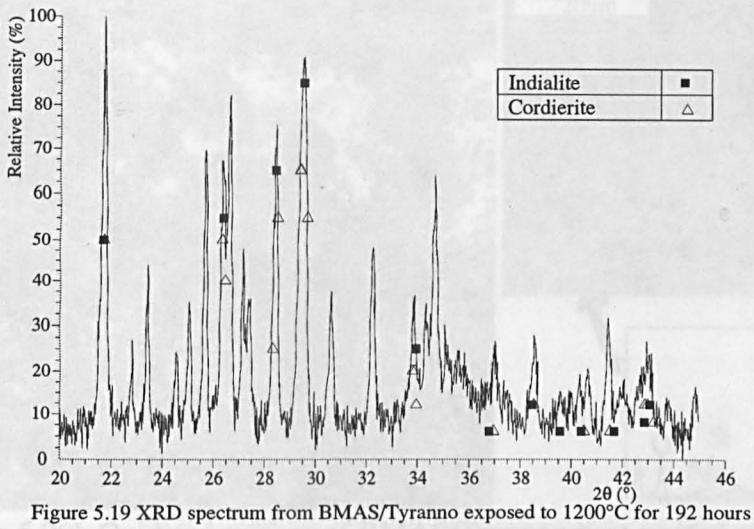

Figure 5.19 XRD spectrum from BMAS/Tyranno exposed to 1200°C for 192 hours

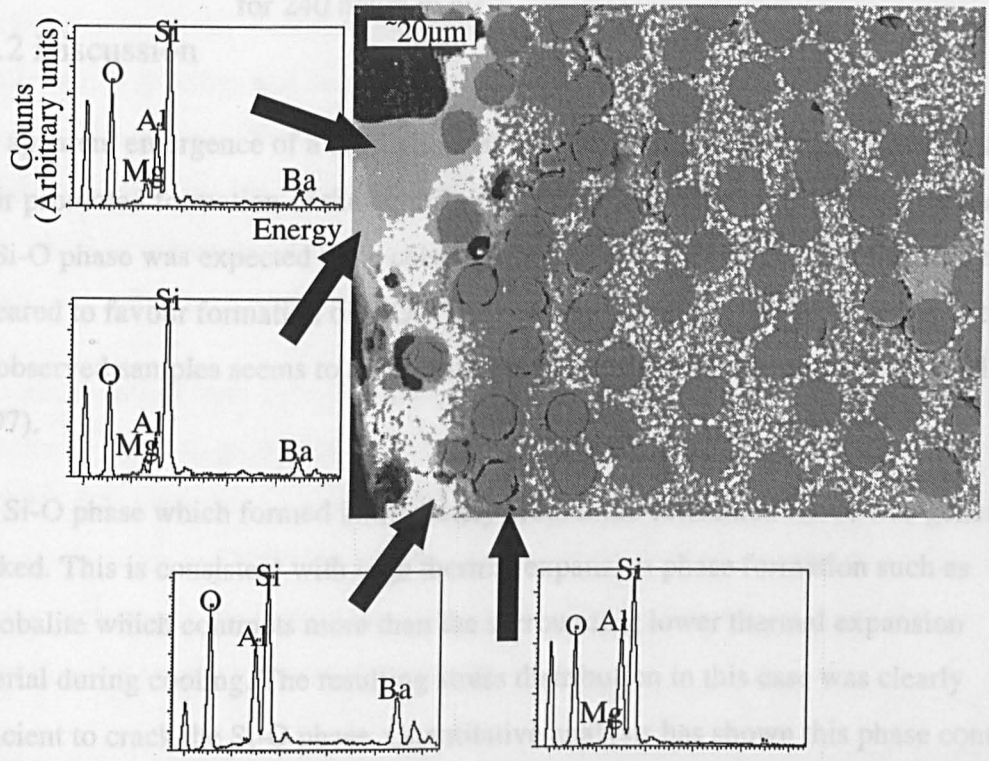

Figure 5.20a Oxidised surface of BMAS/Tyranno heat treated at 1200°C for 72 hours in air

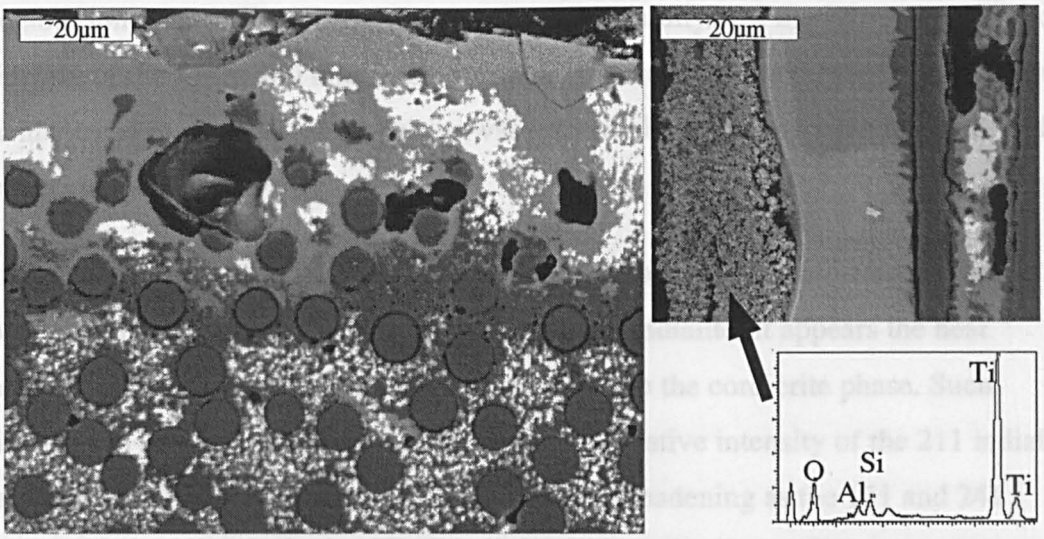

Figure 5.20b Oxidised surface of BMAS/Tyranno heat treated at 1200°C for 240 hours in air

5.3.2 Discussion

The apparent emergence of a third phase at the surface seems to infer the heat treatment in air promoted formation of the equilibrium bariumosumilite phase. Similarly the Ba-Al-Si-O phase was expected to be celsian. The surplus of Si at the site of the fibres appeared to favour formation of SiO_2. The equivalence of the oxidation depth between the observed samples seems to agree with the passivation witnessed by Sunn et al, (1997).

The Si-O phase which formed immediately around the consumed fibres was generally cracked. This is consistent with high thermal expansion phase formation such as cristobalite which contracts more than the surrounding lower thermal expansion material during cooling. The resulting stress distribution in this case was clearly sufficient to crack the Si-O phase. Quantitative analysis has shown this phase contains Si and O in the ratio 1:2.

The high concentration of Ti at the surface in the form of a porous scale was surprising since the fibres contain only 1-2wt% and are the only source for this element. Ti and Ba can be confused in EDS analysis since the BaL_{α} (4.46keV) and the TiK_{α} (4.51keV) lines are close together. However Ba is characterised by three lines of decreasing intensity (BaL_{α} , $BaL_{\beta1}$ and $BaL_{\beta2}$) whereas Ti displays only two lines (TiK_{α} and $TiK_{\beta1}$) which exhibit different peak ratios to Ba. In the instance of the surface scale only two lines are evident with energy levels and a ratio which tends to indicate Ti rather than Ba.

The hour long exposure to 1100°C seemed to successfully seal the UD composite from oxidation of the fibres and interfaces within the interior of the test-pieces to the extent that any trend in mechanical properties was impossible to detect within the scatter of the reported results.

Initial observation of the XRD trace may suggest orthorhombic cordierite is present but closer examination reveals the major MAS phase is indialite. It appears the heat treatment used here results in the gradual transition to the cordierite phase. Such evidence can be gleaned from the reduction in the relative intensity of the 211 indialite peak. Coincident with this observation is the peak broadening as the 151 and 241 cordierite peaks become more pronounced. The close proximity of the peaks between the two systems make identification difficult. The indialite and cordierite phases have similar lattice spacings and hence provide similar fingerprints in XRD spectra. The presence of indialite in the AR composite adds further evidence for the low ceraming temperature suggested in Chapter 3. Hirose et al (1984) found orthorhombic cordierite when MAS powder was heat treated at 1300-1400°C. Lower temperatures (1000-1200) were found to favour development of indialite.

Heat treatments of both Tyranno and Nicalon fibres at elevated temperatures are expected to result in growth of the β-SiC phase. Evidence exists for such growth within the XRD data from the increased intensity and narrowing of the β-SiC peak at 35.74° as the exposure time at 1200°C was increased. It has not proved possible to analyse the grain growth due to the limitations of the X-Ray Diffractometer used and the poor signal to noise ratio found with the samples used.

At the exposed surface the diphasic matrix microstructure of indialite/cordierite and celsian evolved into a Ba-Mg-Al-Si-O phase (probably bariumosumilite) with clusters of a Mg deficient phase (probably celsian). After long ageing periods the penetration of this zone was marked by a band of indialite/cordierite. Beyond this border the matrix microstructure was essentially stable but oxidation of fibres near the exposed surfaces resulted in strong chemical bonding between the fibre and matrix. The embrittled region at the surface was found to reach a maximum average depth of 70μm for the 240 hour exposure period.

Treatments at higher temperatures (>1350°C) in chapter 3 for only short durations (3 hours) have shown the matrix was metastable and transforms to the bariumosumilite

throughout the sample section. These results compare to the findings of this exposure to temperatures of 1200°C and below which show the bulk of the matrix is stable with only a thin (<70μm) surface layer being transformed to other phases. Such a finding emphasises that during the creep testing which will be reported in the next section the matrix should remain stable even for long exposure periods of <250hours.

5.4 Conclusions

In common with other composite systems which rely on carbon rich layers to dissipate the energy of matrix cracks, oxygen embrittlement was observed from temperatures above 600°C for 'standard' testing rates. During low strain rate testing this oxidation degradation was possibly as low as 450°C. Oxidation modified both the sliding stress at the interface and the fibre strength. At temperatures where matrix creep occurred composite strength was generally higher. This was attributed to either shear yielding at the interface of either the silica layer or the surrounding matrix or to crack blunting within the matrix. At higher temperatures the silica bridging mechanism has been used to successfully seal interfaces at exposed fibre ends for operation below the matrix cracking threshold. However slow testing at 950°C has shown even tunnel cracking in the 90° plies precipitates premature failure.

The insidious oxidation through the matrix by diffusion was assessed at 1200°C but penetration depths were generally low.

The speed at which oxidation impaired composite strength was related to the roughness of the fibre and matrix at the interface and the separation between them once the solid lubricant carbon was removed.

The overall oxidation process can be described in three temperature windows for BMAS/Tyranno:

Low temperature band: Carbon volatilization from the interface. Loss of this solid lubricant may increase interfacial shear stress. Conversely it may drop in composites with previously thick carbon rich interfaces.

Intermediate temperature band: Lower fibre strength from decomposition of silicon oxycarbide phase. Silica formation strongly bonds fibre to matrix in the crack wake causing local fibre stress concentrations and premature failure.

High temperature band: Matrix flow results in either exclusion of oxygen from fibres until composite failure or localized shear yielding at oxidized interfaces which dissipates fibre stress concentrations. Creep of fibres may also allow dissipation of stress concentrations to other nearby fibres.

Chapter 6 Time Dependent Properties at Elevated Temperatures

The response of GMCs and GCMCs to loading at high temperatures is of particular relevance since most envisaged applications will involve moderate loading at the upper end of the maximum temperature range. For lower temperature applications it is realistic to assume designers will tend to use metal alloys. This chapter will review the literature on time dependent properties at high temperature for both GMC and GCMCs. The results of creep tests for BMAS/Tyranno will be presented from single and multiple load applications. Further work on AS glass/Nicalon will also be shown with attempts to model the behaviour in terms of the stress state of the matrix and fibre and the strain accumulated.

6.1 Review of Time Dependent Properties

The earliest creep testing of SiC yarn type fibres reinforcing a glass-ceramic matrix described in the literature was by Prewo (1980). He performed a wide range of tests on the original LAS/Nicalon from Corning. Within this work the creep properties were assessed between 700 and 1100°C. The creep testing was by 3 point flexure. Creep was found to initiate, albeit at a very low level, from 900°C. The creep exponents found at 900 and 1000°C were claimed to show dominance of diffusional creep of the fibres. The higher exponent at 1100°C was suggested to indicate the presence of a creeping glassy phase at matrix grain boundaries.

Khobaib and Zawada (1991) tested an aluminosilicate glass matrix composite reinforced with Nicalon fibres in tension at 600, 700 & 750°C. Creep was found to follow those described classically as in metals; primary, secondary (steady state) and tertiary creep were all observed. Strains to failure were relatively low at <0.5%. The testing of a glass matrix meant the gripping arrangement could be at the same temperature as the test specimen. Failures were accompanied by two regions at the fracture surfaces. The region near the exposed edge was found to be flat and featureless and was thought to represent the creep zone. The other 'overload' region showed extensive fibre pull-out. The two zones were postulated to be fast and slow crack growth zones. The creep failures were attributed to embrittling chemistry changes at the interface. The embrittled interface was thought to act in conjunction with interfacial

pitting which increased the probability of crack formation which later resulted in failure.

Of particular relevance to the work conducted here is the work of Wu and Holmes (1993). Wu and Holmes tested both UD and 0,90° CAS with 40% Nicalon fibres in tensile creep tests. The testing atmosphere was pure argon and the main temperature of interest was 1200°C. The argon atmosphere permitted testing at relatively high stresses (60 to 250MPa). The testing regime involved creep for a maximum duration of 100 hours after which time the samples were polished and examined for microstructural damage modes. Despite the high stresses all unidirectional samples tested survived the initial 100hours except those at 250MPa which ruptured within 70 minutes. The most surprising element of their work was the performance of the 0,90° composite which, despite having only half the fibres in the loading direction, had a lower creep accumulation and creep rate than the UD composite at the two stresses where both were tested (60 and 100MPa). This demonstrated the importance of the 90° plies to the properties. The performance was linked to hydrostatic constraint imposed on the matrix by the transverse fibres. The recovery upon removal of the load was also found to be greater for the 0,90° composite. The creep rates for the composites were found to be dominated by the fibres since the stress exponent of ~1.3 at 100 hours was similar to that found for Nicalon fibres. For both composite architectures a constantly decreasing creep rate was observed despite fibre fragmentation in the UD sample under 200MPa applied stress (i.e. steady state creep was not seen). The cause of the decreasing creep rate was thought to be fibre grain growth and realignment of off-axis fibres through creep deformation of the matrix which would then be able to take a greater share of the applied load. The creep damage was summarized into three categories: low, moderate and high stresses. At low stresses cavities formed within the matrix. At moderate stresses periodic fibre fracture and cavities were observed. At the highest testing stress the composite failed within a short duration from rupture of matrix crack bridging fibres.

Weber et al (1994) manufactured an LVDT arrangement which seemed to enable direct comparison between tensile and flexural creep testing. The material under observation was the Corning UD CAS/Nicalon system, (as investigated by Wu and Holmes above in the tensile mode). Testing was conducted at 1200°C in argon at stresses from 50 to 150MPa. Test durations were relatively short at typically 50hours. Steady state creep

was not observed within the test period for any of the applied stresses. Fibre instability was blamed for the transient creep behaviour as fibre grain growth was observed within the outer periphery of the Nicalon fibres only. A model for the different creep properties from the two average grain sizes was suggested. The reasoning behind this was that an increase in grain size generally decreases the speed of diffusional creep mechanisms. Matrix creep was investigated by transverse compressive loading of the composite. In this testing mode the fibres were expected to contribute very little to the creep rate. From the findings the matrix was estimated to carry only ~5% of the applied load at the 1200°C test temperature. The creep rates they found with the flexure facility agreed very well with the tensile creep results of Wu and Holmes.

Holmes et al (1993) have tested a long fibre reinforced composite with greater thermal stability. The reinforcement was monofilament SCS-6 (SiC deposited on a carbon core by CVD, approximate diameter 140μm). The silicon nitride matrix was densified by hot pressing (HPSN). During tensile creep testing an initial primary creep region of up to 75 hours was found to cede to a steady state creep regime. The behaviour was indicative of stress transfer to the fibres in the primary creep regime. The study differed from the glass-ceramic results reported above since steady state creep after 50-75 hours was observed. The steady state creep behaviour was due to the greater stability of the reinforcement. The test temperatures of 1200 to 1350°C in air and stresses of 75 to 200MPa could be tolerated but at 250MPa fast loading was found to promote rapid failure. Slower loading was able to raise the stress rupture time to over 100 hours as the matrix had a greater time to transfer load to the fibres without matrix crack formation. The damage regimes included periodic fibre fracture and matrix cracking at the highest stress and loading rate.

For composites where the matrix creep resistance is higher than the reinforcing fibres, matrix cracking has been shown to occur (Hilmas et al, 1993). Such a reversal results in fibre stress being transferred to the matrix. Ultimately matrix cracking leaves the less creep resistant fibres highly stressed by bridging the matrix cracks and composite failure can rapidly occur. Therefore to ensure component longevity under creep conditions it is preferable for the reinforcing fibres to demonstrate higher creep resistance than the matrix to avoid matrix fracture (Holmes, 1995).

Sutherland et al (1995) tested and modelled the behaviour of a borosilicate glass matrix with Nicalon fibre reinforcement and the Harwell BMAS/Tyranno composite. Small

test temperature adjustments allowed the effects of different matrix viscosities to be investigated with respect ot the rate of load transfer to the elastic fibres for the BS/ Nicalon. The extremely low viscosity of the matrix (load transfer was of the order of seconds to several minutes) meant the apparent creep strains probably included an element of transverse creep from lateral force applied by the extensometer. The modelling was based on a spring and dashpot in parallel. The time for load transfer from the Harwell 0,90° BMAS/Tyranno composite was calculated to be a maximum of ~5000s for testing at 1125°C. The model was used to obtain creep rates of the matrix and fibres separately.

Within this chapter results are presented for two different testing arrangements. In the first section results on UD BMAS/Tyranno (tile NPP14) tested in the flexural mode will appear. Subsequent sections will concentrate on the tensile mode. Two different composites were tested in creep and cyclic creep in the tensile mode: an aluminosilicate glass with UD Nicalon fibres from Schott, Germany and the UD BMAS/Tyranno already described.

6.2 Flexural creep and cyclic creep of BMAS/Tyranno

This section presents mechanical property results from flexural creep testing and the effects of load cycling at elevated temperature. A single temperature of 1100°C was selected to represent a condition where appreciable creep was expected of the fibres as well as the matrix. All the test specimens were heat treated at 1100°C for one hour to prevent easy oxygen infiltration paths by the surface sealing described by Plucknett et al (1994, 1995).

The BMAS/Tyranno glass-ceramic composite had a unidirectional (UD) lay-up, fibre volume fraction ~39% (tile NPP14).

Testing was conducted in an Instron high temperature ceramics testing facility mounted within the load frame of a servohydraulic Instron model 8501. The four point bend jig had 40mm outer and 20mm inner spans. The specimen central deflection for all testing was measured by a central LVDT with 2mm of travel. Heating to high temperature was at 15°C/min and 15 minutes was allowed for the temperature of the test facility to equilibrate. Data sampling was at 20Hz for monotonic testing and every second for the creep and cyclic creep testing.

The monotonic properties were studied to provide a reference for longer term high temperature studies. An actuator displacement rate of 0.5mm/min, which equates to a strain rate of approximately 5×10^{-3}/min, was used for monotonic flexure testing. Useful relative data with the advantage of much lower material usage are a feature of this testing mode. Load/extension data was used for analysis of the apparent elastic modulus during cycling and then reduced for strain versus time plots. Typical specimen dimensions were 2.6×2.5×50mm.

Loading of creep and cyclic creep tests was controlled at a rate of 0.6kN/min (~18.5MPa/s). This loading rate was chosen to prevent overshoot of the creep load thereby minimizing cracking likely to be introduced by the higher transient stress level. The maximum duration for any creep or cyclic creep test was set at 5×10^5s (~139hours). Work with the cross ply BMAS/Tyranno combination suggested that maximum creep stresses of up to 80% of the monotonic flexural strength at 1100°C could be sustained (West et al, 1995). For this reason creep curves for stresses of 240, 210 and 180MPa will be presented (these equate to ~80, 70 and 60% of the apparent flexural strength of 301MPa at 1100°C).

For cyclic creep the same stresses quoted above were applied. The stress was applied and removed at the same rate and held for various times ranging from no hold time (triangular wave) to 240minutes (8 hour cycle time). Periods under load and recovery were equal. During recovery it was necessary to maintain a lower load of 10MPa to ensure continued alignment of the flexure jig.

6.2.1 Flexural Monotonic Properties of UD BMAS/Tyranno

Typical monotonic properties of the UD composite at room temperature and 1100°C are presented in figure 6.1 and summarized in table 6.1. The flexural strength at the higher temperature was ~36% of that at room temperature. The room temperature plots show deviations from linearity above 400MPa. The higher temperature bend tests were linear virtually to failure.

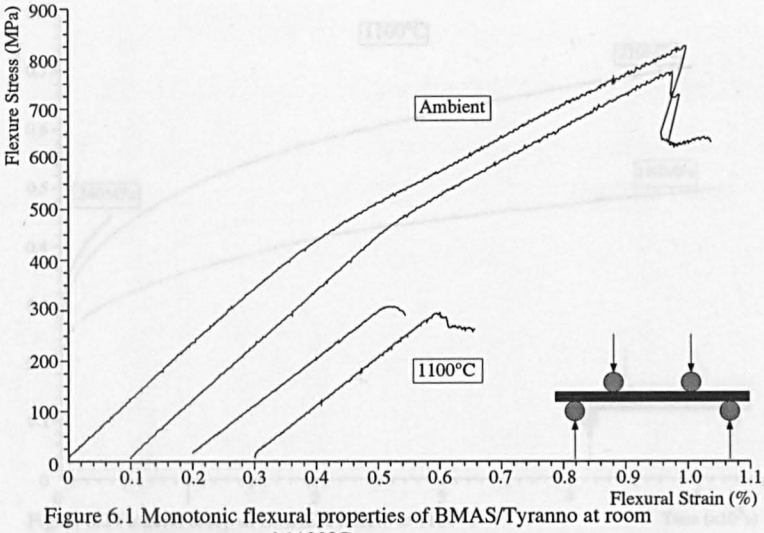

Figure 6.1 Monotonic flexural properties of BMAS/Tyranno at room temperature and 1100°C

Table 6.1 Monotonic flexural properties at room temperature and 1100°C for UD BMAS/Tyranno

Temperature (°C)	Flexural Strength (MPa)	E (20 to 200MPa) GPa
20	824	114.0
1100	301	94.5

6.2.2 Flexural Creep of UD BMAS/Tyranno

The results of the creep tests at 240, 210 and 180MPa are shown in figure 6.2. Failure at the higher stress was quite rapid, occurring shortly after 11 hours. The tests at the lower creep stresses lasted for over 5×10^5s (>138 hours). As observed in other research on similar composites (Wu and Holmes, 1993; Weber et al, 1994) the creep rate did not reach a steady state but gradually decreased. A similar decreasing creep rate was observed for *cross-ply* BMAS/Tyranno of the same composition where testing for times of up to 250hours at 1100°C revealed no steady state creep regime. The creep rates for the three tests are given in table 6.2. The microstructure of the sample crept at 210MPa for 5×10^5s is shown in figure 6.3.

A creep stress of 180MPa was also tried at 1200°C but the creep accumulation was greater than the transducer range within 20 hours (fig 6.4).

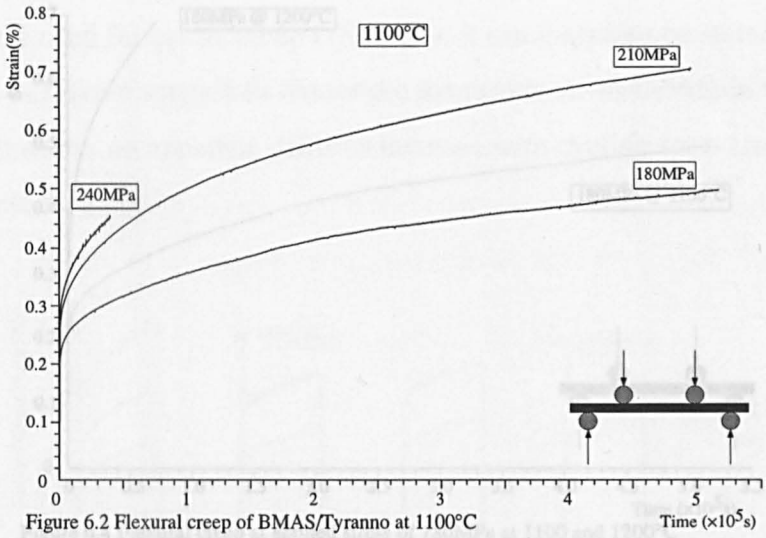

Figure 6.2 Flexural creep of BMAS/Tyranno at 1100°C

Table 6.2 Creep data for BMAS/Tyranno at 1100°C

Creep Stress (MPa)	Failure y/n?	Strain at 138 Hours	Final Strain Rate (/s)
240	yes	4.46×10^{-3}*	1.93×10^{-8}*
210	no	7.04×10^{-3}	3.58×10^{-9}
180	no	4.91×10^{-3}	2.07×10^{-9}

* Results at point of failure

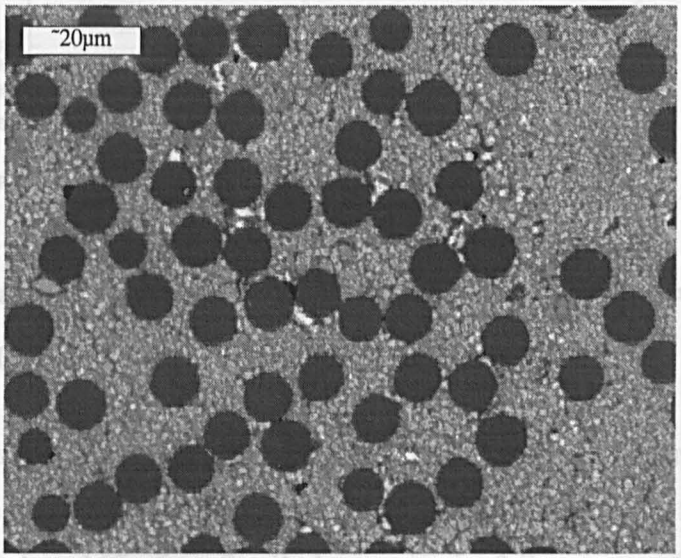

Figure 6.3 Section through sample crept at 210MPa at 1100°C showing no discernible damage of AR material

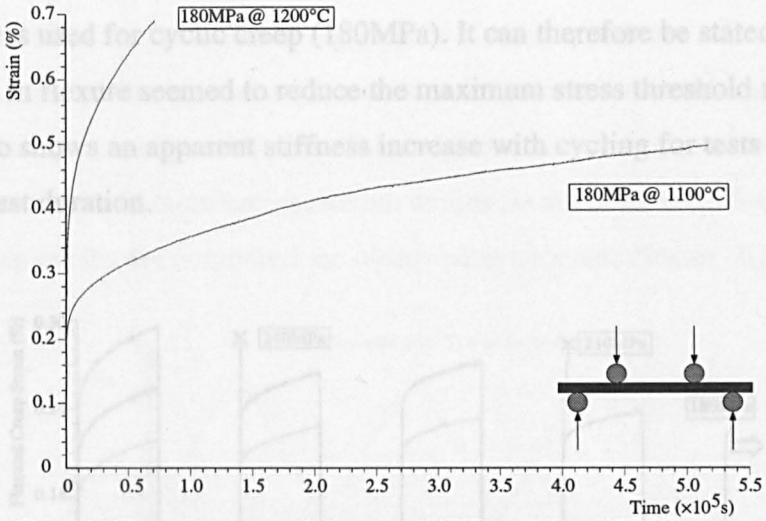

Figure 6.4 Flexural creep at applied stress of 180MPa at 1100 and 1200°C

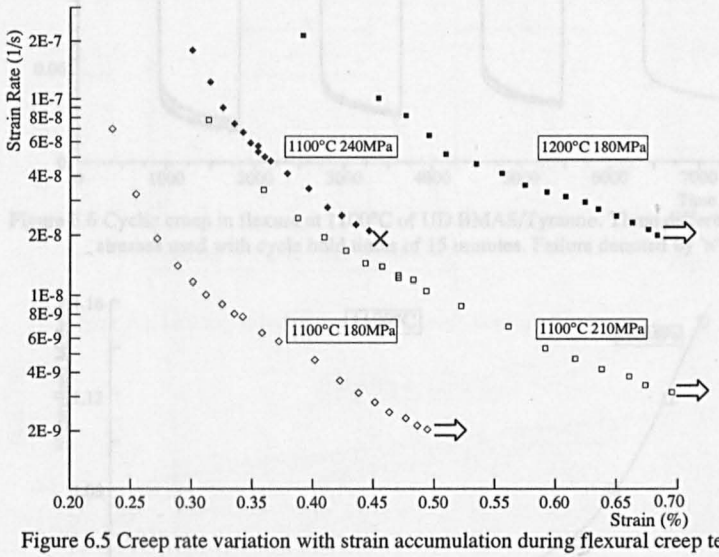

Figure 6.5 Creep rate variation with strain accumulation during flexural creep testing

6.2.3 Flexural Cyclic Creep of UD BMAS/Tyranno

The highest stress used for cyclic creep (240MPa) saw specimen failure upon application of the creep load for the second time, ie at 30 minutes as a fifteen minute hold time was employed (fig 6.6). Similarly, composite failure was assured when a maximum cycle load of 210MPa was applied. During monotonic creep testing the composite could be crept for $>5\times10^5$s at 210MPa. Despite noting failure at 240MPa in flexural creep the same stress was used here for cyclic creep since some possibility of crack closure and healing during the relaxation half of the cycle could have prevented early failure. This was not the case. The sample with maximum cycle stress of 210MPa in figure 6.6 demonstrates failure after three complete cycles and one minute at the stress for the fourth time. Such failures could have been predicted from analysis of the apparent flexural elastic modulus which tended to decrease with each cycle if failure

was to occur as in figure 6.7. The composite seemed able to survive the test duration at the lowest stress used for cyclic creep (180MPa). It can therefore be stated that cycling the creep load in flexure seemed to reduce the maximum stress threshold to 180MPa. Figure 6.7 also shows an apparent stiffness increase with cycling for tests which survived the test duration.

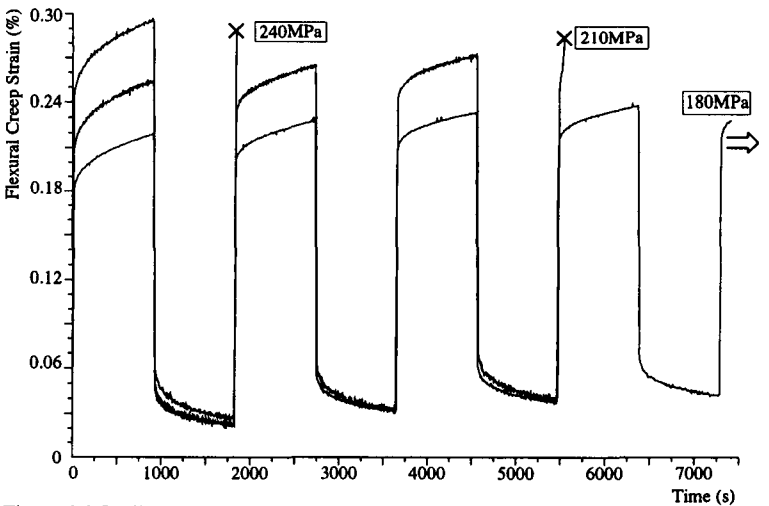

Figure 6.6 Cyclic creep in flexure at 1100°C of UD BMAS/Tyranno. Three different stresses used with cycle hold times of 15 minutes. Failure denoted by 'x'

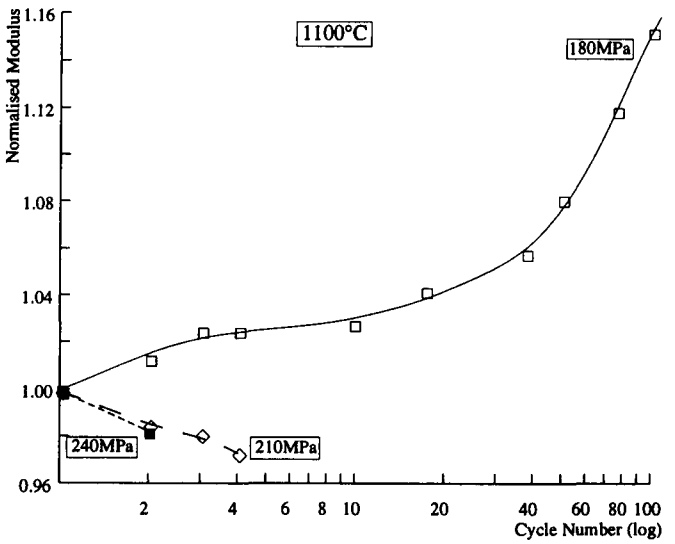

Figure 6.7 Apparent flexural elastic modulus development during cyclic creep

With the maximum sustainable cyclic creep stress established it was possible to change other test parameters such as the hold times used during the cycle at maximum and minimum loads. The hold times were always maintained equal during the stressed and unstressed segments of the cycle for an individual test but this hold time was varied for different samples. With no hold times the loading cycle was effectively a triangular wave form (fig. 6.8). With hold times the cycle was approximately a square wave with finite loading and unloading times. The hold times have been varied from the triangular

to 240min hold times (which equates to an eight hour cycle time). The resulting peak and minimum strains are presented in figure 6.9 as 'strain envelopes'. Close examination of the maximum and minimum curves which form the strain envelope reveals they slowly converge with time. This behaviour stems from reduced strain differences between maximum and minimum strains on successive cycles. When individual creep cycles are compared the observation becomes clearer (fig 6.10).

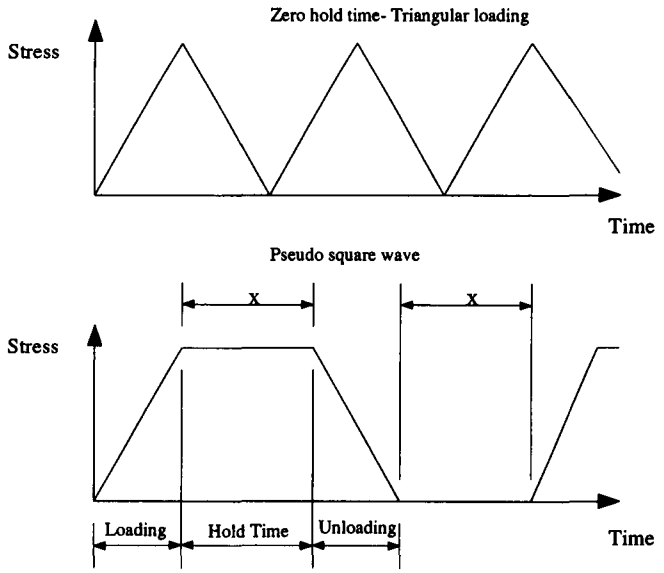

Figure 6.8 Loading waveforms used for cyclic loading

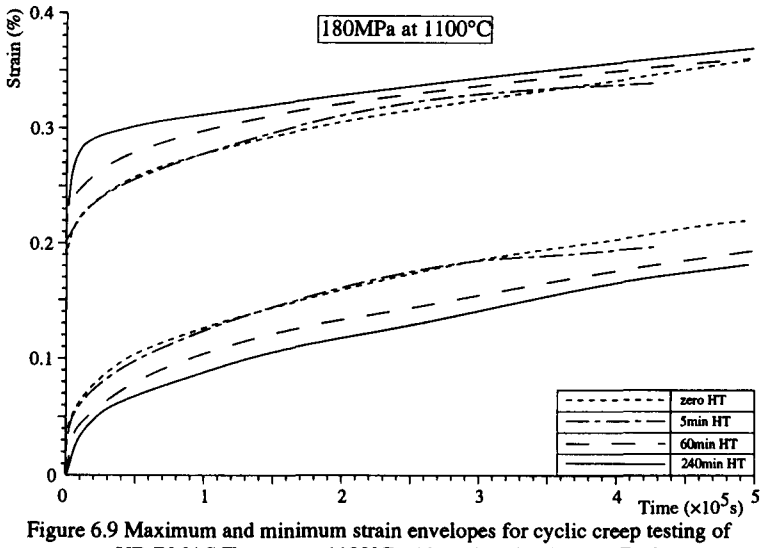

Figure 6.9 Maximum and minimum strain envelopes for cyclic creep testing of UD BMAS/Tyranno at 1100°C with various hold times. Peak cycle stress of 180MPa

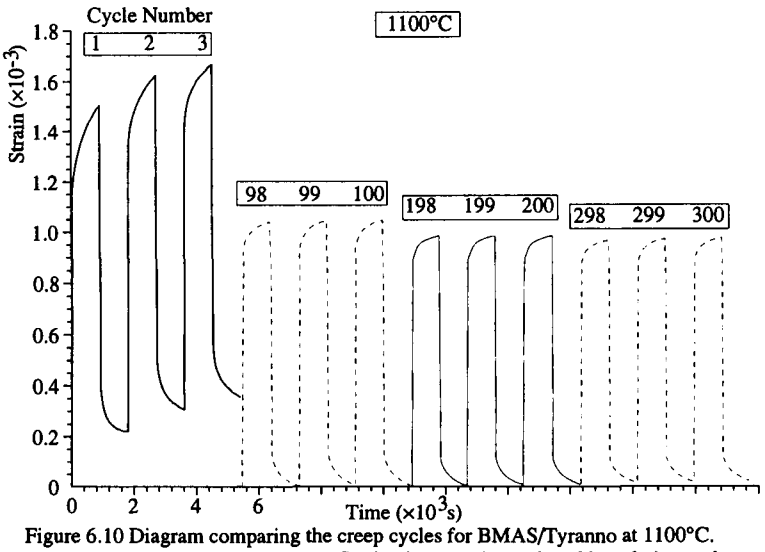

Figure 6.10 Diagram comparing the creep cycles for BMAS/Tyranno at 1100°C. Hold times of 15 minutes. Strain plots are shown for 100 cycle intervals. Accumulated strain has been subtracted.

For the cyclic tests with different hold time which survived the loading for 500 000s the residual flexural strength at high temperature was measured. All of the strength results were higher than the flexural strength found without the cyclic loading at high temperature. The minimum flexural strength increase found was 20%. As previously noted the elastic modulus also seemed to increase in these bend to failure tests at high temperature.

6.2.4 Discussion

The relatively low 1100°C strength compared to that at room temperature shows that only small breaches in matrix integrity were required to impair composite properties at elevated temperatures. The heat treatment prior to testing successfully excluded oxygen ingress by plugging easy oxidation paths but it cannot prevent oxygen entering the composite after matrix cracking has been initiated. The degrading effects of oxidising environments were discussed in chapter 5 but the monotonic flexure results presented here provided a benchmark by which to assess the creep and cyclic creep performance.

Failure during creep at 240MPa was a clear indication that oxygen was entering the composite. At 210 and 180MPa this was clearly not happening since the samples survived the test duration of 5×10^5s and displayed no degradation in residual strength. Indeed the residual strengths at this temperature were even improved. From this evidence it can be deduced that matrix cracking occurred either during loading to 240MPa or some time thereafter to enable oxygen transport to the interior with resulting oxidation of the interface and fibre.

The steadily decreasing strain rate has previously been attributed to fibre microstructural evolution in the form of grain growth, evidence of which was shown in the heat treatment investigation of chapter 5. However, as will be discussed later, with this mode of testing this is not the only possible cause for the creep rate reduction.

The capability of the composite to sustain a higher stress under a single load application creep test, as opposed to the cyclic creep testing, is again symptomatic of oxygen ingress at lower stress levels during cyclic loading. Failure seemed to occur during, or soon after, the loading segment of the creep cycle. The exact reason for this embrittlement is not known. However it is possible the embrittlement of the outer tensile surface of the test beam may allow crack initiation at a lower composite applied stress. With oxygen diffusion through the matrix surface, fibres have been shown to oxidise (Pharaoh et al, 1993). It is known the strength and elastic modulus of Nicalon and Tyranno fibres are reduced by growth of silica on the fibre surface. Gogotsi and Yoshimura (1995) have successfully modelled both the strength and elastic modulus in terms of the depth of the silica layer on the fibre surface. The strength was modelled using a simple fracture mechanics approach where the depth of silica acted as the effective flaw size. The elastic modulus of the oxidised fibre was found to be closely approximated by a rule of mixtures calculation, where the silica tube with modulus 70GPa encircled the reduced diameter fibre, which still maintained the initial fibre modulus. With the modulus of the oxidised fibre reduced in the composite surface, the matrix stress would be higher on reloading (as predicted by the rule of mixtures). With sufficient depth of embrittlement at the composite surface and high enough composite applied stress, surface cracking may initiate as, locally, the matrix fracture stress is exceeded. Since this crack would be at the composite tensile surface the interior would be exposed to the environment. Thus further embrittlement would progress in the vicinity of the crack thereby assisting crack propagation and composite failure.

During a creep cycle the constituent with the highest creep rate transfers load to the more creep resistant component as shown by Holmes and Wu (1995), fig 6.11. For glass ceramic matrix composites the matrix usually has a higher creep rate than the fibres. At the end of the loading transient the matrix witnesses its highest stress level but a stress redistribution due to the creep mismatch leads to a gradual decline in matrix stress as load is shed to the fibres. At a certain (low) matrix stress the creep rate will be the same as that of the fibres (the fibres assuming a higher proportion of the creep

stress). On unloading of the composite the matrix can be placed into compression due to elastic fibre contraction. The matrix can then creep in compression but when the load is reapplied the maximum matrix stress will be lower. Thus the apparent composite creep strain accumulated per cycle decreases with cycling as there is less load transfer from the lower modulus matrix to the stiffer fibres. The fibre creep properties dominate as they assume a greater proportion of the creep stress. However even if both the matrix and fibre only exhibited secondary creep there will always be a primary creep portion on reloading due to the transient stress redistribution.

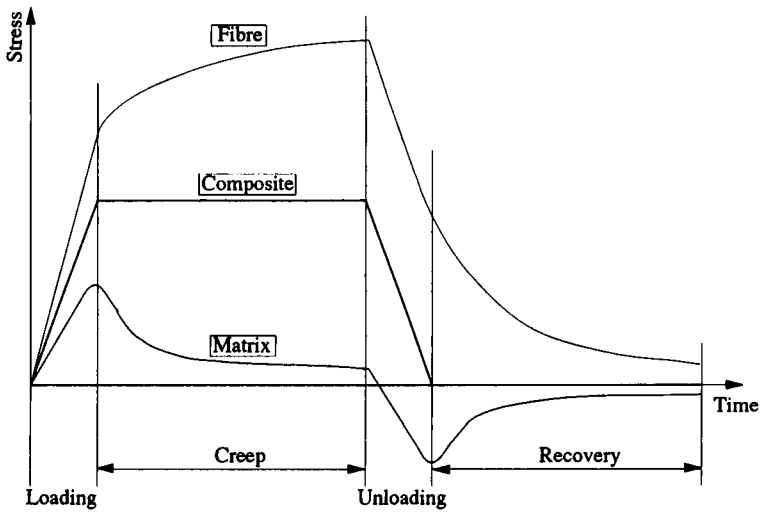

Figure 6.11 Schematic diagram of the stress redistibution between matrix and fibre during cyclic creep. After Holmes and Wu (1995)

The above description of stress redistribution in conjunction with the surface embrittlement theory expounded above could also explain why the failure threshold stress is lower for cyclic creep. As already stated the matrix stress is highest at the end of the loading transient. In a single load application creep test the matrix stress steadily decays. Therefore if the fibres at the exposed surface become embrittled the local matrix stress may not necessarily increase significantly unless fibre fractures occur. In cyclic creep tests the matrix stress becomes negative upon composite unloading and correspondingly decays back towards zero stress during the hold time. From this stress state reloading would clearly result in a tensile matrix stress which at the surface would be higher due to reduced stiffness fibres and possibly above the matrix fracture strength. Hence surface embrittlement would have a greater reduction in composite performance under cyclic creep loading.

The creep envelopes for all the hold times were remarkably similar as shown in figure 6.9. There were initial variations between the maximum and minimum strains for different hold times but after a short period the trend was similar. The amount of creep

during a cycle clearly increased with the hold time thereby explaining the larger strain envelopes for the longer hold times but the gradient of the curves in the figure, which describes the amount of creep strain not recovered during the relaxation period, is alike for all of the hold times tested.

Despite the assertion that fibres near the exposed surface actually experience a reduction in their elastic modulus during cyclic loading an elastic modulus increase was observed for the composite. Several factors are possible for this occurrence such as matrix or fibre elastic modulus increments or a redistribution in matrix stress.

The shrinkage observed in Tyranno and Nicalon fibres has also been noted to increase the elastic modulus. Hochet et al (1997) noted a 13GPa increment in the fibre elastic modulus at room temperature (180GPa to 193GPa) after a five hour heat treatment of Tyranno fibres at 1200°C.

Matrix elastic modulus increases are possible through the devitrification of residual glass. While this may not increase the room temperature elastic modulus significantly the reduction in the amount of glass at the grain boundaries would increase the apparent viscosity of the matrix at elevated temperatures. Thus less viscous deformation would occur during loading, making the apparent stiffness higher.

A process synonymous with the matrix cracking which invalidates the flexure stress calculations is possible during creep. Under an applied stress at high temperature, creep on the tensile side of the test beam will have a tendency to shift the previously central neutral axis towards the compressive side of the beam. This gradual migration of the neutral axis could manifest itself as a reduction in the creep rate and also an increase in the apparent elastic modulus since a greater volume of the matrix, than that allowed for in the linear elastic bend equations, is under stress.

The flexural strength improvement could result from an increase in the matrix cracking threshold, consistent with an increase in the interfacial shear stress or from the stress redistribution from matrix rich areas to in-line fibres thereby delaying the onset of small cracks prior to bulk matrix cracking with the resultant oxygen ingress. Similarly the explanation given above of the movement of the neutral axis would reduce the stress on the tensile face and therefore delay matrix cracking until a higher composite stress was reached. The residual strengths obtained after cyclic creep testing approximate to the bulk matrix microcracking stress evident in the flexural stress strain plots from room

temperature of figure 6.1. Isolated microcracks at lower stresses do not show as modulus changes to the bulk composite in stress-strain plots and have little effect at room temperature. At high temperature such cracks allow oxygen ingress and subsequent composite embrittlement with premature failure.

The final explanation for improved residual strengths after testing is the compressive stress induced in the matrix by elastic fibre contraction. This stress must be overcome in addition to the normal fracture strength thus preventing matrix cracking and excluding the environment until later in the loading ramp.

When a composite sample survived the cyclic creep experiments it appeared the accumulated strain was very much lower than that obtained from single load application creep tests at the same stress. Figure 6.12 compares the creep and cyclic creep (240min hold time) at 180MPa. The creep strain accumulation at 5×10^5s for the creep run was 4.91×10^{-3}. For the cyclic creep run the strain at this time was typically 3.72×10^{-3}. If the time spent at the creep load is directly compared then for the creep test the creep strain at 2.5×10^5s was 4.32×10^{-3}. This is still much higher than the cyclic creep strain for the full test duration. It could be that this lower rate of creep accumulation due to the recovery half of a cycle is advantageous and could extend the lifetimes of components made from such composites. This will be discussed in greater depth in the modelling section.

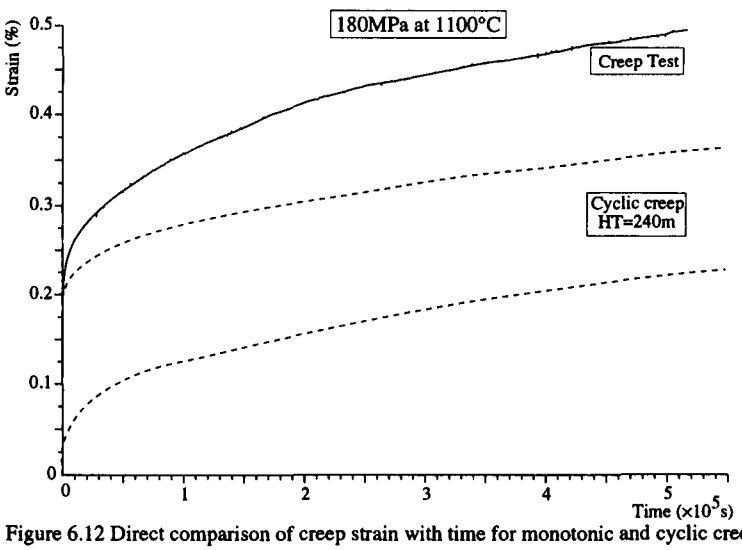

Figure 6.12 Direct comparison of creep strain with time for monotonic and cyclic creep

6.3 Tensile Creep of UD BMAS/Tyranno

Further to the creep testing of UD BMAS/Tyranno in the flexural mode, uniaxial creep

studies at 1100 to 1200°C have been undertaken. The BMAS matrix has a higher temperature capability than the aluminosilicate glass tested which will be reported in section 6.4. In the BMAS/Tyranno composite system samples can be tested at temperatures where both matrix and fibres creep.

6.3.1 Monotonic Tensile Properties of UD BMAS/Tyranno

To place the following results in context the tensile properties at high temperatures must be briefly reviewed. Monotonic tensile tests at 1150 and 1200°C and a cross head speed of 0.2mm/min yielded ultimate strengths of 300 and 299MPa respectively. However, the rate of 1MPa/s used during loading to the required creep stress was not low enough to prevent premature failure at 175.4MPa. From the plots of figure 6.13 it can be seen the lower strength corresponds to a pronounced deviation in the stress strain plot found during uniaxial testing. The difference in the two loading rates was approximately a factor of three, i.e. the 0.2mm/min test was three times quicker than that at 1MPa/s. Therefore it can be assumed the maximum sustainable creep stress at 1200°C was somewhere below this ceiling. The flexural strength at 1100°C of UD BMAS/Tyranno was also approximately 300MPa. Also of note in figure 6.13 is the lower elastic modulus at the lower testing rate.

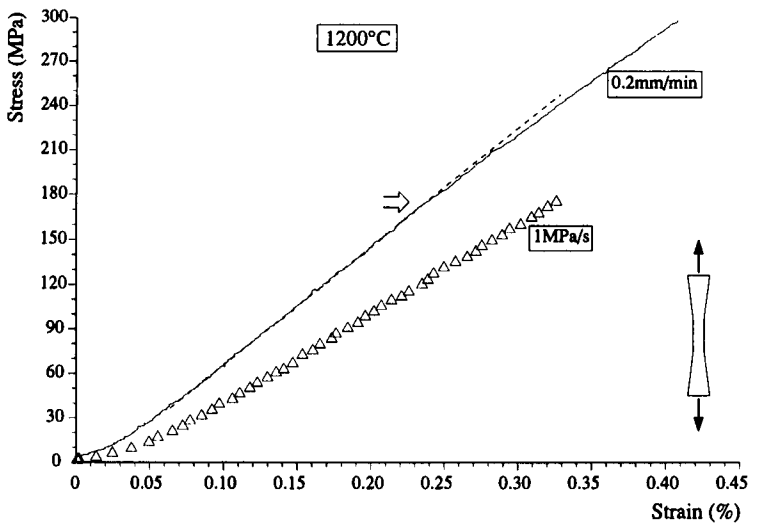

Figure 6.13 Tensile stress strain behaviour at 1200°C for uniaxial tensile test and sample which failed at 174.5MPa during load up for creep testing

6.3.2 Tensile Creep Testing

In the first phase of tensile creep testing of BMAS/Tyranno samples were heat treated at 1100°C for one hour prior to testing. The testing method involved mounting the sample in the pull-rods, then the short furnace was put into place. Extra insulation was

then added around the points at which the pull-rods emerged from the furnace. The extensometer was then located and heating started at 15°C/min. At the set temperature a 15minute hold was allowed before load application. Loading was automatic at a rate of 1MPa/s. The results of creep with an applied stress of 100MPa are given in fig 6.14 as strain against elapsed time and in fig 6.15 as strain rate against strain. The three test temperatures were 1100, 1150 and 1200°C.

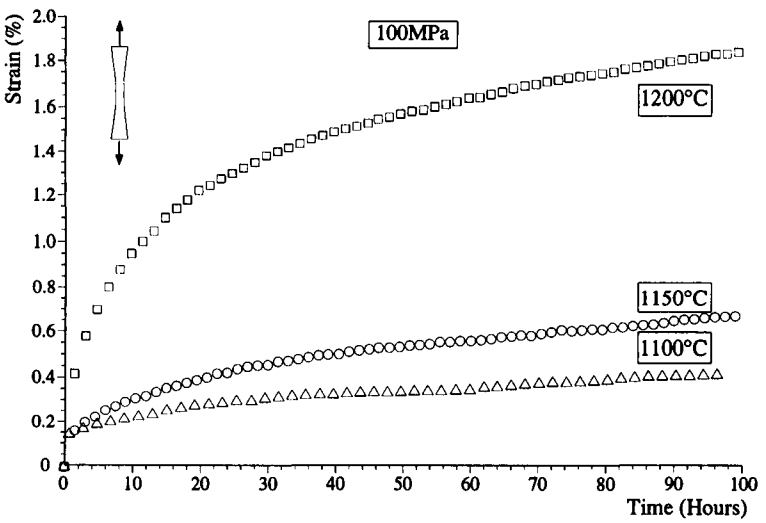

Figure 6.14 Creep curves for a stress of 100MPa at 1100, 1150 and 1200°C for unidirectional BMAS/Tyranno. Pre treatment of 1 hour at 1100°C

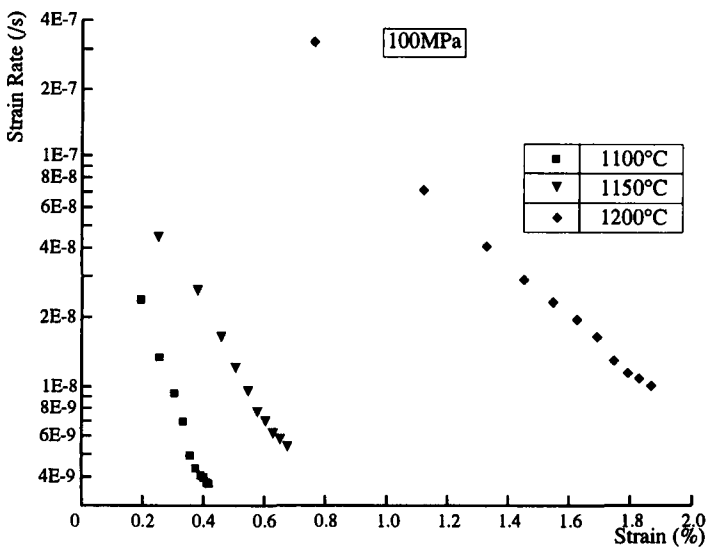

Figure 6.15 Strain rate versus strain for UD BMAS/Tyranno subjected to 100MPa at 1100, 1150 and 1200°C

As with all work on both Nicalon and Tyranno reinforced composites the creep rate was found to steadily decrease at all the exposure temperatures (fig 6.15). The composite could withstand the loading of 100MPa for 100hours at the three temperatures used. Minimum creep rates and degree of strain accumulation are given in Table 6.3.

Table 6.3 Strain rate and strain accumulation at 100 hours for UD BMAS/Tyranno

Temperature (°C)	1100	1150	1200
100 Hour Strain (ε_{100})	4.27E-3	6.74E-3	18.35E-3
100 Hour Strain Rate (/s)($\dot{\varepsilon}_{100}$)	3.84E-9	5.82E-9	1.04E-8

The rates can be compared directly with those of Wu and Holmes (1993). At 60 and 120MPa they found CASII/Nicalon accumulated 0.58 and 1.36% strain at 1200°C in argon after 100hours. The corresponding 100hour strain rates were 0.46 and 1.1×10^{-8}/s. This shows the creep rates were similar but the CASII/Nicalon showed a lower creep accumulation.

When the output from the extensometer was recorded during warm up to temperature it became clear the composite had not reached equilibrium during the 15 minute hold at temperature. Indeed a shrinkage was observed which precipitated the dilatometer stability investigation reported in chapter 3. It appeared that whenever UD BMAS/ Tyranno was exposed to temperatures in excess of 1100°C a longitudinal shrinkage was observed which continued for several hours. The effect of this shrinkage on the creep properties was therefore investigated by heat treating the sample to be tested *in situ* for 24hours prior to creep testing. Apart from this addition no other modifications were made to the testing method. The results of the 24hour exposure to 1200°C is compared directly in figure 6.16 with a non-heat treated sample. Both creep tests were at an applied stress of 100MPa at 1200°C. Similarly the creep rates with respect to the accumulated strain are presented in figure 6.17.

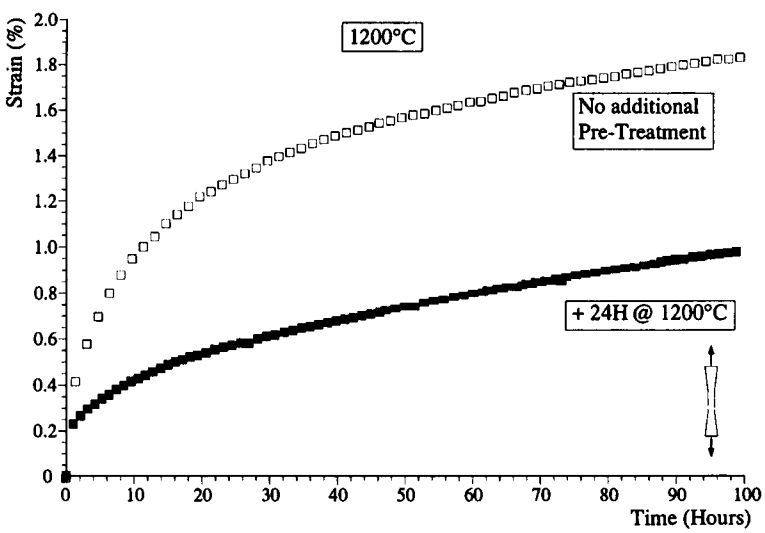

Figure 6.16 Effects of 24 hour hold at 1200°C prior to creep testing at 1200°C and 100MPa. Unidirectional BMAS/Tyranno.

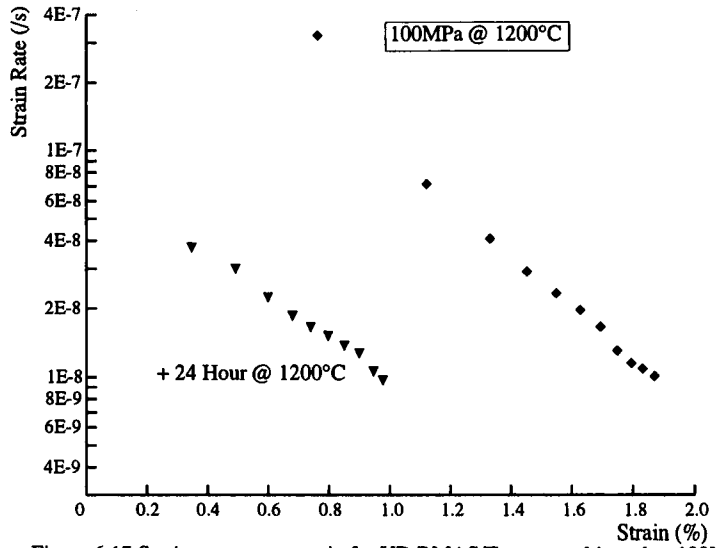

Figure 6.17 Strain rate versus strain for UD BMAS/Tyranno subjected to 100MPa at 1200°C showing effect of 24 hour at 1200°C pre-treatment

As can be seen there was a remarkable disparity between the two with markedly lower strain accumulation after the 24 hour pre treatment. However the 100 hour creep rates were not dissimilar. These final rates are given in Table 6.4.

Table 6.4 Effect of heat treatment at 1200°C on strain rate and strain accumulation

Composite condition	**As Received**	**24 hour @ 1200°C**
100 Hour Strain (ε_{100})	18.35E-3	9.80E-3
100 Hour Strain Rate (/s) ($\dot{\varepsilon}_{100}$)	1.04E-8	1.00E-8

The results show the strain accumulation after the pre treatment is nearly one half that of the non heat treated sample. This result reverses the relative performance of the BMAS and the CAS matrix composites as the BMAS/Tyranno shows a demonstrably lower creep accumulation after the stabilising heat treatment. Despite close examination of the polished gauge sections of crept samples it was not possible to discern any features indicative of creep damage (fig 6.18). Surface oxidation seems to be the only evidence of high temperature exposure.

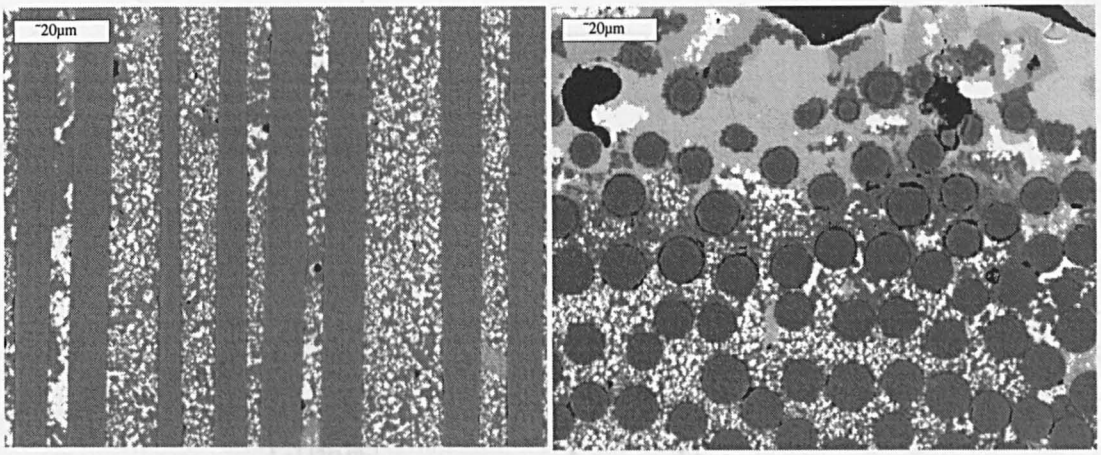

Figure 6.18 Transverse and longitudinal images of UD BMAS/Tyranno crept at 1200°C for 100 hours. No damage could be discerned over the as received composite except an oxidised surface layer (shown)

Despite the monotonic strength testing results, it was possible to load to 200MPa, as the following incremental creep plot shows, fig 6.19. An initial creep stress of 125MPa was applied for ~100 hours after which time the load was incremented to 150MPa. After a further 100 hours the sample was loaded to 200MPa. Failure at this stress only occurred after an additional 18.6 hours.

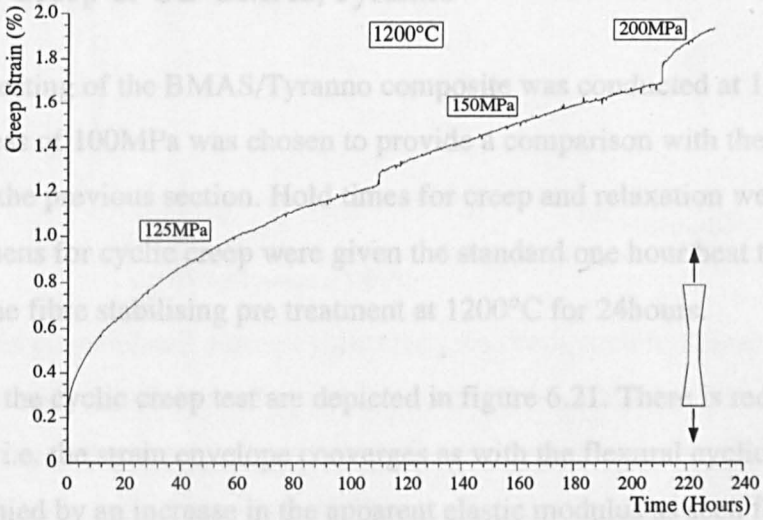

Figure 6.19 Tensile creep of UD BMAS/Tyranno, tile NPP12, creep stresses of 125, 150 and 200MPa

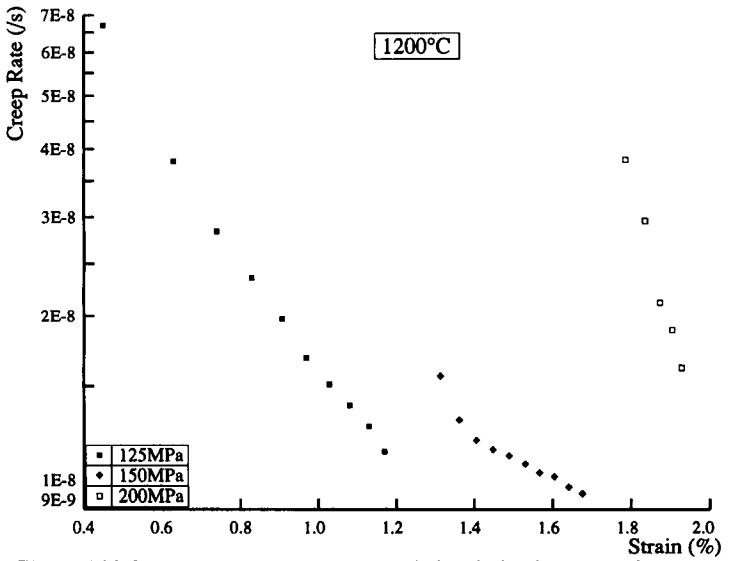

Figure 6.20 Creep rate versus creep accumulation during incremental creep at 1200°C

The above incremental creep test was originally designed to facilitate calculation of a stress exponent. However it can be seen from figure 6.20 that the 100hour creep rate at 150MPa (0.96×10^{-8}) was lower than the 100hour creep rate at 125MPa (1.14×10^{-8}). Because of this it has not been possible to calculate a stress exponent.

6.3.3 Cyclic Creep of UD BMAS/Tyranno

Cyclic creep testing of the BMAS/Tyranno composite was conducted at 1200°C. The maximum stress of 100MPa was chosen to provide a comparison with the standard creep tests of the previous section. Hold times for creep and relaxation were set at 12 hours. Specimens for cyclic creep were given the standard one hour heat treatment at 1100°C and the fibre stabilising pre treatment at 1200°C for 24hours.

The results of the cyclic creep test are depicted in figure 6.21. There is reduced strain on each cycle i.e. the strain envelope converges as with the flexural cyclic creep. This was accompanied by an increase in the apparent elastic modulus as seen for both the BMAS/Tyranno flexural cyclic creep and AS/Nicalon tensile cyclic creep. The increasing modulus with cycling is shown in figure 6.22.

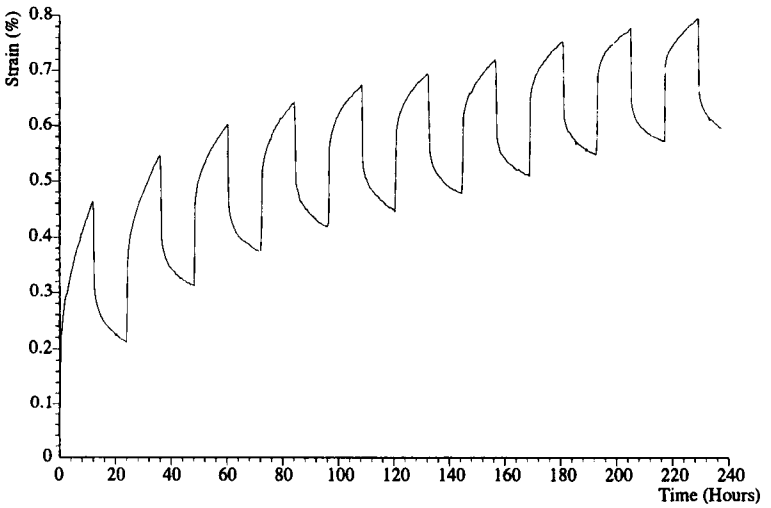

Figure 6.21 Tensile cyclic creep of UD BMAS/Tyranno at 1200°C and 100MPa Cycle hold times of 12 hours.

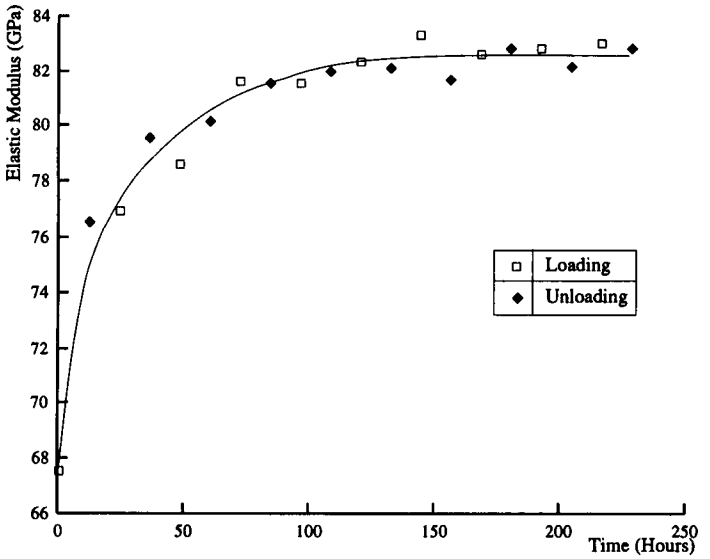

Figure 6.22 Evolution of apparent elastic modulus during cyclic creep of UD BMAS/Tyranno at 1200°C

When the strain accumulated during cyclic creep was compared to the standard creep test, strain was again much lower for the cyclic test. To enable a fair comparison, time at load was compared, not total elapsed time. During cyclic creep the total strain at the end of the 10^{th} cycle at load (i.e. after 216 hours of testing) was 7.9×10^{-3}. For the standard creep test the final strain at 100 hours was 9.8×10^{-3}. When the strain rate against strain plots were compared the two appeared similar (fig 6.23). The finding seems to suggest that for a given strain the strain rate for standard testing and cyclic testing is the same. This must be qualified by stating this only holds true on the loading segment of the cycle and if the previous maximum cycle strain has been exceeded. To test this the maximum strain on the first cycle was recorded. The second cycle was then scrutinised to discover the time at which the same strain level was attained. The difference between the two times was calculated and subtracted from the whole of the

second loading cycle. This was repeated on successive cycles. The results are shown in figure 6.24 with the standard creep test under the same testing conditions.

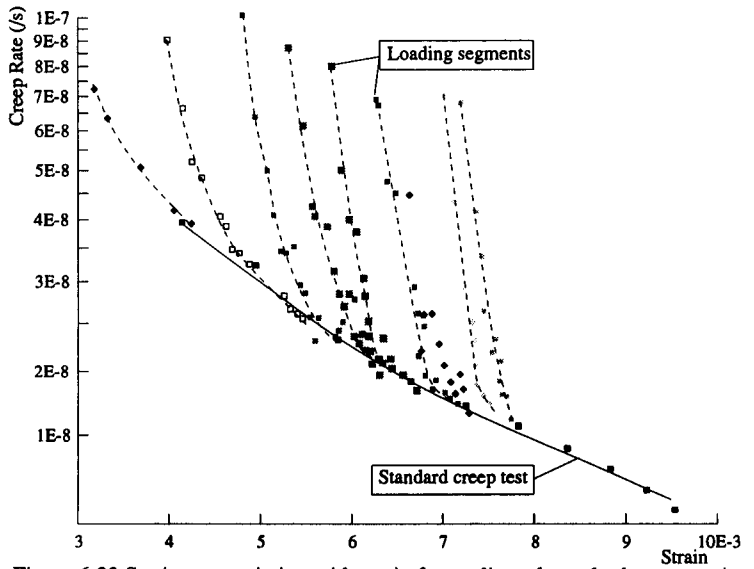

Figure 6.23 Strain rate variation with strain for cyclic and standard creep testing at 1200°C and 100MPa

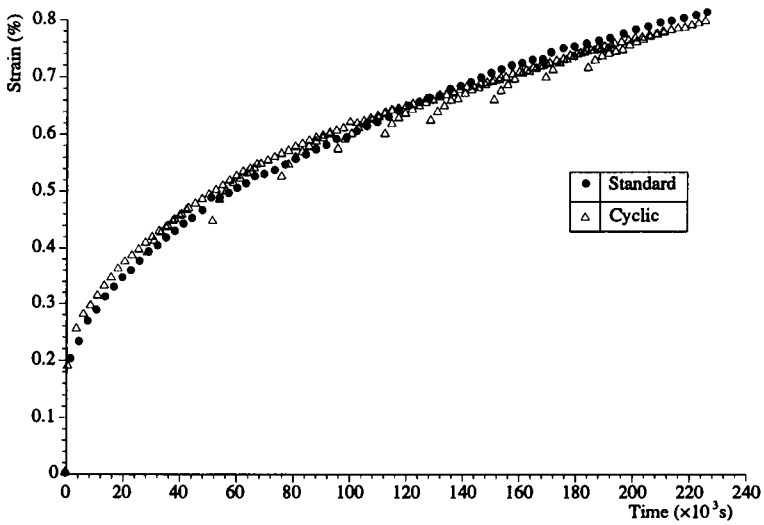

Figure 6.24 Comparison of cyclic and standard creep. Cyclic loading curves have strain matched by subtraction of varying periods (see text)

It can be seen the 240 hours of cyclic creep testing was equivalent in terms of strain accumulation and strain rate to approximately 63 hours of a standard creep test. The time subtracted from each successive cycle represents the interval necessary for load transfer from the matrix to the fibres and also a component for the primary creep of the fibres. This time interval was nearly constant at between 12.5 and 13.2 hours.

The oxidation of this sample was much more severe than the standard creep test due to the longer exposure duration. Micrographs of the sample have shown a planar region at the exposed sample surface (fig 6.25). Fibres within this region have become strongly bonded to the matrix as evinced by the fractures through the fibres even longitudinal to the fibre. Also at the fibre-matrix interface bubbles seemed to have formed. The

bubbles were most probably the product of oxidation of the carbon interface or fibres since decomposition of the silicon oxycarbide phase is responsible for SiO and CO evolution. High fugacities can build up at the interface as gas transport through the matrix is rate controlling. It seems the lifetime limitation of this composite system is the exposure time in the oxidising environment since embrittlement begins at the surface. With crack initiation and growth in this embrittled region on reloading oxidation can progress to the interior.

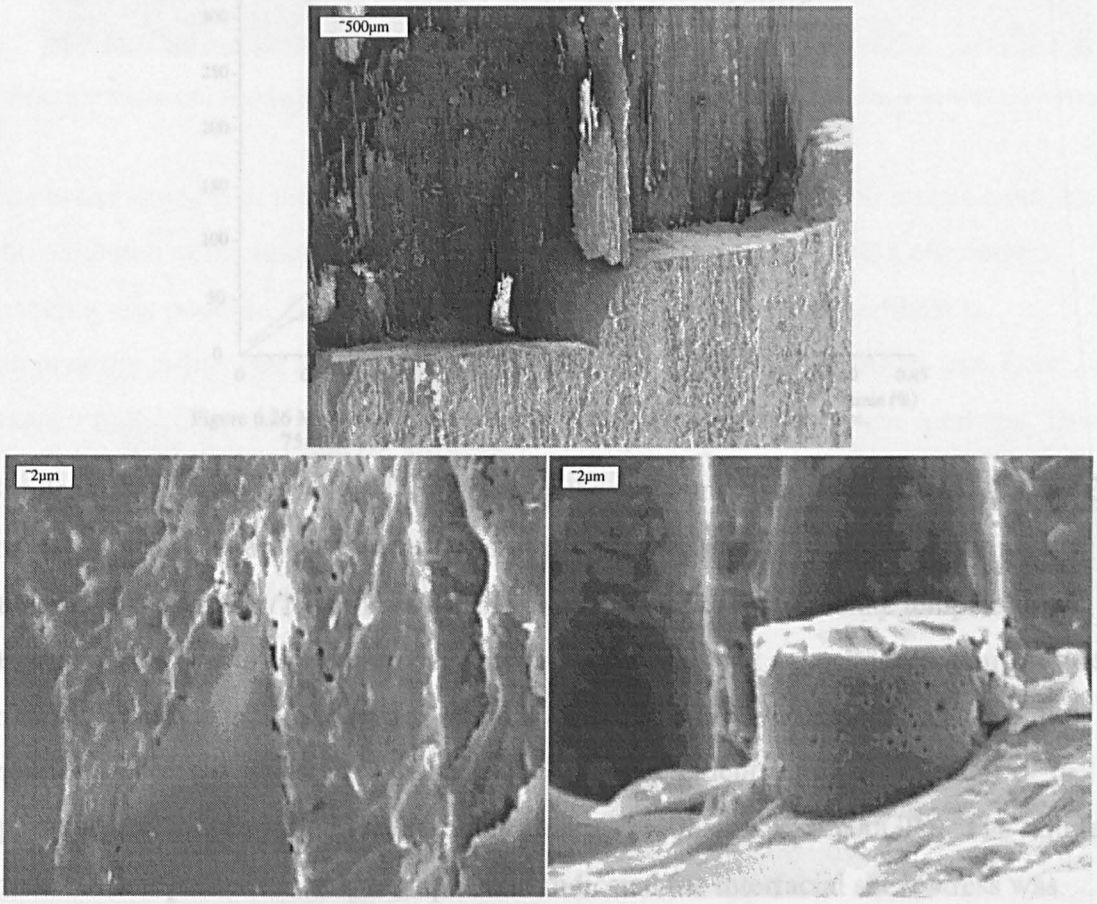

Figure 6.25 Degradation noted after cyclic creep at 1200°C and 100MPa at the interfaces and fibre surfaces at exposed UD BMAS/Tyranno near surface regions

6.4 Tensile Creep of UD Aluminosilicate/Nicalon

The provision of Aluminosilicate/Nicalon (AS/Nicalon) allows investigation into a system where mechanical behaviour can be explored at temperatures where the matrix creeps extensively but the fibres exhibit purely Hookean behaviour.

A similar system has been investigated by Khobaib and Zawada (1991) where the low temperatures necessary for matrix flow enabled hot gripping to be utilised.

6.4.1 Monotonic Tensile Properties of UD AS/Nicalon

Testing of this system has been conducted only at room temperature and two other temperatures (750 and 800°C). The glass softening point was quoted by the manufacturers as 745°C. The resultant tensile stress strain plots are shown in fig 6.26.

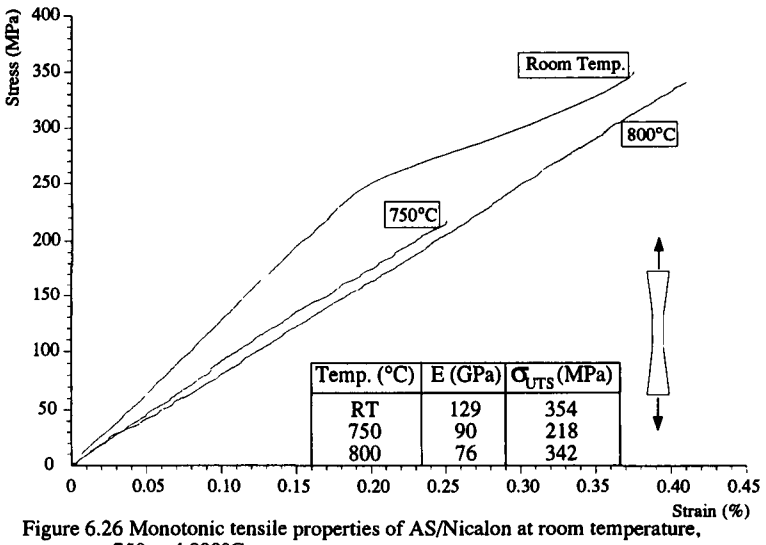

Figure 6.26 Monotonic tensile properties of AS/Nicalon at room temperature, 750 and 800°C

Similar strengths were obtained from testing at room temperature and 800°C. At 750°C the strength was severely degraded. These results seem similar to the increase in strength of the BMAS/Tyranno system when compared to intermediate temperature strengths. However the retention of higher strength occurs at a much lower temperature in this system due to the lower temperature capability of the matrix. The elastic modulus decreased significantly with temperature increments until, at 800°C, it approximated that expected for the fibres alone ($V_f = 0.4$ and $E_f = 200GPa$). The failure mode of fibre pull-out at room temperature indicated the interfacial shear stress was low. This has been proven by fibre indentation testing where an interfacial shear stress of 18MPa was measured, (Boccaccini et al, 1997).

The pull-out failure mode was not mirrored at 750 or 800°C, here brittle failure with no pull-out defined the fracture surfaces (fig 6.27).

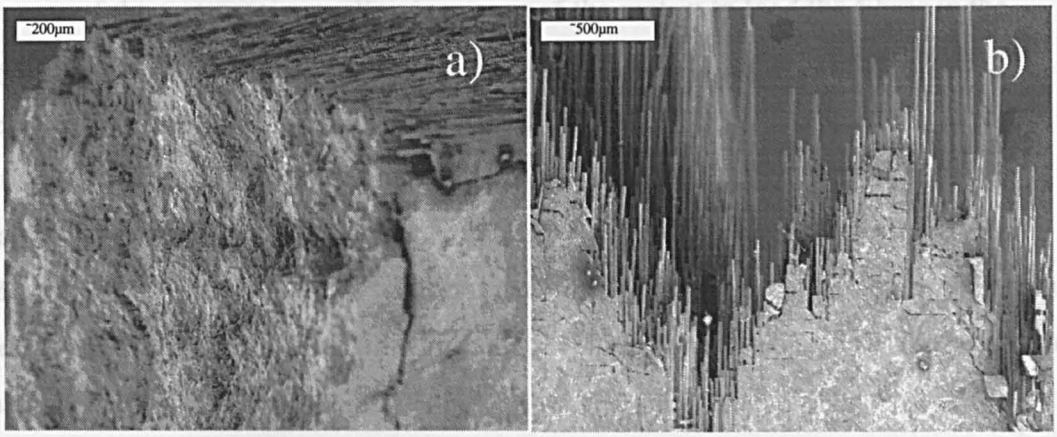

Figure 6.27 Micrographs depicting a) Brittle fracture and b) 'Ductile' failure from testing at750°C and room temperature respectively

The lower strength of the sample tested at 750°C was probably due to matrix cracking and oxidation of the interface. At 800°C the low viscosity of the matrix ensured no cracking was possible. Hence the load transfer from the matrix to the fibres is temperature influenced and can also be enhanced by reducing the loading rate. Load transfer to the fibres also appears as a reduction in the composite elastic modulus. This has been demonstrated by varying the loading rate and measuring the composite elastic modulus from the resulting stress-strain plot in the region 0-50MPa. The same sample was used at all the testing rates. The results of this test can be viewed in figure 6.28.

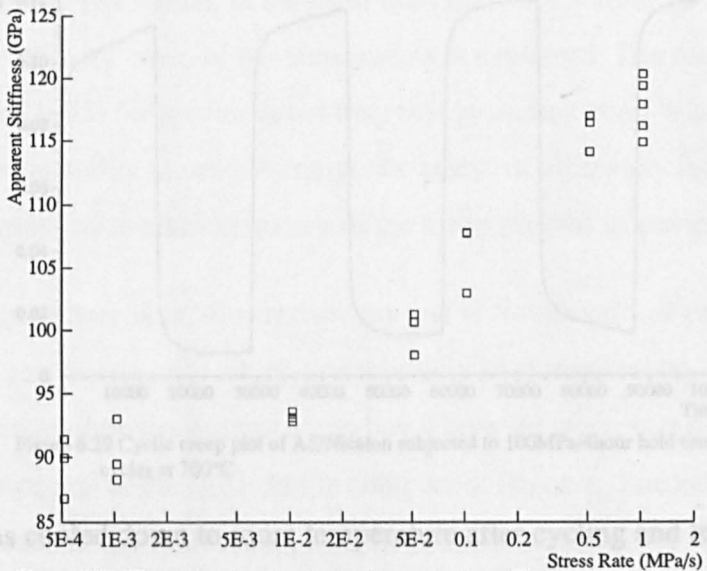

Figure 6.28 Plot indicating the change in composite stiffness with loading rate at 750°C

6.4.2 Cyclic Creep of AS/Nicalon

The fibres reinforcing the glass aluminosilicate matrix are known to be fully elastic at the temperatures used for testing this composite (e.g. Hochet et al, 1997). Therefore

with the warm gripping used here the fibres were rigidly constrained at the gripped segments of the test specimen allowing creep of the matrix to load the fibres in the gauge section elastically. Again it should be stated hot gripping would be expected to give different results. With hot gripping, the fibres would be able to move readily relative to the reduced viscosity matrix. This would explain how none of the AS/ Nicalon composite samples tested failed during creep testing. Samples did fail during load up at approximately 175MPa but not once loading had been completed. This result differs from the study by Khobaib and Zawada (1991) who noted tertiary creep prior to failure.

The results of cycling of AS/Nicalon is shown in figure 6.29. If the modulus of the fibres is taken as 200GPa and the matrix is considered to creep until it has shed all its load then a total strain of 1.25×10^{-3} could be expected. These results will be discussed in greater detail on the modelling of composite creep section.

The AS/Nicalon system appeared to show an elastic modulus increment on subsequent cycles. This is in common with the BMAS/Tyranno system as seen in the flexure testing. This finding will also be discussed in the modelling section.

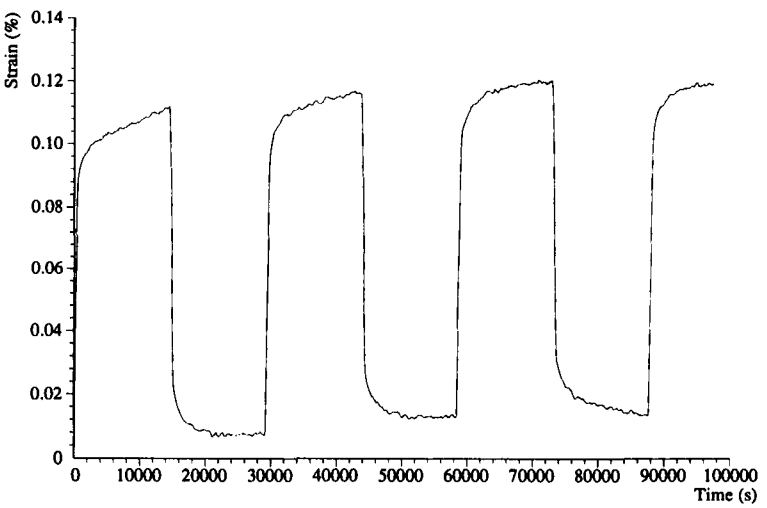

Figure 6.29 Cyclic creep plot of AS/Nicalon subjected to 100MPa/4hour hold time cycles at 700°C

This sample was cooled down to room temperature after cycling and tensile tested. The strength was found to be lower than that obtained for the as received sample (268MPa as opposed to 354MPa). Examination of the fracture surface revealed there was extensive pull-out in the central region but a large zone of flat topography was also seen at the periphery of sample (fig 6.30).

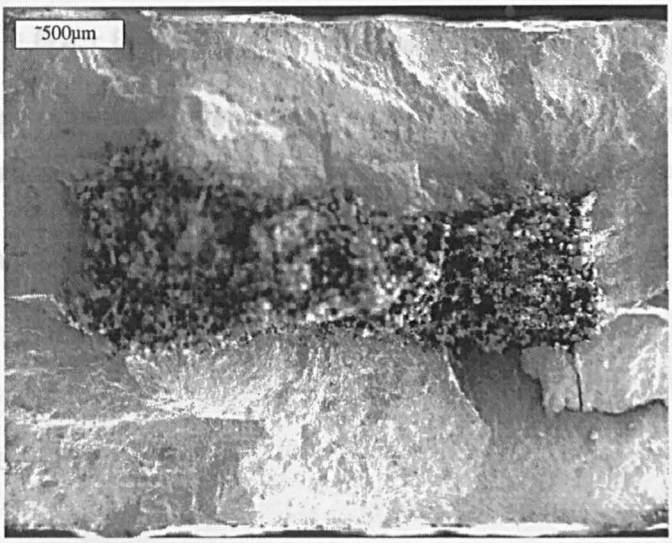

Figure 6.30 'Ductile' central region surrounded by brittle, oxidised peripheral zone

This region was also observed for the heat treatment studies in chapter 5 of BMAS/ Tyranno where the cause was oxygen diffusion through the matrix. This process is more rapid in glassy materials and would therefore explain the greater depth of embrittlement from the surface in this system.

6.5 Modelling of High Temperature Behaviour

Holmes and Wu (1995) have provided a model for describing creep behaviour. Provided in Appendix I is a BASIC program which was composed with the Holmes and Wu equations listed. The model, in the form used here, is a simple 1D analytical approach where primary creep of the constituents is neglected. The reader is directed to Holmes and Wu (1995) for greater detail than that presented here. While the model, as used here, has little ability to predict composite creep, or ultimately failure, it can be used to demonstrate certain key elements of the creep process in composites.

Their model is used here in an illustrative way and is simplified to a two component system of fibre and matrix only which undergo only secondary creep. The creep of each phase is assumed to obey the general creep law where the strain rate of each constituent is directly proportional to the stress in the component (σ_f or σ_m) raised to the power 'n' (the stress exponent of the individual phase). For the modelling here the stress exponent for the matrix was set equal to 1.

For the case where no slipping occurs at the interface it is assumed the strain rate of each phase is equal to the strain rate of the composite, i.e.:

$$\dot{\varepsilon}_{c,tot} = \dot{\varepsilon}_{f,tot} = \dot{\varepsilon}_{f,el} + \dot{\varepsilon}_f = \dot{\sigma}_f / E_f + \dot{\varepsilon}_f = \dot{\varepsilon}_{m,tot} = \dot{\varepsilon}_{m,el} + \dot{\varepsilon}_m = \dot{\sigma}_m / E_m + \dot{\varepsilon}_m \quad (6.1)$$

where the subscripts c, f and m refer to composite, fibre and matrix respectively and the total (tot) strain in each phase is composed of elastic (el) and creep elements.

From the rule of mixtures:

$$V_f \sigma_f + V_m \sigma_m = \sigma_c \quad (6.2)$$

Or in terms of stress state:

$$V_f \dot{\sigma}_f + V_m \dot{\sigma}_m = \dot{\sigma}_c \quad (6.3)$$

From the above equations:

$$\dot{\varepsilon}_{c,tot} = \frac{1}{E_c}(\dot{\sigma}_c + V_f E_f \dot{\varepsilon}_f + V_m E_m \dot{\varepsilon}_m) = \dot{\varepsilon}_{c,el} + < \varepsilon_f >_f + < \varepsilon_m >_m \quad (6.4)$$

Where the final two terms are the creep components of the composite strain rate given by:

$$< \dot{\varepsilon}_f >_f + < \dot{\varepsilon}_m >_m = V_f \frac{E_f}{E_c} \dot{\varepsilon}_f + V_m \frac{E_m}{E_c} \dot{\varepsilon}_m \quad (6.5)$$

For a uniaxial aligned fibre composite the overall creep rate is equal to the weighted mean value of the constituent creep rates. To find the stress in each component the stress redistribution due to elastic and creep strains over a finite period must be calculated. For a two phase system:

$$\dot{\sigma}_f = \frac{E_f}{E_c}\{\dot{\sigma}_c + V_m E_m (\dot{\varepsilon}_m - \dot{\varepsilon}_f)\} \quad (6.6)$$

similarly:

$$\dot{\sigma}_m = \frac{E_m}{E_c}\{\dot{\sigma}_c + V_f E_m (\dot{\varepsilon}_f - \dot{\varepsilon}_m)\} \quad (6.7)$$

The model allows updating of the component stresses over different loading histories.

During a standard creep test load is transferred to the higher creep resistant component. If this process takes place at a temperature and stress at which both components creep,

then at some elapsed time the matrix and fibre creep rate match and a steady state condition is reached. In glass-ceramic SiC based fibre reinforced composites a lower stress in the matrix is necessary to match the fibre creep rate as the fibres have much greater creep resistance. However the matrix can still contribute to the performance of the composite by acting as a 'damper' to slow down the loading of the fibres. Following the analogy, in the standard creep test the 'damper' becomes fully extended and so acts almost solely to shield the fibres from the environment (Weber et al, 1994, calculated that the matrix only sustains ~5% of the creep stress at 1200°C in CAS/Nicalon). However if the load is removed and recovery permitted by holding at a lower stress the damping effect can be utilised again. If the loading hold time is less than the time necessary for the steady state matrix and fibre stresses to be reached a lower creep accumulation can be expected since the fibres will not reach the higher load as experienced during standard creep testing. Benefits also accrue if the loading time is longer since the time spent by the fibres at the maximum stress is reduced.

The above principles are illustrated in figure 6.31. This figure represents the stress distributions during cyclic testing. Primary creep is neglected and the fibres are considered elastic. Also depicted, for direct comparison, are the predictions for a standard creep test.

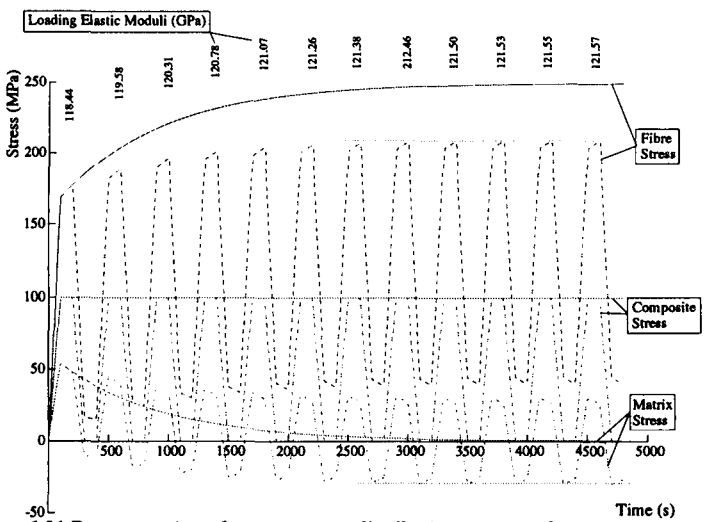

Figure 6.31 Demonstration of creep stress redistributions to a steady state. Fibres were treated as elastic. Cyclic (broken lines) and single cycle loading (solid lines) are compared. Also shown are loading elastic moduli

The simple model shows how the maximum tensile stress in the matrix decreases with the number of cycles until a steady state is reached. This level for a stress exponent equal to '1' and elastic fibres is the same as the compressive stress on unloading. The advantage of the cyclic loading is clearly demonstrated by the much lower stress in the fibres when compared to the standard creep test. The reason for the converging 'strain

envelope' can also now be deduced. The maximum creep of the matrix occurs on the first cycle since it 'sees' the highest stress at the end of the loading transient. The highest strain occurs because the strain rate is considered to be directly proportional to the stress (i.e. n=1). On subsequent cycles the matrix has a lower stress to shed to the fibres so the difference between successive strain maxima and minima is lower.

From the strain and stress values gathered from the model it was also possible to calculate the apparent elastic moduli on each of the loading cycles. For the example conditions used, the elastic modulus was found to increase with the number of cycles (fig 6.31). Since the fibres were considered elastic, the increase is believed to be due to the stress state of the matrix. As with the reduced 'strain envelope' the lower the matrix stress the less it creeps. When the matrix stress is positive the matrix yielding has the effect of increasing the composite strain as seen on a stress-strain plot. If the matrix stress is lower, the proportionality of stress and strain rate, results in lower creep so an apparently higher elastic modulus is measured.

The above explanation provides insight as to why the creep envelopes were so similar during flexural cyclic creep considering the large variation in hold times. It is suggested the hold times used were all shorter than the time necessary for load transfer from the matrix to the fibre to reach the steady condition. The result could have meant the vacillation of the matrix stress either side of zero, during the cycling, as a consequence the fibre stress would oscillate about some average stress but with a perturbation size dependent on the cycle time. This average stress on the fibre would have been the same for all the hold times and hence the similarity in the 'creep envelopes'.

If fibre creep was incorporated in the model the matrix stress would not decay to zero, rather it would decay to a value where the creep rate was the same as the fibre.

Incorporation of the creep properties of the fibres is fraught with oversimplification. Limited studies of the creep of Tyranno fibres have been presented in the literature. Emig and Wirth (1995) tested Tyranno fibre bundles in air and argon between 400 and 1300°C. The creep testing they performed did not result in useful data as the fibres were found to shrink under the applied loads. This was attributed to collapse of channels formed during the pyrolysis processing stage resulting in a lower pore volume fraction. This shrinkage was also found to be dependent on the atmosphere. Low oxygen partial pressures or inert atmospheres have been found to enhance the β-SiC grain growth

(Bodet et al, 1996).

Creep of unstable fibres has been modelled by Jia et al, (1993). The problem of β-SiC grain growth and decomposition of the silicon oxycarbide phase was modelled by a rheological approach. Here deformation was modelled as viscous flow of a concentrated suspension. Fibres such as the Tyranno and Nicalon ceramic grades creep by grain boundary sliding, creep is therefore controlled by the grain size and the grain boundary character. Thus with increasing grain size fibre viscosity was predicted to increase. Instability of the microstructure means steady state creep was not achieved. However Bodet et al (1996) tested Nicalon fibres in different atmospheres (Ar, CO and an Ar/CO mix) in an attempt to prevent fibre decomposition. In the CO/Ar atmosphere no grain growth was observed and the creep rates all reached steady state. In the pure Ar atmosphere both grain growth and unstable creep was noted. Fibre shrinkage was only seen in the pure Ar environment but not in CO. These results have implications for composite systems since the low matrix diffusivity may allow build up of gases (specifically CO) at the interface. Hence, during testing, it is possible the environment surrounding the fibres constantly changes with consequences for the rate of fibre decomposition or grain size evolution.

6.6 Discussion

The stability of the carbon rich interface has limited the investigation of both the BMAS and AS matrix composites to below their matrix cracking thresholds. When creep testing has been performed above the microcracking stress in inert atmospheres, enhanced creep of the crack bridging fibres occurs (Wu and Holmes, 1993). In inert atmospheres the fibre degradation can be severe since no passivating layer is able to form. The resulting lifetimes, once microcracking has been established were consequently much lower: Wu and Holmes found CASII/Nicalon failed in 70minutes at 250MPa (>cracking threshold) but managed >100hours at 200MPa in Ar at 1200°C.

Higher stability interfaces and fibres would clearly be advantageous. Sun et al, (1996, 1997) have presented results on a BMAS/Nicalon composite system with a BN interface (depth~300nm) protected by a SiC overlayer (100nm). This system is claimed to offer greater oxidative stability which has been demonstrated by static fatigue in three point bend in air (Sun et al, 1997). The interface was found to degrade more rapidly at 600°C than at 950°C from BN volatilisation. At 950°C more rapid sealing of

the interface was muted for the greater strength retention. At 600°C the closure of the interfacial void was too slow to prevent oxidation along the BN/fibre interface.

The strength of the BMAS/BN/Nicalon was found to increase, compared to room temperature results, during tensile testing at 1100 and 1200°C (Sun et al, 1996). It was claimed that creep testing of the system above the microcracking stress was possible with no deleterious effects on composite life. However at the proportional limit stress the presence of matrix cracking is questionable. Deviations in the stress strain plot at such high temperatures can be the manifestation of load transfer from the matrix. Substantiation of this claim may be seen in the low elastic modulus after this stress which is the same as that expected for the fibres alone. Thus the creep testing at 138 and 103MPa for the system does not conclusively demonstrate a property advantage over the BMAS/Tyranno tested here.

In common with the BMAS/Tyranno the system studied by Sun et al, (1996), showed no signs of creep damage for the times, temperatures and stresses investigated. However an increase in the glassy phase was seen as well as phase separation via spinodal decomposition. This is somewhat ironic since the non-equilibrium diphasic pairing of cordierite and celsian in the BMAS/Tyranno composite appears to possess greater thermal stability than the near monophasic bariumosumilite matrix of Sun et al, (1996). The two composites have both shown surface reaction zones caused by oxygen diffusion through the matrix. Sun et al also noted the ability of this layer to function as a passivating barrier limiting further oxygen diffusion.

Nicalon and Tyranno both display very poor creep properties when compared to pure SiC. However a new generation of SiC fibres by both UBE Industries and Nippon Carbon Co. with lower oxygen content is expected to offer higher performance at elevated temperatures. The Hi-Nicalon fibre has been shown to have a temperature capability of ~150°C greater than the conventional ceramic grade Nicalon (Tressler and DiCarlo, 1995; Bodet et al, 1995). Under development is the near stoichiometric SiC 'Hi-Nicalon S' fibre with ~0.2wt% oxygen which is expected to withstand even higher temperatures. The higher elastic modulus of this fibre (~410MPa) is expected to provide superior reinforcement through assumption of a greater proportion of composite applied stress. The lower oxygen content of the new Nicalon range of fibres cannot be matched in the Tyranno fibres. Introduction of the titanium content of the fibre as titanium alkoxide means ~5wt% of oxygen is present in the final 'LOX-E' fibre (Hochet al,

1997).

A comparison of various composites and fibre reinforcement is given in figure 6.32. The superiority of the ceramic materials and composites over that of a monolithic superalloy is clear. The data of Bodet et al (1996) for Nicalon fibres in a CO/Ar mix with pp of CO of 40kPa is in close accord with the creep data of the CASII and BMAS matrix composites (see fig 6.32). The correlation becomes greater when an allowance is made for the greater stress on the fibres within the composite, i.e. for a 33% volume fraction the actual stress on the fibres is approximately 3 times the composite stress. The SCS-6 silicon nitride reinforced composite provides an illustration of the creep properties which may be expected if the stoichiometric SiC Hi-Nicalon S fibres are used for these materials.

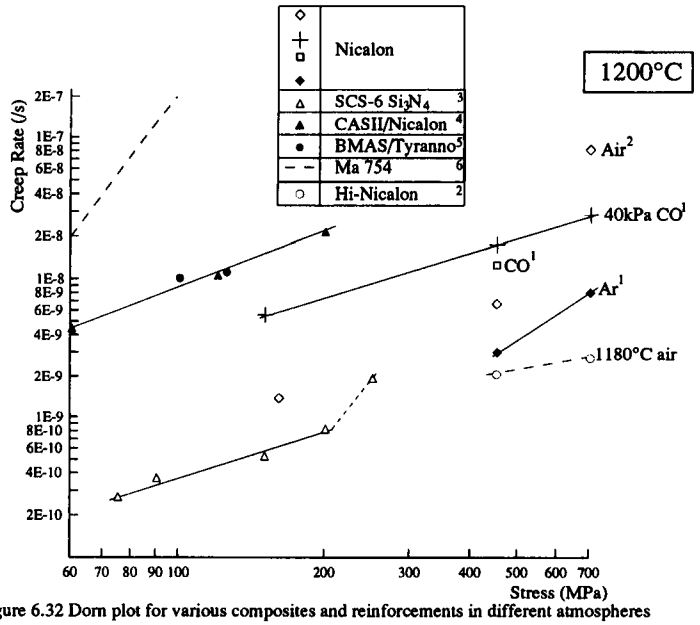

Figure 6.32 Dorn plot for various composites and reinforcements in different atmospheres
1) Bodet et al 1996, 2) Bodet et al, 1995, 3) Holmes et al, 1993, 4) Wu and Holmes, 1993, 5) Current work, 6) Stephens and Nix, 1985

6.7 Conclusions

The high temperature time dependent properties of two composite systems, a GMC and a GCMC, have been investigated. In the former, lower temperature system the temperature used was sufficient for extensive matrix creep but low enough for the fibres to remain linear elastic. In the GCMC both fibres and matrix displayed plastic, time dependent properties when loaded to the investigated temperature range.

In the AS/Nicalon composite the creep strain tended to a limit which was asymptotic to the extension of the fibres alone. This strain to a first approximation could be predicted from the fibre volume fraction, composite applied stress and fibre stiffness. Increasing

the test temperature merely reduced the time necessary to reach the final extension.

In BMAS/Tyranno a constantly decreasing creep rate was observed. Despite alternative possible causes being suggested for this finding in the flexural testing mode, the tensile testing has shown the finding was related to the fibre instability at high temperatures.

Cyclic creep testing in bend has revealed a lower maximum applied stress could be sustained than the standard single load application creep testing. The difference was described in terms of embrittlement of the near surface region.

The testing atmosphere of air placed a limiting maximum on the composite applied stress during testing which coincided with the matrix cracking threshold. Oxygen diffusion through the matrix blighted the high temperature properties of both the systems tested. The deleterious effects were most pronounced in the glass matrix system due to higher gas diffusion rates in non-crystalline materials.

At 1100°C in bend the BMAS/Tyranno could sustain only ~70% of the fast fracture strength at that temperature and only ~60% when the load was cycled. In tension at 1200°C these fractions were not as well defined but both lie below 50% of the fast fracture strength.

In bend the residual composite strength at high temperature after cycling was higher than testing of as received composite. This was attributed to redistributions in matrix stress from matrix rich zones (effectively relieving matrix stress concentrations where microcracking was likely to initiate at low applied stress) and from compressive stress imposed by elastic fibre contraction during unloading.

During cycling at high temperatures in both testing modes and composite systems an apparent elastic modulus increase was observed. This was explained by use of a simple 1D analytical model as outlined by Holmes and Wu, (1995). The modelling also made clear the lower total creep strains observed for the cyclic creep testing over the standard creep testing. The matrix stress decay during loading at high temperature and reversal upon load removal was demonstrated to maintain a lower load in the reinforcing fibres.

Although no stress exponent could be determined due to the limitations imposed by the testing environment, the similarity between the 100 hour creep rates and strain accumulation between this work and that by Wu and Holmes ,(1993), and Weber et al, (1994), seems to suggest fibres dictate the creep performance. It was postulated this

may be to the extent that this form of testing may represent a form of fibre bundle creep evaluation at the temperatures used.

The BMAS/Tyranno system was found to offer similar levels of creep performance to the BMAS/BN/Nicalon system. This system seemed to offer no increase in the maximum creep stress but may outperform in static fatigue where the slower oxidation of BN may permit a greater window for crack healing.

Thus lower oxygen content fibres may be the next development in composite performance at high temperature but higher stability interfaces will be required to exploit the higher creep potential and increased elastic modulus. Without this development, accidental overloads will lead to rapid interfacial oxidation through surface connected matrix cracks.

PAGE NUMBERING AS ORIGINAL

References

Aveston J, Cooper G A and Kelly A, (1971), in 'The Properties of Fibre Composites', NPL Conf. Proc., (IPC Publishing Guildford, 1971) 15-26

Aveston J and Kelly A, (1973), J. Mater. Sci., 8, 352-62

Benson P M, Spear K E, Pantano C G (1988) Ceram. Eng. Sci. Proc., 9 663-70

Berger M H, Hochet N, Lavaste and Bunsell A R, (1996), In Proceedings of ECCM-7, 14-16 May, 1996.

Beyerle D S, Spearing S M, Zok F W, Evans A G, (1992a), J. Am. Ceram. Soc., 75[10]2719-25

Beyerle D S, Spearing S M, Evans A G, (1992b), J. Am. Ceram. Soc., 75[12]3321-30

Bischoff E, Ruhle M, Sbaizero O, Evans A G, (1989), J. Am. Ceram. Soc., 72(5)741-5

Bleay S M and Scott V D, (1992) J. Mater. Sci., 27, 825-38

Boccaccini A R, West G, Janczak J, Lewis M H and Kern H, (1997) J of Mats. Eng. and Perf., Vol. 6, No 3, 1997, pp344-348

Bodet R, Bourrat X, Lamon J and Naslain R, (1995) J. Mater. Sci., 30, 661-77

Bodet R, Lamon J, Jia N and Tressler R E, (1996), J. Am. Ceram. Soc., 79(10)2673-86

Bollet F, Galiotis C and Reece M J, (1996), In Proceedings of ECCM-7, 14-16 May, 1996, 505-510

Bonney L A and Cooper R F, (1990) J. Am. Ceram. Soc., 73[10]2916-21

Brennan J J, (1984), Corning report- Contract no. N00014-82-C-0096, Project no. NR32-616/10-30-81

Brennan J J, Chyung K, Taylor M P, (1984), European patent application no. 84630050.7, 21/11/84

Brennan J J, (1986) Tailoring Multiphase and Composite Ceramics (eds. Tressler R E, Messing G L, Pantano C G, Newnham R E), pp549-60, Plenum Press, New York

Brennan J J, Chyung K and Tayler P M, (1986), US Patent No. 4589900 May 20

Brennan JJ and Prewo KM, (1982), J. Mater. Sci., 17, 2370-83

Budiansky B, Hutchinson J W and Evans A G, (1986), J. Mech. Phys Solids, 34, 2, 167-89

Bunsell A R, (1992), Chapter in "Ceramic Matrix Composites" Ed Warren R, Pub. Blackie and Son Ltd., ISBN 0-216-92682-3 pp12-30

Bunsell AR, Berger M H and Hochet N, (1995), High-Temp. Ceram. Matrix Comps. II: Man & Mats. Dev., (Eds Evans AG & Naslain R) Ceram. Trans. 58, 85-94

Cady C, Heredia F E and Evans A G, (1995), J. Am. Ceram. Soc., 78[8]2065-78

Cain M G, Daniel A M and Lewis MH, (1993), J. Mater. Sci. Lett., 17, 246-52

Cao H and Thouless M D, (1990), J. Am. Ceram. Soc., 73[7]2091-94

Chaim R and Heuer A H, (1987), Adv. Cer. Mat 2[2]154-58

Chaim R and Heuer A H, (1991), J. Am. Ceram. Soc., 74[7]1663-7

Chaim R and Heuer A H, (1992), J. Am. Ceram. Soc., 75[6]1512-21

Charalambides P G and Evans A G, (1989) J. Am. Ceram. Soc., 72[5]746-53

Chawla N, Holmes J W and Mansfield J F, (1995), Mats. Char., 35(4)199-206

Chermant J L and Holmes J W, (1995), High-Temp. Ceram. Matrix Comps. II: Des. Durability and Perf., (Eds Evans AG & Naslain R) Ceram. Trans. 58, pp95-106

Churchman-Davies J J, (1996), Personal communication

Cook J and Gordon J E, 1964 Proc. R. Soc., A228, 508

Cooper R F, Chyung K, J, (1987), Mater. Sci., 22, 3148-60

Cox B N, Marshall D B, (1994), Acta. Metall., 42[2]341-63

Curtin W A, (1991), J. Am. Ceram. Soc., 74, 2837-45

Daniel A M, Elizalde M R, Sanchez J M, Janczak J, Martinez-Esnaola J M, (1997), in

Key Engineering Materials Vols. 127-131, 599-608, *Proceedings of the first international conference in Ceramic and Metal Matrix Composites: CMMC 96,* Eds Fuentes M, Martinez-Esnaola J M, Daniel A M

Daniel I M, Anastassopoulos G, Lee J-W, (1993), Comp Sci and Tech 46, 105-13

Davis J B, Lofvander J P A, Evans A G, Bischoff E and Emiliani M L, (1993) J. Am. Ceram. Soc., 76, 1249

Droillard C and Lamon J, (1996), J. Am. Ceram. Soc., 79(4)849-58

Emig G and Wirth R, (1995), J. Mater. Sci., 30, 5813-18

Evans A G, (1990), J. Am. Ceram. Soc., 73[2]187-206

Evans A G, (1993), paper 2 presented at an AGARD workshop entitled 'Introduction of Ceramics into Aerospace Composites'

Evans A G and Marshall D B, (1989), Acta. Metall., 37, 10, 2567-83

Evans A G, Zok F W, McMeeking R M and Du Z Z, (1996), J. Am. Ceram. Soc., 79[9]2345-52

Filipuzzi L, Camus G, Naslain R, Thebault J, (1994a). J. Am. Ceram. Soc., 77[2]459-66

Fillipuzzi L and Naslain R, (1994). J. Am. Ceram. Soc., 77[2]467-80

Fischbach D B, Lemoine P M and Yen G V, (1988), J. Mater. Sci., 23, 987-983

Frety N, Molins R and Boussage M (1992) J. Mater. Sci., 27, 5084-5090

Gadkaree K P, (1994), J. Mater. Sci., 29, 2417-24

Garrett K W and Bailey, (1977), J. Mater. Sci., 12, 157

Gogotsi Y G and Yoshimura M (1994), J. Mater. Sci. Lett., 13, 680-3

Gogotsi Y G and Yoshimura M (1995), J. Am. Ceram. Soc., 78 (6), 1439-50

Griffith A.A. Phil Trans R Soc, (1921) A221, 163-198

Harris B, Habib F A and Cooke R G, (1992), Proc. R. Soc., A437, 109-31

He M Y, Hutchinson J W, (1989), Int. J. Solids. Struct. 25, 1053-67

He M Y, Evans A G and Curtin W A, (1993), Acta. Metall., 41, 3, 871-8

Hirose Y, Doi H and Kamigaito O, (1984), J. Mater. Sci. Lett., 3,95-96

Hochet N, Berger M H and Bunsell A R, (1997), to appear in J of Micro.

Holmes J W, (1992), J. of Comp. Mats., 26, 6, 916-932

Holmes J W, Park Y H and Jones J W, (1993), J. Am. Ceram. Soc., 76(5),1281-93

Holmes J.W. and. Wu, X, (1995), In "Elevated temperature mechanical behaviour of ceramic matrix composites" Eds. Nair S, Jakus K, Butterworth Heinmann

Huger M, Souchard S and Gault C, (1993), J. Mater. Sci. Lett., 12,414-16

Hutchinson J W and Jensen H, (1990), Mech. Mater., 9, 139-63

Hutchinson J W and Suo Z, Appl. Mech. Rev., 28(1991)63

Inglis C E, (1913) Trans. Inst. Naval. Arch. 55, 219

Irwin G R, (1958) Hanbuck der Physik, V6, p551, Springer, Berlin

Ishikawa T, Ichikawa H and Teranishi H, (1987) Proc. Electrochem. Soc. 88-5; Proc. Symp. High Temp. Mater. Chem., 4, 205

Ishikawa T (1994), Comp. Sci. & Tech., 51, 135-44

Jones R H, Henager C H and Tortotelli P F, (1993), J. of Materials, December 26-29

Khobaib M, Zawada L, (1991), Ceram. Eng. Sci. Proc., 12[7-8]pp. 1537-55

Kim R Y and Katz A P, (1988), Ceram. Eng. Sci. Proc., 9, 853

Kim H S, Yong J A, Rawlings R D and Rogers P S, (1991), Mats., Sci. and Tech., 7, 155-157

Kim H-E and Moorhead A J, (1991) J. Am. Ceram. Soc., 74[3]666-9

Kim R Y and Pagano N J, (1991) J. Am. Ceram. Soc., 74, 1082-90

Kimber A C, Keer J G, (1982), J. Mater. Sci. Lett., 1, 353

Knight J C and Page T F, (1987) Br Ceram Trans J, 86, 154-60

Kotil T, Holmes J W and Comminou M, (1990), J. Am. Ceram. Soc., 73[7]1879-83

Kumar A and Knowles K M, (1996a), Acta. Metall., 44(7)2901-21

Kumar A and Knowles K M, (1996b), J. Am. Ceram. Soc., 79[9]2364-74

Kumar A and Knowles K M, (1996c), J. Am. Ceram. Soc., 79[9]2375-8

Lambrinou K, van der Biest O, Boccaccini A R and Taplin D M R, (1996), J. European Cer. Soc., in press

Lamon J, (1988), in Fatigue of Advanced Materials, 111-130

Lara-Curzio E and Ferber M K, (1994), J. Mater. Sci., 29, 6152-8

Lewis M H, (1989a) in "Materials Development in Turbo-Machinery Design" p248-57 Eds D.M.R. Taplin, J.F. Knott and M.H. Lewis, Inst. of Met. Parsons Press, Trinity College, Dublin

Lewis and Murthy, (1991), Comp. Sci. & Tech., 42, 221-49

Lewis M H, Chamberlain A, Daniel A M, Razzell A G and Sutherland S, (1993), paper 10 presented at a workshop held by the AGARD structures and materials panel

Lewis M H, Daniel A M, Chamberlain A, Pharaoh M W and Cain M G, (1993b), J. of Microscopy, 169, 109-18

Lewis M H, (1996), in Mechanical Behaviour of Materials at High Temps., 599-624 (Eds. Branco C M et al) Kluver Academic Publishers ISBN 0-7923-4113-9

Lin F, Marieb T, Morrone A, Nutt S, (1988), Mater Res Soc Symp Proc 120, 323-32

Lipowitz J, (1991), J. Am. Ceram. Soc. Bull., 70, 12, 1888-94

Lowden R A, (1991) in Adv. Comp. Mats., Ceram. Trans, 19 (Am. Cer. Soc) 619

Luy E Y and Evans A G, (1987), J. Am. Ceram. Soc., 70(7)466-9

Mah T, Mendiratta M G, Katz A P, Ruh R, Mazidiyasni K S, (1985a), Coms. Am. Ceram. Soc., 68 [1] C-27-30

Mah T, Mendiratta M G, Katz A P, Ruh R, Mazidiyasni K S, (1985b), Coms. Am. Ceram. Soc., 68 [9] C-248-51

Mandell J F, Hong K C C and Grande D H, (1987), Ceram. Eng. Sci. Proc., 7, 937

Marshall D B, (1985), Acta. Metall., 33, 2013

Marshall D B and Evans A G, (1985), J. Am. Ceram. Soc., 68, 225-31

Marshall D B and Oliver W C, (1987), J. Am. Ceram. Soc., 70, 8, 542

Meier B, Franz C, Grathwohl G, Wanek H, Przemeck K. Advanced Structural Fiber Composites. Proceeding of Topical Symposium III on Advanced Structual Fiber Composites of the 8th CIMTEC-World Ceramics Congress and Forum on New Materials. Florence, Italy June 28 to July 4, 1994 (Ed. Vincenzini P) pp743-750

McCartney L N, (1987), Proc. R. Soc. A409, 329

Michalske T A and Freiman S W, (1983), J. Am. Ceram. Soc., 66, 284-8

Murthy V S R and Lewis M H, (1989) J. Mater. Sci. Lett., 8, 571-2

MurthyV S R, Pharaoh M W, Lewis M H, (1990), J. Mater. Sci. Lett., 10, 161-164

Ochlschlegel G, Abraham K, Florke O W, Kristall Tech., 11(1976), 1, 59-72

Okamura K, (1987), Composites 18, 107

Peters P W M, (1997), in *Key Engineering Materials Vols.* 127-131, 1093-1100, *Prceedings of the first international conference in Ceramic and Metal Matrix Composites: CMMC 96,* Eds Fuentes M, Martinez-Esnaola J M, Daniel A M

Pharaoh M P. Centre for Advanced Materials, University of Warwick Internal Report Sept 1991

Pharaoh M W, Daniel A M, Lewis M H (1993), J. Mater. Sci. Lett., 12, 988-1001

Plucknett K P, West G, Taplin D M R, Daniel A M, Sutherland S, Cain R L and Lewis

M H, (1994), *Eighth Int. Conf. on Fracture (Advances in Fracture and Structural Integrity 1994), Kiev, Ukraine, June 1993.*

Plucknett K, Sutherland S, Daniel A M, Cain R L, West G, Taplin D M R and Lewis M H, (1995), J. of Microscopy, 177, 3, 251-63

Pluvinage P, Quenisset J M, (1993) J comp Mats 27, 2, 152-169

Prewo K M, Bacon J F, Dicus D L, SAMPE Q. (1979) 42

Prewo K M, Brennan J J, J. Mater. Sci., 15 (1980) 463-8

Prewo K M, Brennan J J, J. Mater. Sci., (1982), 17, 1201-6

Prewo K M, J. Mater. Sci., (1986), 21, 3590-3600

Prewo K M, J. Mater. Sci., (1987), 22, 2695-2701

Prewo and Batt J A, J. Mater. Sci., (1988), 23, 523-527

Prewo K M, Johnson B, Starret S, (1989), J. Mater. Sci., 24, 1373-79

Pryce A W and Smith P A, (1992), J. Mater. Sci., 27, 2695-2704

Pysher D J, Goretta K C, Hodder R S and Tressler R E, (1989), J. Am. Ceram. Soc., 72[2], 184-8

Raj R, (1993) J. Am. Ceram. Soc. 76[9]2147-74

Sambell R A J, Bowen D H, Phillips D C, (1972a) J. Mater. Sci., 7, 663-75

Sambell R A J, Briggs A, Phillips D C, Bowen D H, (1972b), J. Mater. Sci., 7, 676-81

Schoenlein L H, Jones R H, Henager C H, Schilling C H, Gac F, (1988), Mat. Res. Soc. Symph. Proc. Vol. 120 313-21

Simon G and Bunsell A R, (1984), J. Mater. Sci., 19, 3658-70

Singh D, Singh J P and Wheeler M J, (1996), J. Am. Ceram. Soc., 79[3]591-6

Spearing S M and Zok F W, (1993), Trans. of the ASME, 115, 314-18

Spearing S M, Zok F W, Evans A G, (1994), J. Am. Ceram. Soc., 77[2]562-70

Stewart R L, Chyung K, Taylor M P, Cooper R F, (1986), in Fracture mechanics of Ceramics, V7, Ch. 25, 33-51, Eds, Bradt R C, Evans A G, Hasselman D P H and Lange F F, Plenum Publishing

Stohr J F, (1993) AGARD report 795, 1-1 to 1-16, April

Sun E Y, Nutt S R, Brennan J J, (1994) J. Am. Ceram. Soc., 77(5)1329-39

Sun E Y, Nutt S R, Brennan J J, (1996), J. Am. Ceram. Soc., 79(6)1521-29

Sun E Y, Lin H-T and Brennan J J, (1997), J. Am. Ceram. Soc., 80(3)609-14

Sutherland S, Plucknett K P and Lewis M H, (1995), Composites Engineering, 5, 10, 1367-78

Sutherland S and Cain R L, (1995), Progress Report on BRITE BE4610

Thomas W A, Kopp MW and Sanchez J M, (1993), J. Am. Ceram. Soc., 76[9]2175-9

Thouless M D and Evans A G, (1988), Acta. Metall., 36, 517-22

Thouless M D, Sbaizero O, Sigl S, Evans A G, (1989) J. Am. Ceram. Soc., 72[4]525-32

Tressler R E and DiCarlo J A (1995) High-Temp. Ceram. Matrix Comps. II: Des. Durability and Perf., (Eds Evans AG & Naslain R) Ceram. Trans. 58, p141-56

Vagaggini E, Domergue J-M, Evans A G, (1995) J. Am. Ceram. Soc., 78[10]2709-20

Walter M E and Ravichandran G, (1995), J. of Eng. Materials and Tech., 117, 101-108

Wang S-W and Parvizi-Majidi A, (1990), Ceram. Eng. Sci. Proc., 11, 1607

Wang S-W, Khan A, Sands Rand Vasudevan A K, (1992), J. Mater. Sci. Lett., 11, 739

Wang S-W and Parvizi-Majidi A, (1992), J. Mater. Sci., 27, 5483-96

Weber C H, Lofvander J P A and Evans A G, (1994) J. Am. Ceram. Soc., 77(7)1745-52

Weibull W, (1951), J. Appl Mech. 18(3),293-7

Weiderhorn S M, (1967), J. Am. Ceram. Soc., 50, 407-14

Weihs T P and Nix W D, (1988), Scripta Metall. et Mat., 22, 271

West G, Boccaccini A R, Taplin D M R and Lewis M H, (1995) *ECCM-7, The Institute of Materials, Woodhead Publishing Ltd, London, 1996 Vol 1, 455-60*

Wetherhold RC and Zawada L P (1991), J. Am. Ceram. Soc., 74(8)1997-2000

Windisch C F, Henager C H, Springer G D and Jones R H, (1997), J. Am. Ceram. Soc., 80(3)569-74

Winter W, Bogdanov C, Muller G and Pannhorst W, (1993a), Glastech. Ber., 66, 5, 109-117

Winter W, Berger A, Muller G and Pannhorst W, (1993b), J. Am. Ceram. Soc., 76[7]1837-43

Wu X and Holmes J W, (1993) J. Am. Ceram. Soc., 76[10]2695-700

Xia C, Carr R R and Hutchinson J W, (1993), Acta. Metall., 41[3]2365-76

Yajima S Hasagawa X Hayashi J and Iimua M (1978). J. Mater. Sci., 13, 2569

Yajima S, Okamura K, Hayashi J, Omori M. J. Am. Ceram. Soc., 59 (1976) 324

Yamamura T, Hurushima T, Kimoto M, Ishikawa T, Shibuya M and Iwai T, (1987) High Tech. Ceramics, (Ed. Vincenzini P) Elsevier 737-46

Yamamura T, Ishikawa T, Shibuya M, Hisayuki T and Okamura K (1988), J. Mater. Sci., 23, 2589-94

Zawada L P, and Butkus L M, (1991) J. Am. Ceram. Soc., 74[11]2851-58

Zok F W and Spearing S M, (1992), Acta. Metall., 40,2033

Appendix I

```
10 REM Program for modelling of stress distributions during creep or cyclic creep testing
20 ON ERROR REPORT:PRINT" at line "ERL:CLOSE#0:END
30 deltaT=1
40 sigmaCdot=1E6
50 LoadMax=100E6                          :REM composite loading rate
60 StepsUp=LoadMax/sigmaCdot
70 HoldTime=100                           :REM Enter time in seconds
80 HoldStep=HoldTime
90 Em=70E9:Ef=200E9                       :REM constituent moduli
100 Vf=0.4: Vm=(1-Vf): Ec=(Vf*Ef)+(Vm*Em) :REM composite stiffness
110 nf=1: nm=1                            :REM stress exponents
120 Af=0:Am=2500E-17                      :REM creep constants
130 G%=OPENOUT "modeltest"                :REM filename
140
150 sigmaF=0: sigmaM=0                    :REM initialise variables
160 epsC=0: epsM=0: epsF=0
170 epsMdot=0: epsFdot=0
180 epsCdottot=0: epsMdottot=0: epsFdottot=0
190 sumdeltaT=0
200
210 FOR N=1 TO 500000 STEP deltaT
220   sigmaFdot=(Ef/Ec)*(sigmaCdot+Vm*Em*(epsMdot-epsFdot))          :REM eq 6.1
230   sigmaMdot=(Em/Ec)*(sigmaCdot+Vf*Ef*(epsFdot-epsMdot))          :REM eq 6.1
240   sigmaF=(sigmaFdot*deltaT)+sigmaF                  :REM update stresses
250   sigmaM=(sigmaMdot*deltaT)+sigmaM                  :
260   sigmaC=(Vf*sigmaF)+(Vm*sigmaM)                    :
270
280   epsMdot=Am*(sigmaM^nm): epsFdot=Af*(sigmaF^nf)    :REM calculate strain rates
290
300   epsMdottot=(sigmaMdot/Em)+epsMdot
310   epsFdottot=(sigmaFdot/Ef)+epsFdot
320
330   epsM=epsMdottot*deltaT: epsF=epsFdottot*deltaT
340   epsCdottot=(sigmaCdot+(Vm*Em*epsMdot+Vf*Ef*epsFdot))/Ec
350   epsC=(epsCdottot*deltaT)+epsC
360
370   sumdeltaT=deltaT+sumdeltaT                        :REM elaspsed time
380   REM next line controls ramp switching
390   IF (N-StepsUp) MOD (HoldStep+StepsUp)=0 THEN PROCStepChange ELSE IF N MOD
       ((HoldStep*2)+(2*StepsUp)) =0 THEN PROCLoadup ELSE IF N MOD
       (HoldStep+StepsUp) =0 THEN PROCLoaddown
400   REM next line outputs stresses and composite strain
410   IF sumdeltaT MOD 2=0 THEN BPUT#G%,STR$ sumdeltaT+","+STR$ epsC+","+STR$
       sigmaC+","+STR$ sigmaM+","+STR$ sigmaF
420
430 IF sumdeltaT>(14400/3) THEN 450                     :REM sets max model length
440 NEXT N
450 CLOSE#0:END
460DEF PROCStepChange
470 sigmaCdot=0
480 REM deltaT=500
490ENDPROC
500DEF PROCLoadup
510 sigmaCdot=1E6
520ENDPROC
530DEF PROCLoaddown
540 sigmaCdot=-1E6
550ENDPROC
```